

**Water-swollable rubber with  
nanotechnology-enabled super capacity as  
smart water-leakage sealant**

**By**

Nazila Dehbari



This thesis is presented for the degree of

Doctor of Philosophy of Mechanical Engineering

School of Computer Science, Engineering and Mathematics

Flinders University

July 2017

## SUMMARY

Water-swellaible rubber (WSR) attracts special interest due to their unique properties that can provide critical advantages for applications. They can stop water not only by means of elastic sealing, high resilience and good tensile strength but also by means of swelling in water. These new functional polymers can expand their volumes up to several hundred times the original by absorbing surrounding water. The more water absorbed, the higher the expansion force. WSRs were used in the Euro Tunnel under the straits of Dover and there are some examples in segment tunnel construction for railways, subways and highways in Japan and recently in China.

The main problem of WSR is that hydrophilic super absorbent resin cannot disperse well in hydrophobic rubber, so it can break off from rubber matrix easily which may cause weakening abilities of water-swelling, mechanical properties, long-term water retention, and repeated usage. These issues have spawned a flurry of research to devise longer lasting of superabsorbent polymers (SAPs) in WSR, with higher water absorbency (about 3times) and particular emphasis on sealing applications.

The incompatibility between rubber and SAPs can be mitigated by modifier. By using compatibilizer and neutralizer the dispersion of hydrophilic phase into the hydrophobic continuous phase is greatly improved confirmed by SEM, and therefore, migration of super water-absorbent resin from the rubber matrix dramatically reduced.

Next step basically focused on enhancing mechanical properties of WSR by introducing either hyperbranched (HB) polymer in poly acrylic acid (PAA) hydrogel or electrospun nanofibers. Continuous nanofibers with dual nano-macro nature and ability to bridge scales are considered to provide in situ water channels between SAPs and enhance the mechanical strength at the same time.

The objective of this thesis was to fabricating novel WSR, manufacture of nanofibers and study the behaviour of nanofiber reinforced WSR composites. It was shown that PAA, styrene-butadiene-styrene (SBS), PAA/SBS and poly vinyl alcohol (PVA) nanofibers manufactured using single and/or double needle electrospinning technique are excellent candidates for reinforcement purposes. Based on results, WSR reinforced with PVA and SBS nanofibers possess significant improvements in tensile strength, elongation at break and toughness of WSR composites.

**Chapter 1** provides a general introduction of WSR composites. The classification, background of study, problem statement, were discussed. The objectives and scopes of the study and significance of the research were also introduced in **Chapter 1**.

**Chapter 2** provides an overview of previous research on knowledge sharing and intranets in this area. It introduces the framework for the case study that comprises the main focus of the research described in this thesis. It is also the summary of the published work in a peer-reviewed journal.

**Chapter 3** focuses on the initial investigations of using SAP into the Rubber. Neutralisation and compatibilization effects on WSR is going to be discussed in this chapter.

**Chapter 4** provides a detailed introduction towards the electrospinning of various superabsorbent nanofibers mats. It presents an outlook about the problems and challenges in electrospun nanofiber reinforced polymer composites. In next step, electrospun nanofiber mats were added into conventional WSR and the properties of resultant composite alongside of mechanisms of those fibers on WSR are also discussed.

**Chapter 5** discusses the potential use of nanofibers of PAA and SBS to reinforce WSR composites. The mechanisms and effects of these nanofiber mats in enhancing the mechanical and water swelling properties of WSR are investigated here.

**Chapter 6** relates to the reinforcement of PAA hydrogel by using HB polymer. The physical and mechanical properties of the prepared hydrogels were investigated in this chapter.

**Chapter 7** shows the possibility of significant enhancement of WSR in both swelling ability and mechanical strength by introducing PVA/SBS nanofiber.

**Chapter 8** summarizes the thesis, discusses its findings and contributions, points out limitations of the current work, and also outlines directions for future research.

# TABLE OF CONTENTS

<b>Summary</b>	<b>i</b>
<b>Table of Contents</b>	<b>iv</b>
<b>List of Figures</b>	<b>x</b>
<b>List of Tables</b>	<b>xvii</b>
<b>Abbreviations</b>	<b>xviii</b>
<b>Details of Publications</b>	<b>xx</b>
<b>Conference Abstracts and Oral Presentations</b>	<b>xxii</b>
<b>Declaration</b>	<b>xxiii</b>
<b>Acknowledgements</b>	<b>xxiv</b>
<b>CHAPTER 1 OVERVEIW</b>	<b>1</b>
1.1 Background of Study	1
1.2 Problem Statement	2
1.3 Objective of Study	2
1.4 Scope of the Study	3
1.5 Significant of Research	3
<b>CHAPTER 2 INTRODUCTION OF WSR COMPOSITE</b>	<b>4</b>
2.1 Overview	5
2.2 How does WSR work?	7

2.3 Applications and market	9
2.4 Synthesis and manufacturing process	10
2.4.1 Physical methods	11
2.4.2 Chemical methods	11
2.4.2.1 IPN technology	12
2.4.2.2 Compatibilizing and grafting	14
2.5 Properties of WSR composites	16
2.5.1 Effect of mechanical mixing	16
2.5.2 Effect of IPN networks	19
2.5.3 Effect of fillers	21
2.5.4 Effect of grafting	23
2.5.5 Other methods	23
2.6 Future of WSR	24
2.7 Conclusions	27
2.8 References	28

## **CHAPTER 3 NEUTRALIZATION AND COMPATIBILIZATION EFFECT ON WATER SWELLABLE RUBBER**

**35**

3.1 Introduction	36
3.2 Experiments	37
3.2.1 Materials and preparation	37
3.3 Characterization	38
3.4 Results and discussion	40

3.4.1 Molecular interactions in WSR	40
3.4.2 Water swelling behaviour	41
3.4.3 Morphological study	44
3.4.4 Contact angle	46
3.4.5 Mechanical properties	48
3.5 Conclusions	49
3.6 References	50

**CHAPTER 4 ELECTROSPUN MULTI-SCALE HYBRID NANOFIBER/NET WITH ENHANCED WATER SWELLING ABILITY IN RUBBER COMPOSITES** **53**

4.1 Introduction	54
4.2 Experiments	56
4.2.1 Materials and Preparation of PAA and PAA hybrid solutions	56
4.2.2 Preparation of PAA and PAA hybrid NFN mats	57
4.2.3 Preparation of PAA hybrid NFN mat enhanced WSR composites	58
4.3 Characterizations	59
4.4 Results and discussion	61
4.5 Conclusions	71
4.6 References	72

**CHAPTER 5 ENHANCING WATER SWELLING ABILITY AND MECHANICAL PROPERTIES OF WSR BY PAA/SBS NANOFIBER MATS** **79**

5.1 Introduction	80
------------------	----

5.2 Experiments	81
5.2.1 Materials and Sample preparation	81
5.2.2 Characterizations	83
5.3 Results and discussion	84
5.3.1 Morphology	84
5.3.2 Contact angle of nanofiber mats	86
5.3.3 Mechanical properties of nanofiber mats and composites	87
5.3.4 Swelling ratio of composites	90
5.4 Mechanisms of enhanced swelling ratio and mechanical properties	93
5.5 Conclusions	95
5.6 References	95

**CHAPTER 6 IN SITU POLYMERIZED HYPERBRANCHED POLYMER REINFORCED  
POLY (ACRYLIC ACID) HYDROGELS** **100**

6.1 Introduction	101
6.2 Material preparation and characterisations	103
6.3 Results and discussion	106
6.3.1 Molecular interactions within hydrogels	106
6.3.2 Morphological understanding	108
6.3.3 Water swelling behaviours	110
6.3.4 Mechanical behaviours of hydrogels	111
6.4 Proposed mechanism	118
6.5 Sensor application	120

6.6 Conclusions	123
6.7 References	124
<b>CHAPTER 7 IN SITU FORMED INTERNAL WATER CHANNELS IMPROVING WATER SWELLING AND MECHANICAL PROPERTIES OF WSR COMPOSITES</b>	<b>132</b>
7.1 Introduction	133
7.2 Experiments	134
7.2.1 Materials and methods	134
7.2.2 Sample characterization	135
7.3 Results and discussion	136
7.3.1 Swelling behaviour	136
7.3.2 Contact angle	140
7.3.3 Morphological study	140
7.3.4 Mechanical behaviour	143
7.4 Conclusions	145
7.5 References	145
<b>CHAPTER 8 CONCLUSIONS AND FUTURE DIRECTIONS</b>	<b>148</b>
8.1 Summary	149
8.2 Comparison of Commercial WSR with studied WSR	151
8.2.1 Experiments	153
8.2.2 Results and discussion	154

8.3 Recommendations and Future Directions	158
8.4 References	159

## LIST OF FIGURES

---

- Figure 2.1**| Schematic presentation of (a) SAP chains before and after swelling [12] and (b) sodium polyacrylate networks 7
- Figure 2.2**| Schematic illustration of swelling mechanism of WSR (a) SAP particles (red dots) between cross-linked chains of rubbers, (b) water molecules penetrate to the chains, causing to increase the volume of SAP, and (c) the network of WSR is extensively swollen 8
- Figure 2.3**| Two synthetic methods for preparing interpenetrating polymer networks. A, sequential IPNs, and B, simultaneous IPNs 13
- Figure 2.4**| Schematic mechanism of interpenetrating polymer networks 14
- Figure 2.5**| Micrographs of films of SAP/rubber in ratio 30/100 (a) dispersion from the mixing chamber of a Brabender and (b) dispersion from a two-roll mill 17
- Figure 2.6**| SEM micrographs obtained from cross-sections of (a) (magnification  $\times 7000$ ) unmodified PDMS, and PDMS/PAA IPNs having a PAA contents of (b) (magnification  $\times 7000$ ) 20 wt%, (c) (magnification  $\times 3000$ ) 20 wt%, (d) (magnification  $\times 7000$ ) 30 wt%, (e) (magnification  $\times 7000$ ) 40 wt%, (f) (magnification  $\times 7000$ ) 50 wt%, (g) (magnification  $\times 7000$ ) 60 wt% and (h) swelling behaviour of PDMS/PAA IPNs 20
- Figure 2.7**| Schematic drawings of (a) electrospinning SAP fibers/mats to rubber layers, (b) multi-layering electrospinning of SAP and rubber, (c) co-electrospinning of SAP and rubber and (c) hybrid 3D printing with electrospinning of rubber and SAP to form WSR composites 27

<b>Figure 3.1 </b> Schematic of processing WSR	<b>38</b>
<b>Figure 3.2 </b> FTIR spectra of poly (acrylic acid), pure PDMS and their composites with different ratio of PAA, NaOH and compatibilizer	<b>41</b>
<b>Figure 3.3 </b> Water swellability of WSR composites	<b>42</b>
<b>Figure 3.4 </b> Water swellability of WSR with and without compatibilizer and NaOH	<b>43</b>
<b>Figure 3.5 </b> Water swellability of WSR for first, second and third dry swellings for sample 1	<b>44</b>
<b>Figure 3.6 </b> SEM micrographs of fractured surfaces of a–e samples 1–5 and f pure rubber after immersion in water for 1000 h	<b>45</b>
<b>Figure 3.7 </b> SEM micrographs of fractured surfaces of sample 6 (SAP/rubber), 7 (SAP/ rubber/ compatibilizer) and 8 (SAP/rubber/ compatibilizer/NaOH) in a dry and b swelling states (after 1000 h of soaking in water)	<b>46</b>
<b>Figure 3.8 </b> Optical images of water droplets on pure PAA, pure rubber and all composites	<b>47</b>
<b>Figure 3.9 </b> Effect of using PAA on contact angle of rubber with all composites	<b>47</b>
<b>Figure 4.1 </b> Preparation of electrospun PAA-HB-GO NFN mat	<b>58</b>
<b>Figure 4.2 </b> Scheme of composites preparation with (a) PAA/rubber composite and (b) PAA-HB-GO NFN mat/PAA/rubber composites	<b>59</b>

- Figure 4.3|** SEM images of (a) PAA-EG, (b) PAA-EG+HB, (c) PAA-EG+GO and (d) PAA-EG+HB+GO fibrous mats **62**
- Figure 4.4|** FTIR spectra of 1) PAA, 2) EG, 3) HB, 4) GO, 5) PAA-EG, 6) PAA-EG+HB, 7) PAA-EG+GO and 8) PAA-EG-HB+GO **63**
- Figure 4.5|** Raman spectra graph of 1) GO, 2) PAA-EG, 3) PAA-EG+GO and 4) PAA-EG+HB+GO **65**
- Figure 4.6|** TGA curves of 1) PAA-EG, 2) PAA-EG+HB, 3) PAA-EG+GO and 4) PAA-EG+HB+GO fibrous mats **66**
- Figure 4.7|** (a) Water absorption properties of PAA-EG, PAA-EG+HB, PAA-EG+GO and PAA-EG+HB+GO fibrous mats, (b) Water absorption properties of PAA-EG, PAA-EG+HB, PAA-EG+GO and PAA-EG+HB+GO fibrous mats in 6 h, (c) SEM image of PAA-EG+HB+GO fibrous mat **68**
- Figure 4.8|** Water absorption ability of five composites in (a) 0-6 h and (b) 0-1800 h, and (c) photos of the conventional WSR (1) before and (3) after absorbing water for 1000 h, and WSR+PAA-EG+HB+GO (2) before and (4) after absorbing water for 1000 h **70**
- Figure 4.9|** Schematics of water channel in WSR containing electrospun NFN mat **71**

**Figure 5.1|** Steps of preparation of WSR enhanced with PAA/SBS nanofiber mats (a) the electrospinning machine with two needles setting, (b) the SEM image of the PAA/SBS nanofibers, (c) mixing of PAA/SBS nanofibers with WSR, and (d) the cured composite of WSR+PAA/SBS nanofibers **83**

**Figure 5.2|** SEM micrographs of (a) PAA nanofibers with average diameter of 0.65  $\mu\text{m}$  (solid orange arrows), (b) SBS nanofibers with average diameter of 0.95  $\mu\text{m}$  (dashed blue arrows), (c) PAA/SBS nanofibers with some spider web-like structures (solid green arrows), and WSR+PAA/SBS composites (d) before and (e) after swelling, the bold channels representing PAA nanofibers that have absorbed water (solid orange arrows) **86**

**Figure 5.3|** Contact angle images of (a) SBS nanofiber mat and (b) PAA/SBS nanofiber mat 30 s after a drop of water was put on the surface **87**

**Figure 5.4|** Force-stretch curves of PAA, SBS and PAA/SBS nanofiber mats **88**

**Figure 5.5|** Force-stretch curves of composites with PAA, SBS and PAA/SBS nanofibers before (a) and (b) after immersing in water **89**

**Figure 5.6|** Water swellability of composites in (a) first and (b) second swellings to 650 hrs **92**

**Figure 5.7|** Water swellability of composites after (a) 1<sup>st</sup> and (b) 2<sup>nd</sup> absorbing periods for the first 6 hrs **93**

<b>Figure 5.8 </b> SEM images show the proposed mechanism of WSR containing PAA and SBS nanofiber mats after swelling (Dashed arrows with blue colour pointing SBS nanofibers)	<b>94</b>
<b>Figure 6.1 </b> FTIR spectra of (a) HB powder, (b) PAA and (c) PAA-HB hydrogel	<b>107</b>
<b>Figure 6.2 </b> DSC curves of PAA and PAA hybrid samples	<b>108</b>
<b>Figure 6.3 </b> SEM images of (a) and (b) PAA-HB surfaces and (c) and (d) PAA surfaces two different magnifications of 80 $\mu\text{m}$ and 200 $\mu\text{m}$	<b>109</b>
<b>Figure 6.4 </b> TEM images of PAA-HB hydrogel	<b>110</b>
<b>Figure 6.5 </b> Swelling ratios of PAA and PAA-HB hydrogels immersed in water	<b>111</b>
<b>Figure 6.6 </b> Mechanical properties of PAA and PAA-HB hydrogels	<b>112</b>
<b>Figure 6.7 </b> Stress-strain relationship for PAA-HB hydrogels at different stretch ratios	<b>113</b>
<b>Figure 6.8 </b> Comparison of mechanical properties of PAA with PAA-HB hydrogel for different notch depths. (a) Ultimate tensile strength, (b) elongation at break (c) toughness and (d) stretchability	<b>115</b>

**Figure 6.9**| Hysteresis effect of loading to a certain stretch ( $\lambda=4$ ) and unloading to zero for first and second loadings with different time intervals. All dynamic tests were performed at 50 mm.min<sup>-1</sup> strain rate **117**

**Figure 6.10**| (a) Interpenetrating networks of PAA-HB, (b) schematic structure of a HB molecule, and (c) schematic illustration of possible physical interaction and hydrogen bond formation mechanism between PAA chains and HB molecules **119**

**Figure 6.11**| Effect of pH values on the (a) swelling kinetics and (b) equilibrium swelling ratio (ESR) of PAA and PAA-HB samples **121**

**Figure 6.12**| (a) Change in the SR10/SR2 ratio during three cycles of dynamic swelling revealed higher pH sensitivity of PAA-HB hydrogels compared to that of PAA samples. After 3 cycles, the better dimensional stability of (b) PAA-HB samples compared to that of (c) PAA samples was in general agreement with the enhanced mechanical properties from HB **123**

**Figure 7.1**| Effect of PVA and SBS nanofibers on 1<sup>st</sup> and 2<sup>nd</sup> occasion swelling properties of WSR samples **137**

**Figure 7.2**| Comparison of 1<sup>st</sup> and 2<sup>nd</sup> occasion swelling properties of WSR containing PVA and PVA/SBS nanofibers **138**

**Figure 7.3**| SEM micrographs of (a) WSR/PVA nanofiber, (b) PVA nanofibers, (c) WSR+PVA/SBS nanofiber and (d) WSR after 350 h immersing in water **141**

<b>Figure 7.4 </b> Schematic diagram of water channel formation in the WSR+PVA/SBS nanofiber composite	<b>142</b>
<b>Figure 7.5 </b> Load-extension diagram for WSR, WSR/PVA nanofiber and WSR+PVA/SBS nanofiber in dry state and after first and second swelling	<b>144</b>
<b>Figure 8.1 </b> An example of usage Leakmaster in pre-cast applications such as utility vaults and storage reservoirs	<b>152</b>
<b>Figure 8.2 </b> Swelling Properties of Leakmaster after immersing in water	<b>152</b>
<b>Figure 8.3 </b> Load-extension curves in dry state and after the first and second swelling for a) Commercial WSR and b) WSR+PVA/SBS nanofiber composite	<b>155</b>
<b>Figure 8.4 </b> Water swellability of a) Commercial WSR b) WSR+PVA/SBS nanofiber composite for first and second swelling	<b>156</b>
<b>Figure 8.5 </b> Images of a) commercial WSR and b) studied WSR in dry and after 3 months and 6 months of immersion	<b>157</b>

# LIST OF TABLES

---

2.1 Advantages and disadvantages of physical and chemical methods	11
2.2 Summary of WSR composites with their corresponding manufacturing methods	18
2.3 Effect of different kinds of fillers on water swelling ratio and mechanical properties of WSRs	22
3.1 Composition of prepared WSR composites	38
3.2 Tensile properties of WSR before and after immersion in water	49
4.1 BET specific surface area of PAA and PAA hybrid NFN mats	67
5.1 Mechanical properties of PAA, SBS and PAA/SBS reinforced WSR composites	90
6.1 Change in selected mechanical properties of PAA-HB at different stretch ratios	112
6.2 Different PAA hydrogel toughening methods with mechanical and swelling properties	120
7.1 Mean swelling rate for the WSR composites	139
7.2 Comparison of contact angle and surface energy for different samples	140
7.3 Selected mechanical properties for nanofibers and hybrid composites	143
8.1 Mechanical properties of Leakmaster	153

## ABBREVIATIONS

---

<b>AA</b>	<b>Acrylic acid</b>
<b>CHR</b>	<b>Chlorohydrin rubber</b>
<b>CPA</b>	<b>Crosslinked polyacrylate</b>
<b>CR</b>	<b>Chloroprene Rubber</b>
<b>DSC</b>	<b>Differential scanning calorimeter</b>
<b>DMF</b>	<b>N,N-dimethylformamide</b>
<b>EB</b>	<b>Elongation at break</b>
<b>EG</b>	<b>Ethylene glycol</b>
<b>EPDM</b>	<b>Ethylene propylene diene monomer rubber</b>
<b>FESEM</b>	<b>Field emission scanning electron microscopy</b>
<b>FTIR</b>	<b>Fourier transform infrared spectroscopy</b>
<b>GO</b>	<b>Graphene oxide</b>
<b>HB</b>	<b>Hyperbranched polymer</b>
<b>HNBR</b>	<b>Hydrogenated Nitrile Butadiene Rubber</b>
<b>IPN</b>	<b>Interpenetrating polymer network</b>
<b>MA</b>	<b>Methyl acrylate</b>
<b>MMA</b>	<b>Methyl methacrylate</b>
<b>MPa</b>	<b>Mega pascal</b>
<b>NR</b>	<b>Natural rubber</b>
<b>NBR</b>	<b>Natural butadiene rubber</b>
<b>PAA</b>	<b>Poly acrylic acid</b>
<b>PAN</b>	<b>poly acrylonitrile</b>
<b>PDMS</b>	<b>Poly dimethyl siloxane</b>
<b>PEG</b>	<b>Poly ethylene glycol</b>

<b>PVA</b>	<b>Poly vinyl alcohol</b>
<b>PVC</b>	<b>Poly vinyl chloride</b>
<b>SAP</b>	<b>Super absorbent polymer</b>
<b>SBR</b>	<b>Styrene-butadiene rubber</b>
<b>SEM</b>	<b>Scanning electron microscopy</b>
<b>SBS</b>	<b>Styrene butadiene styrene</b>
<b>SMC</b>	<b>Sheet-moulding compounds</b>
<b>SW</b>	<b>Swelling ratio</b>
<b>TEM</b>	<b>Transmission electron microscopy</b>
<b>THF</b>	<b>Tetrahydrofuran</b>
<b>TGA</b>	<b>Thermogravimetric analysis</b>
<b>TB</b>	<b>Tensile strength at break</b>
<b>WSR</b>	<b>Water swellable rubber</b>

## DETAILS OF PUBLICATIONS

---

### JOURNAL ARTICLES

1. **Nazila Dehbari**, Javad Tavakoli, Jinchao Zhao and Youhong Tang. "In situ formed internal water channels improving water swelling and mechanical properties of water swellable rubber composites". *Journal of Applied Polymer Science* 134 no. 9 (2017) DOI: 10.1002/app.44548.
2. **Nazila Dehbari**, Javad Tavakoli, Simranjeet Singh Khatrao, and Youhong Tang. "In situ polymerized hyperbranched polymer reinforced poly (acrylic acid) hydrogels". *Materials Chemistry Frontiers* (2017) DOI: 10.1039/C7QM00028F.
3. **Nazila Dehbari**, Javad Tavakoli, Jinchao Zhao, and Youhong Tang. "Enhancing water swelling ability and mechanical properties of water-swellable rubber by PAA/SBS nanofiber mats." *Journal of Applied Polymer Science* 133, no. 47 (2016) DOI: 10.1002/app.44213.
4. **Nazila Dehbari**, and Youhong Tang. "Water swellable rubber composites: An update review from preparation to properties." *Journal of Applied Polymer Science* 132, no. 46 (2015) DOI: 10.1002/app.42786.
5. Jinchao Zhao, **Nazila Dehbari**, Wei Han, Leping Huang, and Youhong Tang. "Electrospun multi-scale hybrid nanofiber/net with enhanced water swelling ability in rubber composites." *Materials & Design* 86 (2015): 14-21. DOI: 10.1016/j.matdes.2015.07.105.

6. **Nazila Dehbari**, Jinchao Zhao, Rengui Peng, and Youhong Tang. "Neutralisation and compatibilization effects on novel water-swellaable rubber composites." *Journal of Materials Science* 50, no. 15 (2015): 5157-5164. DOI: 10.1007/s10853-015-9052-7.
  
7. **Nazila Dehbari**, Youhong Tang, and Nima Moazeni. "Polylactic acid based rubber composites and nanocomposites" In: *Rubber based bionanocomposites - preparation*, Visakh P. M. Ed (2017) Springer, UK.

## CONFERENCE ABSTRACTS AND ORAL PRESENTATIONS

---

- 1. Nazila Dehbari**, Javad Tavakoli, Yakani Kambu, and Youhong Tang. "An economic way to toughen poly acrylic acid superabsorbent polymer using hyperbranched polymer". International Conference of Material Science and Engineering Technology (ICMSET), Japan (2016).
- 2. Nazila Dehbari**, Jinchao Zhao, and Youhong Tang. PAA/SBS 3D-blending nanofiber mats as water channels for water swelling rubber composites. International Conference on Nanoscience and Nanotechnology (ICONN) Australia (2016).
- 3. Nazila Dehbari**, and Youhong Tan. "Polylactic acid based rubber composites and nanocomposites". Centre for NanoScale Science and Technology (CNST), Australia (2015).
- 4. Nazila Dehbari**, and Youhong Tang. "Study of kenaf core on poly lactic acid biocomposite". Royal Australian Chemical Institute (RACI) Polymer & Bionanotechnology Symposium (SASPBS'13) – Australia (2013).

# DECLARATION

I certify that this thesis does not incorporate without acknowledgment any material previously submitted for a degree or diploma in any university; and that to the best of my knowledge and belief it does not contain any material previously published or written by another person except where due reference is made in the text.

Signed.....*nazila*.....

Date.....22/03/2017.....

## ACKNOWLEDGEMENTS

I wish to extend my gratitude to a number of people that have made this research a success.

Firstly, I would like to thank my supervisor, Dr Youhong Tang, for believing in me and being a great mentor. He has taught me that the key to a successful career is passion and hard work and for that I am sincerely grateful. During the last few years, his wisdom, immense knowledge and optimism has been a great motivation to me. He has created the foundation on which I have been able to build my research career on.

I would also like to thank my co-supervisors, Professor Amanda Ellis and Associate Professor Karl Sammut for their guidance and encouragement.

I would like to record my gratitude to Dr. Javad Tavakoli for guiding and working with me especially, in particular with the design of the experiments. A big part of this research would not have been possible without keen collaboration of him. I appreciate the fact that he believed in my ideas and undoubtedly, the success in the outcome was achieved because I had the chance to work with such an inspiring team of colleagues.

To all the members of the Tang Research Group, not forgetting the ones who have embarked on a different path to pursue their respective careers, I would like to express my deepest appreciation. I believe that no research is a success without a great team. I would like to extend particular appreciation to Mr. Wei Han, Associate Professor. Jinchao Zhao and Mr. Rengui Peng for being remarkable friends, colleagues and mentors. I gained so much knowledge and skills from Dr. Yang Yu during my research career.

I would like to also thank Dr. Cameron Shearer for all his support and constant guidance particularly with the scanning electron microscopy. It has certainly helped me with a number of experiments and data analysis.

Last but not least, I am truly grateful to my family: my parents and my brothers for truly believing in me and for providing me with a great support system and constantly reminding me to be proud of myself and everything that I have achieved so far. This thesis would not have been close to possible without their constant support and encouragement. I owe thanks to a very special person, my soulmate, Yashar, for his continued and unfailing love, support, patience and understanding during my pursuit of PhD degree that made the completion of thesis possible. I am truly blessed to be surrounded by so much love.

# 1. [OVERVIEW]

Nowadays water shortages are one of the problems which humans are faced due to the rapid industrialisation and population expansion. Unfortunately, considerable amounts of water are lost due to leakage. The rate and amount of leaks differ from one country or region to another. According to data reported by Water Loss Task Force of the International Water Association, the leakage rate is lowest at about 3% in Germany, but very high in the U. K. at over 20% and Australia at 12%.

WSR is a new kind of functional rubber with water sealing and water-swelling properties, which was developed in the 1980s and is currently used to prevent water leakage from pipe or block connections in constructions. This project will develop a novel, easy-to-fabricate and convenient-to-use WSR to improve its ability to prevent water leakage, with high capability and durability, especially for construction joints and cracks.

## 1.1 Background of Study

Classical rubbers have been frequently used to prevent water leakage from pipes, block connections and construction joints. However, they have inherent drawbacks in sealing precision. WSRs are functional polymers that expand their volumes up to several hundred times the original by absorbing surrounding water. WSRs possess not only the general properties of rubber, such as high resilience and good tensile strength, but also water-swelling ability. This functionality provides the materials with sealing or caulking applications. The more water absorbed, the higher the expansion force. WSRs were used in the Euro Tunnel under the straits of Dover and there are

some examples in segment tunnel construction for railways, subways and highways in Japan and recently in China. Most recently, they have been used to seal cracks occurring from the earthquake in Fukushima No. 2 nuclear power plant in Japan.

## **1.2 Problem Statement**

Currently WSRs used have some intrinsic disadvantages, which need to be improved to advance their applications:

1. Incompatibility between hydrophilic SAP and hydrophobic rubber.
2. Uneven water absorption among SAPs and local stress concentration in rubber matrix.

## **1.3 Objectives of Study**

The specific aims of this research are as follows:

- To develop novel methods to fabricate WSR with high capacity of water uptake and manipulate good connection between rubber and SAP particles for applications in sealing.
- To develop novel methods of overcoming the migration of SAPs while controlling their mechanical
- To control the formation of nano-blocks and nano-channels by introducing electrospun fibers in rubber matrix
- To characterise water swelling mechanisms of the proposed smart water-leakage sealant.

## **1.4 Scope of the Study**

In order to execute the objectives of this research, the activities below were performed:

- I. Sample preparation involved the following parts: (a) Processing of WSR by using nanofiller reinforcement and (b) electrospinning of nanofiber-enabled water channels
  
- II. Characterisation of water swelling mechanisms: The capability, durability, aging properties and uniformity of WSR will be characterised to understand the enhanced water swelling mechanisms by FESEM.
  
- III. Mechanical tests: to evaluate the enhanced mechanical properties of WSR, tensile strength, elongation at break, stiffness and hardness test were performed.

## **1.5 Significant of Research**

The significant of this research is improving the performance of WSR using SAPs and nanofibers which can enhance the mechanical properties of WSR, while nanofiber-enabled channels in the rubber matrix allow water to diffuse between isolated hydrophilic SAP phases, achieving high swelling ability for sealing applications. Therefore, the subsequent chapters in this thesis will provide a detail description of the development of novel methods to overcome the limitations of WSR.

## 2. [INTRODUCTION OF WSR COMPOSITE<sup>1</sup>]

This chapter presents a brief review of the recent progress on WSR in terms of their manufacturing methods, synthesis, chemical, physical, and mechanical properties and indicates some challenging problems. To keep the integrity of the knowledge, a brief introduction of WSR has been given following by discussion of critical issues involved in principle fundamentals. A summary of the researches on the physical and mechanical behaviour of different kinds of WSR are presented. Finally, the critical issues and challenges are detailed, and suggestions for potential application have been made based on the authors' knowledge and experience.

1. This work has been published in Journal of Applied Polymer Science: Nazila Dehbari and Youhong Tang. "Water swellable rubber composites: An update review from preparation to properties." Journal of Applied Polymer Science 132.46 (2015) DOI: 10.1002/app.42786.

## 2.1 Overview

Polymer blend systems are new kinds of material that have come into wide use in recent years. The relative ease of mixing, low cost of processing (compared to synthesizing) and novel properties are the major advantages of developing combined polymer materials [1]. One of the most industrially multicomponent blends is WSR. WSR is a kind of functional polymer composed of elastomer with water-absorbent resins. It retains the properties of general rubbers such as high elasticity, resilience and high toughness. Moreover, with the absorption of water its volume can expand to more than 1.5 times the original [2]. The most common hydrophobic rubbers used as a matrix in WSRs are natural rubber, chloroprene rubber, chlorohydrin rubber and silicon rubber specially room temperature vulcanization silicone rubber (RTV Silicone) which is a type of silicone rubber made from a two-component system (base plus curing agent, A+B) [3-9]. They are usually mixed with various water-absorbent materials known as SAPs.

SAP is a kind of hydrophilic polymer (cross-linked hydrogel) having water-absorbing capacity from 100 up to 2000 g/g, in which the absorbed water is scarcely removable even under pressure, because the water molecules are held tightly in the network by hydrogen bonding. Using SAP into rubber will help the water go through its three-dimensional network structures and retain into the rubber structure which can force it to swell. Some of the common SAPs that are commonly using by researchers are cross-linked forms of polyacrylate (acrylic acid and acrylamide), polyvinyl alcohol, poly (ethylene oxide), starch-acrylate copolymer, carboxymethyl cellulose and many other polymers [9-12]. The degree of swelling and swelling rate of SAPs basically depends on the type of rubber, the conditions of the water are using for test such as pH, salinity, temperature, pressure and time of immersing in a solution and also the design of the samples [13].

The dependency of molecular weights and grafting frequencies on swelling behaviour of graft copolymers was investigated by Fanta *et al* [14]. He showed by decreasing the number of grafted chains of polyacrylonitrile (PAN) and increasing their average molecular weight, swelling of starch granules will be enhanced significantly. In a similar work, he reported that incorporation of selected co-monomers such as vinylsulfonic acid, acrylic acid (AA), methyl acrylate (MA), methyl methacrylate (MMA) and styrene has a great influence on water absorbency of the PAN-starch [15]. The first commercial SAP was produced in 1970 through alkaline hydrolysis of starch-g-polyacrylonitrile [2]. Because of their excellent characteristics, SAPs have stimulated considerable interest in various fields. They were industrialized in the US and Japan in the early 1980s as hygienic products and to reduce cost. They are now used in a broad range of applications in health, such as controlled drug delivery, and in agricultural and horticultural applications such as water conservation in soil and soil conditioning [16-19].

Figure 2.1(a) illustrates a typical SAP in dry and water-swollen states. Absorption capacity (ability of WSR to absorb/incorporate water), absorption rate (the rate of transferring mass/volume at the interface between the water and composite) and the swollen gel strength are the three main functional features of SAPs. In the swollen state, however, the mechanical properties of SAPs are relatively weak. By manipulating the structure of hydrogels, such as by increasing the cross-linking density, surface treatment of the SAP and incorporation of suitable polymers, the mechanical, thermal and physical properties of SAPs can be improved [12, 20, 21].

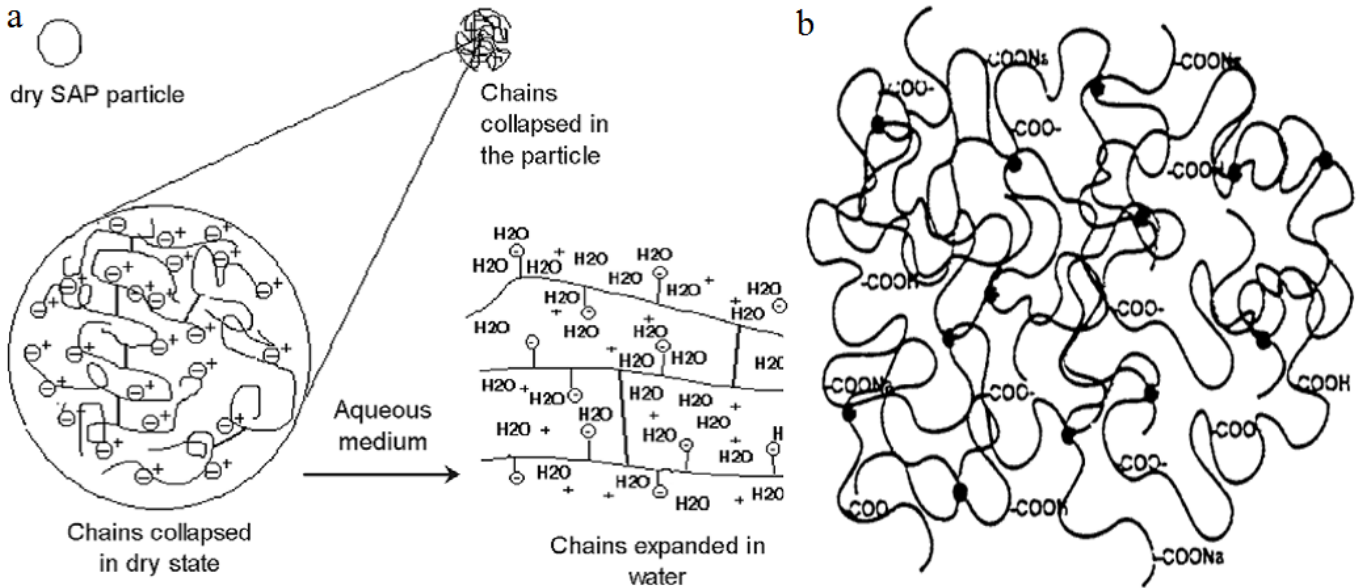


Figure 2.1 Schematic presentation of (a) SAP chains before and after swelling [12] and (b) sodium polyacrylate networks [22]

One of the SAPs with most commercial applications is polyacrylate partially neutralized with sodium hydroxide (NaOH). Sodium atoms in the centre of the molecule are bonded to carbon chains of acrylate. When the polymer comes into contact with water, the concentration of water outside the polymer is higher than that inside it, which draws the water molecules into the network by osmotic pressure formed by the sodium neutralization of the polymer backbone. Due to the cross-linkages between molecules, the polymer chains cannot straighten and, as a result, the particles expand into the network, as shown in Figure 2.1(b) [22]. This expansion continues until the concentration of water is equal within and outside the polymer.

## 2.2 How does WSR work?

WSR can swell in three dimensions and the swelling rate and capacity are proportional to the contact surface area. Generally, the two main forces for the polymer swelling mechanism are the driving force of the solvent into the polymer network and the resistance of the polymer network to expansion. In a thermodynamically balanced state, these two forces should be equal [23]. For WSR, SAP particles have an interaction with water molecules via hydrogen bonding, which is one of the

main driving forces for chains absorbing the water molecules. The water is drawn into the rubber network to be absorbed by SAPs, however, because of the crosslinks of the elastomer chains, dispersion of the water is limited and the absorption ability of SAP also been confined, thus a resistance to expansion develops. This energy disparity manifests itself in an effort to achieve an energy balance by creating a diffusion gradient between the elastomer and the fluid around it, resulting in equilibrium [13, 24]. Figure 2.2 shows the schematic drawing of water swelling mechanism in WSRs. SAP particles inside the cross-linked chains of rubbers (red dots) accelerate the water penetrating into the rubber chains and become bigger and bigger with time increasing.

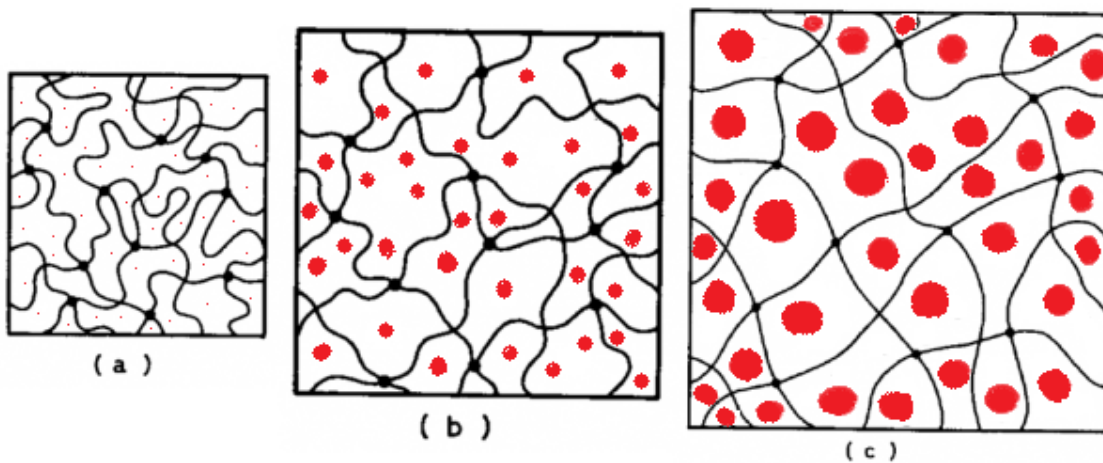


Figure 2.2 Schematic illustration of swelling mechanism of WSR (a) SAP particles (red dots) between cross-linked chains of rubbers, (b) water molecules penetrate to the chains, causing to increase the volume of SAP, and (c) the network of WSR is extensively swollen

When SAP is introduced into a rubber matrix, the degree and rate of swelling of the rubber increase. However, prolonged contact with water causes SAPs migrate from the rubber into the water, so the swellability is ultimately lost, the strength is decreased and the water is polluted. This migration may be caused by high interfacial tension between phases of immiscible polymer blends that lead to coarse and unstable morphology of WSR, narrow interfaces and poor physical and chemical interactions between the phase boundaries. The amount of SAP added into the rubber can

notably affect the strength of the final product. Thus, to prevent reducing the strength of the product, more cross-linking is needed in the remaining elastomer, but on the other hand, a higher cross-link density makes the WSR more rigid and it resists swelling. It is a very important, therefore, to find the right balance between rubber and SAP such that the product has excellent water-absorption property as well as desirable mechanical properties.

### **2.3 Applications and markets**

WSRs have created a wide spectrum of applications which makes them effectively unique for use in various forms by particular major industries. They can be utilized in oil field applications as well as mining and civil engineering, for caulking, sealing of gaps in construction works, cold joints and working joints in concrete, in sewer joints, against slurry walls and in sheet piling especially with irregular wellbore shapes such as poor hole geometry and corroded casing, for sealing downholes, preventing water leakage from pipe or block connections, preservation of airtightness in machinery and apparatus, isolation of open and cased holes, in underground installations such as culverts, subways and sub-sea tunnels, impounding reservoirs, metros and retaining dams. One of the advantages of using WSR is that they are re-usable. As an example, for sealing application, in cold seasons, they can absorb the humidity of environments and swell and fill the gaps. However, in warm seasons, they can return to their original size and again swell in cold weather for next time. The most commercialized elastomers currently used are natural rubber (NR), natural butadiene rubber (NBR), ethylene propylene diene monomer rubber (EPDM), styrene-butadiene rubber (SBR) and Chloroprene Rubber (CR) [13, 25-29]. Many companies currently use WSR simultaneously as both elastic sealing and water blocking such as Rigzone, Rongwei Rubber, Hebei Kailong Guyite Rubber, Bekina Compounds, Zaoqiang Dacheng Rubber, Qinghe Xinao Rubber Seal and Martins Rubber. In terms of global marketing, WSRs are currently used in all over the world. However, the regions that have been making the most use of WSR are Africa, Asia (Central and Southern and the Middle East), Europe and North and Latin America.

Recently, Tendeka company, developed a specific strengthening component to reach a significantly improvements of performance for WSR in saline solutions at low temperatures. By optimisation of the conditions of swelling test, they successfully characterized WSR to isolate over 10,000 frac stages to date [30]. Similarly, the Halliburton Company currently uses elastomers that can swell when exposed to hydrocarbon products, upon exposure to water or a hybrid of oil and water in a single compound. Their products are made by bonding elastomer systems onto oilfield tubulars, with metal end rings installed on each end of the rubber element. The end rings assist in increasing the differential pressure capability and guide the packer when it is run into the hole, They are also can be used for isolating the unwanted zones and resulted in a huge decrease in water cut from 25% to 0.3% [31]. In heavy oil wells, WSR can be installed which use steam to heat the reservoir, causing oil to flow. The high-temperature water swellable packer currently has an upper operational limit of 575°F (302°C) [32]. The most common types of elastomers were using in this field includes NBR, Hydrogenated Nitrile Butadiene Rubber (HNBR), NBR/polyvinyl chloride (PVC), acrylic rubber, co-polymer fluorocarbon (FKM) and terpolymer FKM [33].

## **2.4 Synthesis and manufacturing process**

The properties of WSR depend on two structural parameters: sufficient interfacial tension to create a small phase for dispersing the ingredients uniformly, and strong interface adhesion to assimilate stresses and strains without any disruption of the established morphology [34, 35]. These criteria can be met in different applicable ways such as by increasing the interfacial area by modifying one or two phases or changing the mixing parameters, to transfer applied stress effectively between phases. Blending techniques have been used successfully for the past decades in blend systems to form homogeneous WSRs. Based on the application of WSR, the cost of final product and the environmental condition for using these kind of composites, the processing method should be properly selected. For example, for natural rubber (NR) due to the need of high shear rate to mix the ingredients, the most common process is using 2-roll mill. However, for RTV rubbers

such as silicon rubbers, casting or using internal mixer is more preferable [2, 4]. Manufacturing methods can be classified in two major groups, physical and chemical, as detailed in the following and the brief information about advantages and disadvantages of each method are shown in Table 2.1.

#### **2.4.1 Physical methods**

Mechanical dispersion is one of the most common methods for preparing WSR [3]. For example, internal mixing, Banbury, and two-roll milling are batch mixers. Mixing with an extruder in continuous mixing is a common method for dispersing SAP (powder or resin) into the rubber. A vulcanizing agent and a vulcanization accelerator are mixed during the mixing procedure and other ingredients such as filler, plasticizer, antioxidant or colorants may be incorporated. As in the conventional method, the mixture is then heated until it becomes fully vulcanized, after which it is hot pressed by a compression moulding machine in different moulds, depending on its intended application, to form WSR [5].

#### **2.4.2 Chemical methods**

Without the assistance of chemicals, physical methods cannot provide sufficient adhesion between ingredients due to the marked differences in polarity between rubber and SAP. Therefore, chemical blending techniques have been used to overcome this problem. Using chemical modifications such as interpenetrating polymer network (IPN) technology, grafting, and compatibilizer have been found effective for improving the properties of the final WSR.

### 2.4.2.1 IPN technology

IPNs are defined as combinations of two or more networks from polymeric components, with at least one of the polymers being polymerized and/or cross-linked immediately in the presence of the other polymer(s). The networks interpenetrate each other without any chemical bonds. In synthesizing IPNs, two methods of cross-linking are normally used: sequential and simultaneous, as shown in Figure 2.3 [36]. In sequential cross-linking, an initial mixture consisting of monomer, cross-linking agent and catalyst/initiator is polymerized to form a network, a second combination of monomer and cross-linking agent is then added to that network. Causing the first network to swell, the second network is polymerized within the first network and an IPN will be formed. Reactive polymer chains with initiator or catalyst can also be used instead of monomers to synthesize the networks.

In simultaneous IPN, the polymerizing of two networks is done in a single step. Different monomers or different polymer chains with appropriate cross-linking agents are polymerized together. The advantage of this process is that the two components are cross-linked by reactions and will not interfere with one another [37], such as when a condensation reaction occurs polymerizing one network while the other network is formed by a free radical reaction. Figure 2.4 shows a schematic mechanism of IPNs. This new technology has become widespread, being used in a variety of materials with different purposes such as sheet-moulding compounds (SMCs), membranes, ion-exchange resins, sound damping, dental fillings, artificial joints, tough rubber and plastic materials, and also WSR. It should be noted that IPN can still be considered an expensive technology requiring professional experts and it highly evolves chemical wastes.

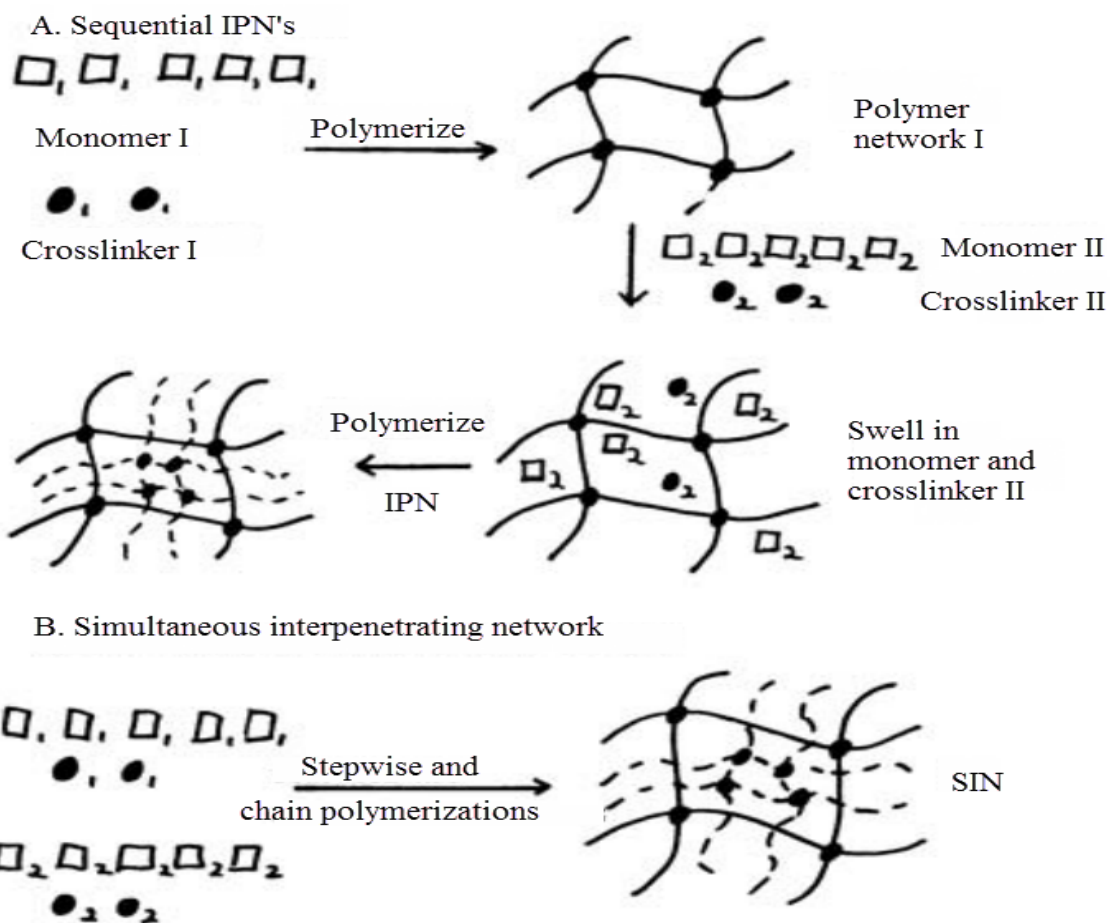


Figure 2.3 Two synthetic methods for preparing interpenetrating polymer networks. A, sequential IPNs, and B, simultaneous IPNs [36]

One of the practical ways to prepare a high performance nanocomposite is using nanoparticles into polymer matrix by introducing simultaneous interpenetrating polymer network. For example, simultaneous IPN is developed for polyimide matrix by using PI/POSS with lower dielectric constant. Enhanced in glass transition temperatures and uniformly embedding of POSS particles with sizes of approximately 50-60 nm of into polyimide matrices shown by SEM [39]. In similar study, the graft-mode of simultaneous IPN method were used to obtain the controlled domains on a nanometre scale between two phases [40]. This method is one of the potential ways to fabricate WSRs with multi-functionalities introduced by nanoparticles. There are two structure for IPN networks: open cell and closed cell. Open cell structure is softer and less dense with air pockets

within the cell structure. Closed cell structure differs in that its cell structure is closed and packed tightly together making it much denser and hard to the touch. Because it is so rigid, closed cell can actually improve the structural stability. Based on application both methods can be used, however, in case of durability (e. g. using WSR in harsh environments), closed cell is more preferable.

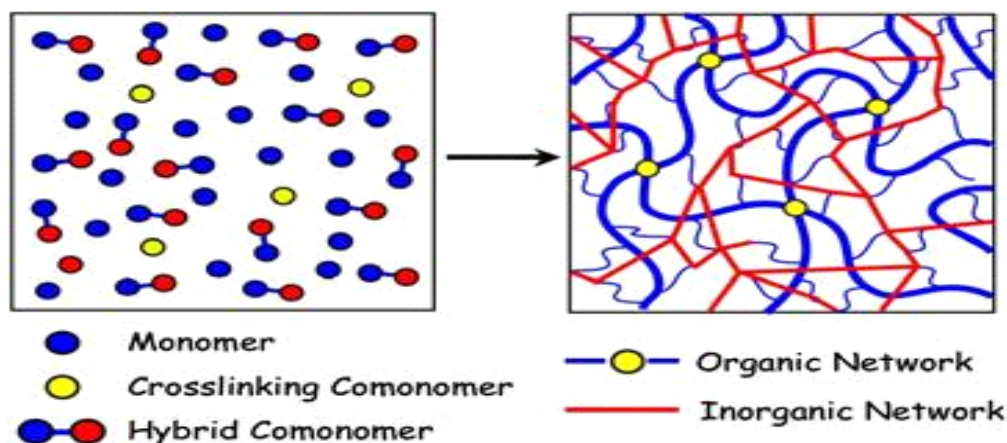


Figure 2.4 Schematic mechanism of interpenetrating polymer networks [38]

### 2.4.2.2 Compatibilizing and grafting

Most polymer blends are immiscible with each other and have inadequate properties for most end uses. Suitable functional additives called compatibilizers have been employed to improve the miscibility of polymers. Compatibilizers can be either block or graft copolymers which include segments of similar structure or solubility parameters to the polymers being mixed (typically at 5-7 wt %). Compatibilizers are used for verification of polymers such as polymer blends, alloys, melts and solutions [41]. The general principles of compatibilization are reduction the interfacial tension between two polymers and finer dispersion to stabilize the morphology against high stresses during the formation and to increase adhesion between the phases [42]. Recently, we report the compatibilizer (aminopropyltriethoxysilane) and neutralizer (sodium hydroxide) effects on the conventional poly (acrylic acid) (PAA)/ poly (dimethylsiloxane) water swellable rubbers and find

that the water swelling ability and durability of the WSR increased by virtue of the synergistic effects of compatibilizer and neutralizer [43].

Grafting is one of the prime techniques for polymer modification which combine a variety of functional components in a single material. Chemical and radiation techniques are the most applicable pathways for performing grafting reactions. Chemical routes are classified in three groups: (1) Redox reaction in which by using redox reagents, radicals can be generated to form a polymer and grafting reaction occurs, (2) Living radical formation, which avoids the chain termination step either by increasing the rate of initiation without changing the rate of propagation or by eliminating chain termination and transfer reactions. Therefore, polymer chains grow in a constant rate with similar chain lengths which provides polymers capable to grow whenever an additional monomer is supplied, (3) Enzymatic technique that expresses the graft reactions can be featured with assistance of enzymes [44]. However, both compatibilizing and grafting methods are not cost effective which limits their usage in large scale.

Table 2.1 advantages and disadvantages of physical and chemical methods

<b>Method</b>	<b>Advantages</b>	<b>Disadvantages</b>
Physical methods	<ul style="list-style-type: none"> <li>• continuous mixing</li> <li>• Easy to process</li> <li>• Cost effective</li> </ul>	<ul style="list-style-type: none"> <li>• Insufficient dispersion</li> <li>• Time consuming</li> </ul>
Chemical methods	<ul style="list-style-type: none"> <li>• Relatively Fast method</li> <li>• Improving the miscibility of polymer blends</li> <li>• Feasible for various kinds of Polymers</li> </ul>	<ul style="list-style-type: none"> <li>• Expensive</li> <li>• Evolves chemical wastes</li> </ul>

## **2.5. Properties of WSR composites**

Depending on different factors, the properties of WSR can be changed. The properties most often investigated for such materials are water swellability, water expansion rate, mechanical properties (e.g. tensile and impact results), and morphological characterization of composites.

### **2.5.1 Effect of mechanical mixing**

Processing techniques and mixing parameters can affect the swellability, phase morphology, distribution and dispersion of SAP into rubber and influence the mechanical properties of the resultant WSR composites. A comprehensive summary of processing methods for different kinds of composites of WSRs which have been successfully produced is listed in Table 2.2. In mechanical mixing, by varying the mixing time, speed and temperature, the properties of WSR composites can be optimised. For instance, Zhang *et al.* reported that if the size of SAP grains is within the range of 74-840  $\mu\text{m}$  the dispersion is not homogeneous. After the resultant WSR was immersed in water the SAPs easily dropped out of the rubber matrix. They suggested that fine SAP powder below 20  $\mu\text{m}$  gave better dispersion [5]. This can be achieved by increasing the high shear rate during the mixing process. Figure 2.5 illustrates the importance of choosing an appropriate mechanical method for the dispersion of SAP into the rubber, with comparison images of samples prepared by (a) Brabender and (b) two-roll mill.

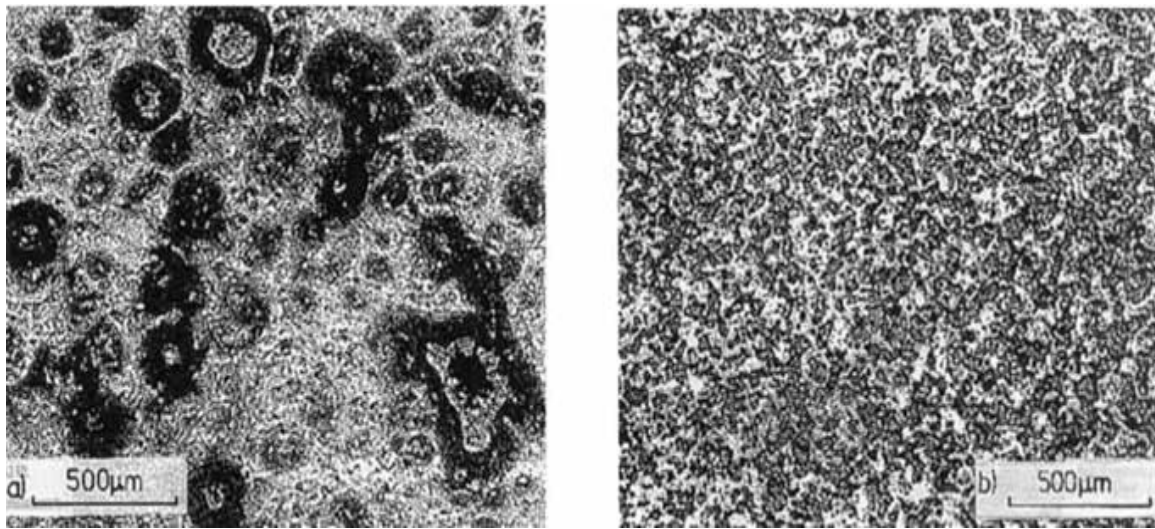


Figure 2.5 Micrographs of films of SAP/rubber in ratio 30/100 (a) dispersion from the mixing chamber of a Brabender and (b) dispersion from a two-roll mill [46]

Table 2.2 Summary of WSR composites with their corresponding manufacturing methods

<b>Polymer</b>	<b>Other substance</b>	<b>Method</b>	<b>Ref</b>
Chlorohydrin rubber (CHR)	PVA-g-PBA (compatibilizer); Cross-linked polyacrylate (SAP)	Grafting	5
CHR	PVA-g-PBA (compatibilizer) Polyethylene glycol (PEG) Precipitated silica (PSA)	Grafting	7
CHR	Precipitated silica reinforcing filler Cross-linked sodium polyacrylate (CSP); Poly(ethylene oxide) (PEO)	Grafting	8
CHR	PVA-g-PBA and cross-linked polyacrylate (CPA)	Grafting	10
Chlorobutadiene rubber (CR)	CSP; reactive clay; P(AA-co-BA)/CR	IPN	3
Polydimethylsiloxane (PDMS)	PAA	IPN	45
Natural rubber (NR)	Sodium polyacrylate	Internal mixer	9
CR	CSP; PEO, PSA	Banbury mixer	1
NR	PEO-b-PBA; CSP; PSA	Open mill	4
NR	PEO; Trimethylpropane trimethacrylate	Open mill	2
NR	SAP; carbon black (reinforcing agent); TBBS (accelerator)	Open mill	27
NR; Chlorobutyl rubber; Ethylene propylene diene (EPDM)	Polyacrylamide (PAM)	Open mill	46
Styrene Butadiene Rubber (SBR)	Cellulose Nanocrystals (CNC)	Solution Casting	47
Styrene Butadiene Rubber (SBR)	Cellulose Nanocrystals (CNC)	Compression molding	47

### 2.5.2 Effect of IPN networks

The morphology of immiscible polymer blends is usually unstable due to high interfacial tension between the phases, which leads to poor physical and chemical interactions across the phase boundaries. IPNs can control the phase morphology of immiscible polymer blends (like interfacial agents) by sharing load between the components without transferring stress across the phase boundaries [3]. This new technology has opened a wide range of variations in the preparation of WSR which can customize the properties to the specific needs of many different applications. Yoo *et al.* prepared PDMS interpenetrating networks of two different molecular weight PDMS, and the swelling, mechanical property and toughness results proved that the load was effectively transferred between the networks [48]. It has been proposed that selected combinations of two networks could provide synergistic performance which could maximize useful properties and minimize unwanted properties [49]. As an example, Jalili *et al.* proved that the addition of 20 wt% PAA to PDMS with IPNs technology produced the dispersed phase as fine particles, resulting in synergistic effects in the new composites. Their observations are explained with visible morphological changes in scanning electron microscope (SEM) results, and with changes in swelling properties [45].

Figure 2.6 shows the variation of swelling with time for the IPNs with different PAA concentrations. This plot exhibits two distinct slopes, with a higher slope at concentrations of PAA greater than 25%. Abbasi *et al.* also observed that in the case of IPNs in the solid state, phase inversion occurred at PAA concentrations of about 60 wt%, but in the swollen state, PAA acted together with the absorbed water as a single phase [45].

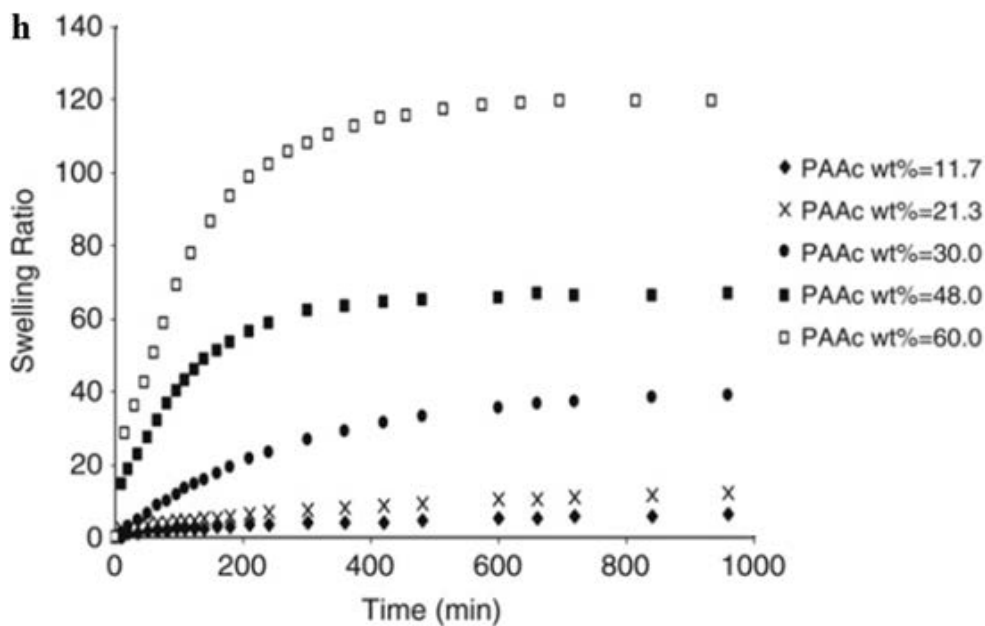
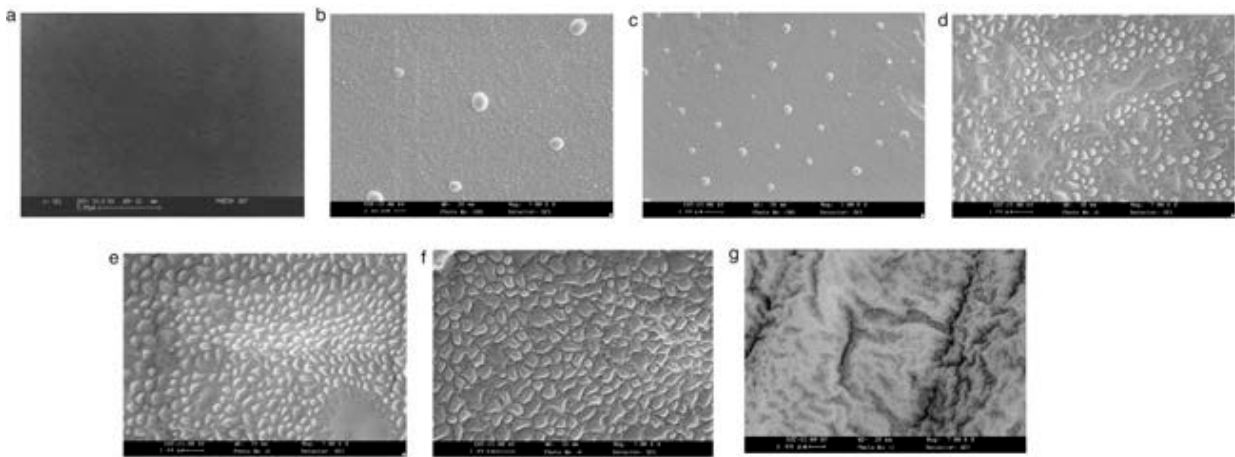


Figure 2.6 SEM micrographs obtained from cross-sections of (a) (magnification  $\times 7000$ ) unmodified PDMS, and PDMS/PAA IPNs having a PAA contents of (b) (magnification  $\times 7000$ ) 20 wt%, (c) (magnification  $\times 3000$ ) 20 wt%, (d) (magnification  $\times 7000$ ) 30 wt%, (e) (magnification  $\times 7000$ ) 40 wt%, (f) (magnification  $\times 7000$ ) 50 wt%, (g) (magnification  $\times 7000$ ) 60 wt% and (h) swelling behaviour of PDMS/PAA IPNs [45]

The main disadvantage of IPN systems is that, sometimes the polymers interpenetrate to such an extent and the swelling of SAPs from the rubber matrix will face some difficulties. In addition due to the lack of an effective interface between non-covalent and covalent systems, IPN method cannot be an effective method.

### 2.5.3 Effect of fillers

Fillers are commonly used to reinforce composites by improving properties such as hardness, tensile strength, tear resistance and abrasion resistance. Compared to other techniques currently used to enhance the efficiency of WSR, the use of reinforcement fillers is one of the most convenient ways to achieve this goal. In WSR, a common reinforcement filler is silica. It is highly polar due to the existence of numerous silanol groups on its surface which can improve not only the mechanical properties but also the water-absorbent properties of the WSR [8].

Zhang and co-workers found that when crosslinked polyacrylate (CPA) grains were dispersed into chlorohydrin rubber (CHR), the SAP grains were isolated from others by a rubber phase and could not give full play to the water-absorbing ability. However, with the addition of poly(ethylene glycol) (PEG) into the system, some water-absorbing routes between water-absorbent grains were built. In other words, the PEG created a bridge between SAPs to transfer the water among them and make the composite swell. By increasing the PEG content, the number of water-absorbing routes within rubber was increased and the water-absorption rate was also increased [7].

The amount of filler plays an important role in compatibilizing WSR [4-6]. For example, Wang et al. found that the optimum range of precipitated silica to improve the water-absorbent properties of WSR (here CR+CSP) is 10-50 phr. The more silica provides more number of elastically effective entanglement points and higher the crosslinking density and the crosslinking restriction force, resulting in a lower degree of swelling [1]. Therefore, with the appropriate amount, the water-absorption properties and the mechanical properties of composites both increase, but if more compatibilizer is added, those properties decrease due to a decrement in the size of the cross-linked networks, limiting the expansion of WSR and its absorption of water and also affecting tensile properties such as elongation at break and strength at break. Table 2.3 shows the use of different reinforcement fillers as compatibilizers and the use of coupling agents for improving specific properties of samples.

Table 2.3 Effect of different kinds of fillers on water swelling ratio and mechanical properties of WSRs

WSR	Fillers	WS (%)	TS and EB	Ref
CR + CSP	PEO 5–30 phr;	550-700		1
	Precipitated silica 10–50 phr	800-500		
NR	PEO 10 phr; trimethylopropane trimethacrylate:2 phr	200(14 days)	TS <sup>a</sup> = 11.1±0.2 EB <sup>a</sup> =642 ± 6 TS <sup>b</sup> =8.0 ± 0.1 EB <sup>b</sup> =702 ± 6	2
CR + CSP	Reactive clay 30 phr; 30% wt P(AA-co-BA)	350	TS <sup>a</sup> =7.7  EB <sup>a</sup> = 1530 TS <sup>b</sup> =2.8 EB <sup>b</sup> =1730	3
NR + CSP	PEO-b-PBA(0.36, 5phr) precipitated silica PEG (10–20 phr)	1200 (10 days)	–	4
CHR + SAP	PVA-g-PBA 10 phr PEG 40 phr PSA 40 phr	568 – –	–	5
CHR + SAP	PVA-g-PBA: 10 phr; (PEG) 40 phr; precipitated silica 40 phr	– 474 545	–	7
CHR + SAP	Precipitated silica 15-50 phr; (PEO) 10 phr	–	TS <sup>a</sup> = 9.0 EB <sup>a</sup> =1070 TS <sup>b</sup> =0.55 EB <sup>b</sup> =350	8
CHR + cross-linked CPA	PVA-g-PBA(%340.4 grafting ): 5 phr	5.5 (for 80 hrs)	TS <sup>a</sup> = 3.09 EB <sup>a</sup> =136.27 TS <sup>b</sup> =0.31 EB <sup>b</sup> =92.48	10
NR + SAP	Carbon black: 10 phr ZnO: 3 phr S: 0.5 phr TBBS: 1 phr	500 (40 phr SAP for 91 days )	TS <sup>b</sup> ≈3.5 EB <sup>b</sup> ≈580	27
PDMS+SAP	Aminopropyltriethoxysilane: 0.036 g;  sodium hydroxide: 5 g	250 (40 phr SAP for 1000 hrs)	TS <sup>a</sup> = 2.29 EB <sup>a</sup> = 171.5  TS <sup>b</sup> = 0.09 EB <sup>b</sup> = 66.3	43

**Note: Tensile Strength (TS, MPa) and Elongation at break (EB, %) before (a) and after (b) swelling**

#### **2.5.4 Effect of grafting**

Graft copolymerization can make the blend system more compatible by reducing the interfacial tension between two phases and increasing the cohesive force between them. Zhang *et al.* showed that the properties of polyvinyl alcohol (PVA) were greatly improved by grafting poly (butyl acrylate) (PBA) with good elasticity due to its long soft side-chains and relatively low glass-transition temperature (-49 °C) onto PVA. At the same time, the branched chains were hydrophobic, and were used as backbone. PBA can serve between hydrophobic rubber and hydrophilic PVA as an amphiphilic graft copolymer [5]. As a result, the water-absorption and water swelling abilities are enhanced. However, when a large amount of graft polymer is added into the mixture, the branched chains of PBA agglomerate by themselves and form a thin layer of continuous paste which can obstruct the passage of water molecules through the rubber to reach the SAPs [6]. Thus the amount of grafted polymer should be optimised to ensure better properties. In a similar experiment, Zhang *et al.* found that the incorporation of PVA-g-PBA into chlorohydrin rubber significantly enhanced not only the water swelling behaviour but also the mechanical properties of WSR before and after water swelling. The blend consisted of 5 phr PVA-g-PBA with a grafting percentage of 340.4%, and the tensile strength increased from 1.87 to 3.09 MPa and 0.27 to 0.31 before and after water swelling, respectively [10].

#### **2.5.5 Other methods**

For fabrication of WSR, some other methods which are not as common as above mentioned techniques can be used. As an example, aqueous suspensions of absorbent polymer are mixed with rubber to make a homogenous solution. The resulting mixtures are then cast into the glass mould and placed into oven till solvent is completely evaporated. Furthermore, the resulting WSR films can be compressed with optimized conditions to obtain non-shrinking, free-standing films for investigating properties [47]. All the mentioned methods have their own advantages and

disadvantages. Based on type of rubber, fillers, condition of experiment and the specified applications, the proper technique should be picked.

## **2.6 Future of WSR**

The main goal of processing WSR is to achieve a high swelling rate in every contact with water without any drop-out from the rubber, with considerable mechanical strength. One of the main disadvantages of common WSRs is that the costs involved in their processing for specific applications are quite high. Complex technologies such as the use of IPNs to improve the properties can increase the cost of the final product. Therefore, utilization of such technologies on a large scale is not economical. Moreover, they are not generally reusable, and their disposal after use can impact on the environment. Based on the research to date, one of the best ways to enhance the swelling kinetics of WSR is the use of reinforcement fillers which prevent migration of SAP particles from the rubber to the water phase.

As we have discussed, fillers can modify composite properties such as swelling behaviour, strength, impact and solvent resistance. However, fillers with low aspect ratios cannot create a major improvement from the properties of unfilled WSR. When the aspect ratio between the longest and the shortest dimension of the filler is greater than a certain amount, the filler (known as fiber) significantly affects the properties of the composite. Electrospinning enables the manufacture of nanofibers in the form of sheet or membrane-type products with virtually any functional polymer, using known and established formulations. Meanwhile, considering their length, fibers can act as routes for the transfer of water between isolated SAP particles within the rubber matrix, increasing the swellability of WSR. Moreover, with the provision of good bonding between fiber and polymer components (both rubber and SAP), strength in the fiber direction is significantly increased. By

bonding to SAP particles, fibers also prevent the migration of SAP from the rubber, with the result that better water swellability can be achieved.

Recently, we reported the improved water absorption property and stability of WSR obtained by using electrospun multi-scaled hybrid fiber mats of crosslinked PAA as water channels, as shown in Figure 2.7(a) which we are going to discuss about it in chapter 4. Electrospinning of various superabsorbent fibers with hyperbranched polymer (HB) and/or graphene oxide (GO) having nano- and submicro-diameter fiber sizes was performed. With hybrid fillers (HB and GO) added into the PAA, spun fiber mats showed the increased water swelling ability due to the presence of spider web-like multi-scale structures and enhanced specific surface areas. The spun fiber mats were added into conventional WSR and the resultant rubber composites showed enhanced water swelling ability. The electrospun fibers acted as internal multi-scale water channels to bridge isolated PAA particles wrapped in hydrophobic rubber together and link the internal PAA with the composite surface to enhance the short- and long-term water swelling ability of rubber composites [50].

On the other hand, further potential for cost-effective seals using simple methods and environmentally friendly processes can arise from innovations in manufacture, especially 3D printing technology and electrospinning methods. Complex technologies such as the use of IPNs to improve printing technology and electrospinning methods are now being used. One of the potential ways to improve the characteristics and performance of WSR is electrospinning of rubber and SAP at the same time, as shown in the probable schematic in Figures 2.7(b) and (c) with SAP and rubber [51]. In this technique, different types of polymers are electrospinning either multilayering (Figure 2.7(b) or simultaneously together mixed (Figure 2.7(c)) to make a mixed fiber mesh. In simultaneously mixing process, two different polymers are electrospun from different syringes at

the same time on the same target collector. In the multilayering system, after the first polymer is electrospun, the second polymer is sequentially electrospinning on the same collector to form a hierarchically ordered structure of different kinds of polymer (here SAP/rubber).

The other promising technique is 3D printing (layer-by layer) rubber and SAP together, inspired by ideas from Compton and Lewis [52] and Tumbleston *et al.* [53] regarding lightweight cellular composites and continuous liquid interface production by 3D printing. In order to achieve controlled composition, geometric shape, function, and complexity 3D printing method is much effective rather than traditional manufacturing procedures. Moreover, in order to generate composites (especially immiscible blends such as rubber and SAP) with controlled structure and adequate physical properties, advanced fabrication techniques are being employed. Hybrid of 3D printing and electrospinning is a good example of such a technique [54, 55]. This new method can be further considered to simplify the fabrication of novel WSR composites with value-added performance by incorporating of 3D printing with electrospinning process, as shown in Figure 2.7(d).

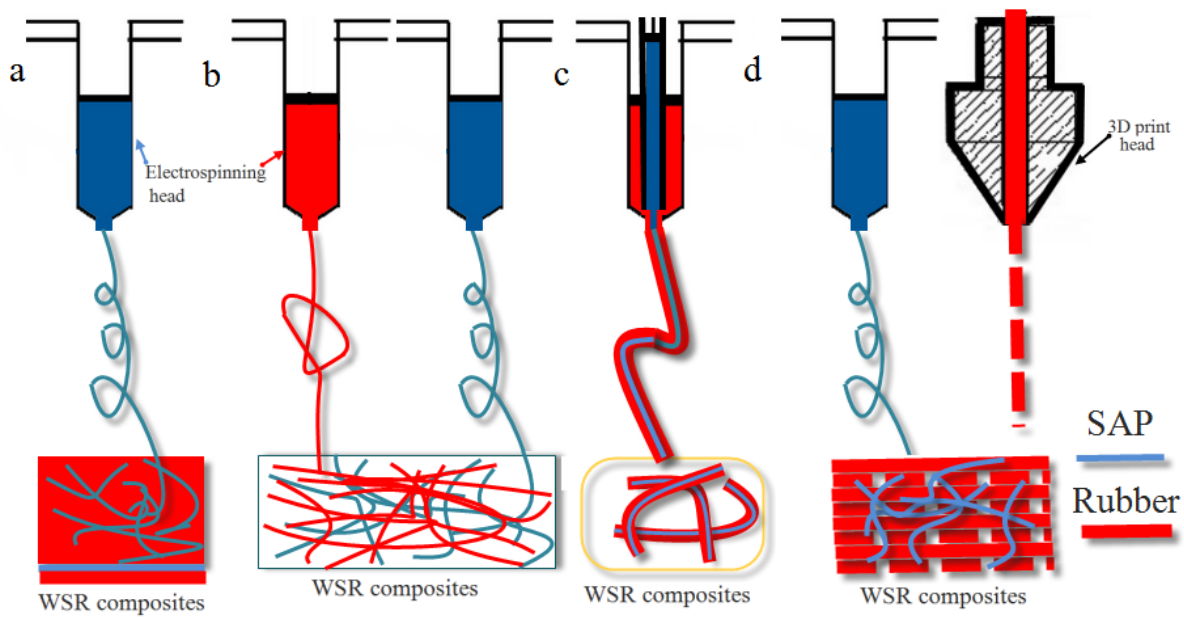


Figure 2.7 Schematic drawings of (a) electrospinning SAP fibers/mats to rubber layers, (b) multi-layering electrospinning of SAP and rubber, (c) co-electrospinning of SAP and rubber and (d) hybrid 3D printing with electrospinning of rubber and SAP to form WSR composites

## 2.7 Conclusions

The use of WSR has been investigated in great depth by many researchers during recent decades. The methods (physical and chemical) used for processing have a huge effect on the properties of WSR. Indeed, modifications of this new kind of polymer constitute another direction of development in this area, involving features such as reinforcement fillers, compatibilizers or coupling agents, with the aim of imparting specific desirable properties. This approach to tailor-made materials has been successfully applied to synthetic and natural rubbers. Interfacial interaction promotes adhesion of hydrophobic rubber to hydrophilic substrate and, as a result, great increments in water-absorption ratio have been observed relative to unmodified WSRs. We expect that, with the introduction of hydrophilic fibers into the WSR as internal water channels as well as reinforcement, greater absorption properties in combination with considerable mechanical strength should be achieved. With the further development of electrospinning and 3D printing technologies,

WSR composites with desirable properties can be fabricated in a cost-effective and environmentally friendly manner.

In next chapter the first step of modification of WSR composite by using a compatibilizer, and neutralising of PAA and their effects on swelling ratio and also mechanical properties will be investigated.

## 2.8 References

1. Wang, G., Li, M. and Chen, X., 1998. Preparation and water-absorbent properties of a water-swellaable rubber. *Journal of applied polymer science*, 68(8), pp.1219-1225.
2. Nakason, C., Nakaramontri, Y., Kaesaman, A., Kangwansukpamonkon, W. and Kiatkamjornwong, S., 2013. Synthesis and characterization of water swellaable natural rubber vulcanizates. *European Polymer Journal*, 49(5), pp.1098-1110.
3. Liu, C., Ding, J., Zhou, L. and Chen, S., 2006. Mechanical properties, water-swelling behavior, and morphology of water-swellaable rubber prepared using crosslinked sodium polyacrylate. *Journal of applied polymer science*, 102(2), pp.1489-1496.
4. Wang, C., Zhang, G., Dong, Y., Chen, X. and Tan, H., 2002. Study on a water-swellaable rubber compatibilized by amphiphilic block polymer based on poly (ethylene oxide) and poly (butyl acrylate). *Journal of applied polymer science*, 86(12), pp.3120-3125.
5. Zhang, Z., Zhang, G., Li, D., Liu, Z. and Chen, X., 1999. Chlorohydrin water-swellaable rubber compatibilized by an amphiphilic graft copolymer. II. Effects of PVA-g-PBA and CPA on water-swelling behaviors. *Journal of applied polymer science*, 74(13), pp.3145-3152.

6. Zhang, G., Zhang, Z., Xie, F., Hu, X., Luo, X. and Chen, X., 2000. Chlorohydrin water swellable rubber compatibilized by an amphiphilic graft copolymer. I. Synthesis and characterization of compatibilizer PVA-g-PBA. *Journal of applied polymer science*, 75(8), pp.977-986.
7. Zhang, Z., Zhang, G., Wang, C., Liu, D., Liu, Z. and Chen, X., 2001. Chlorohydrin water-swellable rubber compatibilized by an amphiphilic graft copolymer. III. Effects of PEG and PSA on water-swelling behavior. *Journal of applied polymer science*, 79(14), pp.2509-2516.
8. Wang, G., Li, M. and Chen, X., 1999. Effects of fillers on mechanical properties of a water-swellable rubber. *Journal of applied polymer science*, 72(4), pp.577-584.
9. Park, J.H. and Kim, D., 2001. Preparation and characterization of water-swellable natural rubbers. *Journal of applied polymer science*, 80(1), pp.115-121.
10. Zhang, Z., Zhang, G., Zhang, Y., Wang, Z., Yu, D., Hu, X., Hu, C. and Tang, X., 2004. Mechanical properties, water swelling behavior, and morphology of swellable rubber compatibilized by PVA-g-PBA. *Polymer Engineering & Science*, 44(1), pp.72-78.
11. Buchholz, F.L. and Graham, A.T., 1998. Modern superabsorbent polymer technology. *John! Wiley & Sons, Inc*, 605 Third Ave, New York, NY 10016, USA, 1998. 279.
12. Zohuriaan-Mehr, M.J. and Kabiri, K., 2008. Superabsorbent polymer materials: a review. *Iranian polymer journal*, 17(6), p.451.
13. Seyger, R., Resink, S., Harms, H. and Hibberd, R., 2013. The future of swelling elastomers: An elastomer manufacturer's view of swelling elastomer developments and market trends. *The Journal of Engineering Research [TJER]*, 10(1), pp.50-64.

14. Fanta, G.F., Burr, R.C., Russell, C.R. and Rist, C.E., 1970. Copolymers of starch and polyacrylonitrile. Influence of granule swelling on copolymer composition under various reaction conditions. *Journal of Macromolecular Science—Chemistry*, 4(2), pp.331-339.
15. Fanta, G.F., Burr, R.C., Doane, W.M. and Russell, C.R., 1978. Absorbent polymers from starch and flour through graft polymerization of acrylonitrile and comonomer mixtures. *Starch-Stärke*, 30(7), pp.237-242.
16. Sakiyama, T., Chu, C.H., Fujii, T. and Yano, T., 1993. Preparation of a polyelectrolyte complex gel from chitosan and  $\kappa$ -carrageenan and its pH-sensitive swelling. *Journal of Applied Polymer Science*, 50(11), pp.2021-2025.
17. Yoshida, M., Asano, M. and Kumakura, M., 1989. A new temperature-sensitive hydrogel with  $\alpha$ -amino acid group as side chain of polymer. *European polymer journal*, 25(12), pp.1197-1202.
18. Shiga, T., Hirose, Y., Okada, A. and Kurauchi, T., 1993. Bending of ionic polymer gel caused by swelling under sinusoidally varying electric fields. *Journal of Applied Polymer Science*, 47(1), pp.113-119.
19. Shiga, T., Hirose, Y., Okada, A. and Kurauchi, T., 1992. Bending of poly (vinyl alcohol)–poly (sodium acrylate) composite hydrogel in electric fields. *Journal of Applied Polymer Science*, 44(2), pp.249-253.
20. Kabiri, K., Omidian, H., Zohuriaan-Mehr, M.J. and Doroudiani, S., 2011. Superabsorbent hydrogel composites and nanocomposites: a review. *Polymer composites*, 32(2), pp.277-289.
21. Yu, Y., De Andrade, L.C.X., Fang, L., Ma, J., Zhang, W. and Tang, Y., 2015. Graphene oxide and hyperbranched polymer-toughened hydrogels with improved absorption properties and durability. *Journal of Materials Science*, 50(9), pp.3457-3466..

22. How do superabsorbent polymers work? Retrieved 10 April 2015, from M2 Polymer Technologies, Inc.: [http:// www.m2polymer.com/html/superabsorbent\\_polymers.html](http://www.m2polymer.com/html/superabsorbent_polymers.html).
23. Flory, P.J. and Rehner Jr, J., 1943. Statistical mechanics of cross-linked polymer networks I. Rubberlike elasticity. *The Journal of Chemical Physics*, *11*(11), pp.512-520.
24. Treloar, L.R.G., 1975. *The physics of rubber elasticity*. Oxford University Press, USA.
25. Choi, S. and Justice, L.J., Zeon Chemicals LP, 2012. *Water swellable rubber composition having stable swelling property at high temperatures*. U.S. Patent Application 13/447,611.
26. Korte, J.R., Thurston, J.J. and Goodson, J.E., Baker Hughes Incorporated, 2012. *Water swelling rubber compound for use in reactive packers and other downhole tools*. U.S. Patent 8,181,708.
27. Saijun, D., Nakason, C., Kaesaman, A. and Klinpituksa, P., 2009. Water absorption and mechanical properties of water-swellable natural rubber. *Sonklanakarin Journal of Science and Technology*, *31*(5), p.561.
28. Pal, K., Rajasekar, R., Kang, D.J., Zhang, Z.X., Pal, S.K., Das, C.K. and Kim, J.K., 2010. Effect of fillers on natural rubber/high styrene rubber blends with nano silica: morphology and wear. *Materials & Design*, *31*(2), pp.677-686.
29. Fiorini, M. and Barbiroli, G., 2000. A global performance index to assess the quality of elastomers. *Polymer testing*, *19*(8), pp.967-973.
30. McKay, E. High performance water swelling elastomers save time and money in the Bakken. Tendeka website. Retrieved 10 April 2015 from <http://tendeka.com/news-and-events/high-performance-water-swelling-elastomers-save-time-and-money-in-the-bakke/>.
31. Akhtar, M., Qamar, S.Z. and Pervez, T., 2012. Swelling elastomer applications in oil and gas industry. *J. Trends Dev. Mach. Assoc. Technol*, *16*(1), pp.71-74.

32. How does a swellable packer work? (n. d.). Retrieved 10 April 2015, from Rigzone: [http://www.rigzone.com/training/insight.asp?insight\\_id=353&c\\_id=24](http://www.rigzone.com/training/insight.asp?insight_id=353&c_id=24).
33. Chai, A.B., Andriyana, A., Verron, E. and Johan, M.R., 2013. Mechanical characteristics of swollen elastomers under cyclic loading. *Materials & Design*, 44, pp.566-572.
34. Favis, B.D., 1990. The effect of processing parameters on the morphology of an immiscible binary blend. *Journal of applied polymer science*, 39(2), pp.285-300.
35. Sundararaj, U. and Macosko, C.W., 1995. Drop breakup and coalescence in polymer blends: the effects of concentration and compatibilization. *Macromolecules*, 28(8), pp.2647-2657.
36. Sperling, L.H. and Hu, R., 2003. Interpenetrating polymer networks. In *Polymer blends handbook* (pp. 417-447). Springer Netherlands.
37. Sperling, L.H. and Mishra, V.B.A.T., 1996. The current status of interpenetrating polymer networks. *Polymers for Advanced Technologies*, 7(4), pp.197-208.
38. Silverstein, M. S. (n. d.). Poly HIPE: Porous polymers synthesized within high internal phase emulsions (HIPE). The Macromolecular Materials Group website. Retrieved from 10 April 2015, from <http://matwww.technion.ac.il/Silverstein/HIPE>.
39. Chen, W.Y., Ho, K.S., Hsieh, T.H., Chang, F.C. and Wang, Y.Z., 2006. Simultaneous Preparation of PI/POSS Semi-IPN Nanocomposites. *Macromolecular rapid communications*, 27(6), pp.452-457.
40. Dongyan, T., Liangsheng, Q., Zheng, J. and Weimin, C., 2002. Preparation, morphology, and thermoelectric property studies of BaTiO<sub>3</sub> superfine fiber/castor oil polyurethane-based IPN nanocomposites. *Journal of applied polymer science*, 84(4), pp.709-715.

41. Gaylord, G. N. In Copolymers, Poly blends, and Composites, 1975. Platzer, N. A. J., Ed., American Chemical Society: Washington, DC, pp.76-84.
42. Utracki, L.A., 2002. Compatibilization of polymer blends. *The Canadian Journal of Chemical Engineering*, 80(6), pp.1008-1016.
43. Dehbari, N., Zhao, J., Peng, R. and Tang, Y., 2015. Neutralisation and compatibilisation effects on novel water-swellaible rubber composites. *Journal of Materials Science*, 50(15), pp.5157-5164.
44. Bhattacharya, A. and Misra, B.N., 2004. Grafting: a versatile means to modify polymers: techniques, factors and applications. *Progress in polymer science*, 29(8), pp.767-814.
45. Jalili, K., Abbasi, F., Oskoe, S.S. and Alinejad, Z., 2009. Relationships between the morphology, swelling and mechanical properties of poly (dimethyl siloxane)/poly (acrylic acid) interpenetrating networks. *Journal of the mechanical behavior of biomedical materials*, 2(5), pp.534-541.
46. Hron, P., Vymazalova, Z. and Lopour, P., 1997. Water-swellaible rubbers containing powdery poly (acrylamide) hydrogel. *Macromolecular Materials and Engineering*, 245(1), pp.203-210.
47. Annamalai, P.K., Dagnon, K.L., Monemian, S., Foster, E.J., Rowan, S.J. and Weder, C., 2014. Water-Responsive Mechanically Adaptive Nanocomposites Based on Styrene-Butadiene Rubber and Cellulose Nanocrystals Processing Matters. *ACS applied materials & interfaces*, 6(2), pp.967-976.
48. Yoo, S.H., Cohen, C. and Hui, C.Y., 2006. Mechanical and swelling properties of PDMS interpenetrating polymer networks. *Polymer*, 47(17), pp.6226-6235.

49. Weber, G.R., 2012. *Interpenetrating polymer network adhesives* (Doctoral dissertation, University of Washington).
50. Zhao, J., Dehbari, N., Han, W., Huang, L. and Tang, Y., 2015. Electrospun multi-scale hybrid nanofiber/net with enhanced water swelling ability in rubber composites. *Materials & Design*, 86, pp.14-21.
51. Elahi, F., Lu, W., Guoping, G. and Khan, F., 2013. Core-shell fibers for biomedical applications—A review. *Bioengineering & Biomedical Science*, 3(1), pp.1-14.
52. Compton, B.G. and Lewis, J.A., 2014. 3D-printing of lightweight cellular composites. *Advanced materials*, 26(34), pp.5930-5935.
53. Tumbleston, J.R., Shirvanyants, D., Ermoshkin, N., Januszewicz, R., Johnson, A.R., Kelly, D., Chen, K., Pinschmidt, R., Rolland, J.P., Ermoshkin, A. and Samulski, E.T., 2015. Continuous liquid interface production of 3D objects. *Science*, 347(6228), pp.1349-1352.
54. Kidoaki, S., Kwon, I.K. and Matsuda, T., 2005. Mesoscopic spatial designs of nano-and microfiber meshes for tissue-engineering matrix and scaffold based on newly devised multilayering and mixing electrospinning techniques. *Biomaterials*, 26(1), pp.37-46.
55. Xu, T., Binder, K.W., Albanna, M.Z., Dice, D., Zhao, W., Yoo, J.J. and Atala, A., 2012. Hybrid printing of mechanically and biologically improved constructs for cartilage tissue engineering applications. *Biofabrication*, 5(1), p.015001.

### **3. [NEUTRALIZATION AND COMPATIBILIZATION EFFECT ON WATER SWELLABLE RUBBER <sup>1]</sup>**

The objective of this chapter is preparation novel WSR followed by the modification of rubber matrix and PAA by using NaOH as a neutralizer and Silane coupling agent as a compatibilizer. The characterization of WSR has been tested by infrared spectroscopic (FTIR) and scanning electron microscopy (SEM) and physical and mechanical properties before and after swelling of all composite have been tested and compared as well.

1. This work has been published in Journal of Materials Science: Nazila Dehbari, Jinchao Zhao, Rengui Peng, and Youhong Tang. "Neutralisation and compatibilization effects on novel water-swelling rubber composites." Journal of Materials Science 50, no. 15 (2015): 5157-5164. DOI: 10.1007/s10853-015-9052-7

### 3.1 Introduction

SAPs have been the subject of much research in recent decades [1]. Due to the presence of a three-dimensional network, SAPs can absorb and retain a large amount of water increasing in volume a hundred- or thousand-fold without dissolving in the water. SAPs are used in a variety of applications such as medicine, sanitary goods, the food industry and agricultural and horticultural applications [1–6]. Despite the capacity of SAPs to absorb large amounts of water, they do not have enough gel strength for certain applications. On the other hand, rubber has inherently good resilience, elasticity and stability but lacks water absorbency. Thus, by mixing SAP and rubber with an optimised ratio, a new material has been introduced and is known as WSR. WSRs possess the general properties of rubber, such as high elasticity, resilience and high toughness, but also they can expand their volume up to 1.5 times the original when in contact with water [7]. Having both water absorbency and stability, WSRs can be widely used in sealing industries [8].

Among the common elastomer matrixes used in the production of WSRs, such as natural rubber, chloroprene rubber and chlorohydrin rubber, silicon rubbers, especially poly (dimethylsiloxane) rubber (PDMS), have more advantages than other elastomers. Its low glass transition temperature ( $-125^{\circ}\text{C}$ ), unique flexibility, very low mechanical loss factor, high gas permeability, high compressibility, usability over a wide temperature range and essentially non-toxic nature [9–11] make PDMS suitable for many varied applications, such as the mechanical interconnection layer between two silicon wafers, ion selective membranes, accelerometers and sensor applications[12–15]. The water-absorbent resins include starch, cellulose, poly (ethylene oxide), poly (acrylic acid) (PAA), poly (vinyl alcohol) and poly (acrylamide). Among these, PAA displays excellent hydrophilicity with a higher degree of absorption and absorption rate than the other water-absorbent resins [7, 16, 17]. Mechanical mixing and chemical grafting are two common methods generally used to prepare WSRs [16]. However, studies [7, 17–19] have shown that SAPs do not disperse well in rubber due to their different polarity, such that the SAP easily separates from

the rubber network over a long-period contact with water. As a result, the swelling property, long-term water retention, repeatability and mechanical properties of the rubber are weakened, and no satisfactory effect can be expected. The present chapter was conducted for the purpose of overcoming the abovementioned problems. Here, WSR was prepared by the blending of PDMS as a rubber matrix, PAA as a superabsorbent resin and sodium hydroxide (NaOH) as a neutraliser. Besides, to improve the interactions between the ingredients, a silane coupling agent served as a compatibilizer in the blend system. The effects of neutralization and compatibilization on various properties of the WSR were investigated as well.

## **3.2 Experiments**

### **3.2.1 Materials and preparation**

PDMS was obtained from Sigma-Aldrich, Australia. The formulation consisted of two parts, part A (a PDMS monomer) and part B (a hardener/curing agent), which were mixed together in a ratio of 1/1. PAA solution (Sigma-Aldrich, Australia) was used as a SAP. NaOH (Sigma-Aldrich, Australia) was used to neutralise PAA, and aminopropyltriethoxysilane was used as a silane coupling agent (KH-550, Sigma-Aldrich, Australia). Different amounts of PAA, NaOH and part A of PDMS in proper order were mixed together continuously until the mixture reached apparent homogeneity. PDMS part B was then added to the mixture for curing. Next, the batch was laid up on a dry and clean glass mould at room temperature for about 4 h. After curing, all WSR films were cut into samples of  $10 \times 50 \times 1$  mm for mechanical testing. Figure 3.1 shows the preparation procedures of the WSR composite samples. A similar process was used to produce WSR with compatibilizer KH 550. It was first added to NaOH and PAA and mixed carefully, and the rest of the experiment was repeated. Table 3.1 provides a summary of the composition of the WSR composites used in this study.



Figure 3.1 Schematic of processing WSR

### 3.3 Characterization

The functional groups of pure rubber (PDMS), pure PAA, modified PAAs and all WSR composites were investigated by a Fourier transform infrared (FTIR) spectrometer (Perkin-Elmer, USA). The number of scans was 32, with a resolution of 4 cm<sup>-1</sup>. The surface morphologies of the various composites of WSR were inspected by scanning electron microscopy (SEM, Philips CM200, Netherlands) at 200 kV. To retain the original morphology of the samples, they were placed in liquid nitrogen for 0.5 h and then were broken down into two pieces and freeze dried overnight. Finally, in order to improve electric conductivity before characterization, the cross-section areas of all samples were sputter coated with gold.

Table 3.1 Composition of prepared WSR composites

Sample	Composition
1	2.5 gr PAA+ 4 gr Rubber+0.5 gr NaOH
2	3 gr PAA+ 4 gr Rubber+0.5 gr NaOH
3	3.5 gr PAA+ 4 gr Rubber+0.5 gr NaOH
4	4 gr PAA+ 4 gr Rubber+0.5 gr NaOH
5	2.5 gr PAA+ 4 gr Rubber+0.7 gr NaOH
6	2.5 gr PAA+ 4 gr Rubber
7	2.5 gr PAA+ 4 gr Rubber +KH550
8	2.5 gr PAA+ 4 gr Rubber+0.5 gr NaOH+KH550

Contact angle is a quantitative measure of the wetting of a solid by a liquid. It is defined geometrically as the angle formed by a liquid at the three-phase boundary where a liquid, gas and solid intersect. For comparison of the wettability of samples, a drop of deionised (DI) water was dropped onto a plane solid surface of a WSR sample and an image was taken. The contact angles of all composites were measured based on the images taken.

The vulcanized strips of WSR were cut into sheets measuring  $40 \times 20 \times 1$  mm, each of which was weighed accurately and then immersed into 80.0 g of DI water at room temperature from 1 h to several days. The samples were taken out at specified intervals. To remove excess water from the surface, the samples were gently blotted with tissue paper before the weight of each swollen sample was recorded. This process was repeated at several time intervals. The water swelling ratio was calculated by the formula:

$$(W_2 - W_1)/W_1 * 100$$

where  $W_2$  and  $W_1$  are the weights of the WSR after a certain immersion period and the initial dry samples, respectively.

Next, each sample was dried at below 70 °C until it achieved a constant weight. Then the dried sample was again soaked in DI water at room temperature. At a specified time, it was taken out, the moisture on the surface was removed and weight of the sample was measured. The second and third water swelling ratios by weight were calculated using the following formulas:

$$(W_4 - W_3)/W_3 * 100$$

where  $W_3$  and  $W_4$  are the weights of a sample before and after the second water swelling, respectively, and

$$(W_5 - W_4)/W_4 * 100$$

where  $W_4$  and  $W_5$  are the weights of a sample before and after the third water swelling, respectively.

The stress–strain behaviour of the samples was investigated using a tensile testing machine (Instron, USA) with a crosshead speed of 50 mm.min<sup>-1</sup> and an initial gauge length of 40 mm. The tensile strength at break (TB) and elongation at break (EB) were then determined based on the stress–strain curves, at least three samples being tested for each experiment.

### **3.4 Results and discussion**

#### **3.4.1 Molecular interactions in WSR**

The functional groups of the WSR composites were investigated by FTIR, and the results are shown in Figure 3.2, which shows that the FTIR spectra of most of the WSR composites were similar to those of the PDMS rubber. It is observed that the main absorption peaks of PDMS are related to its different functional groups of 1259 cm<sup>-1</sup> (CH<sub>3</sub> symmetric bending in Si–CH<sub>3</sub>), 1076 and 1018 cm<sup>-1</sup> (Si–O–Si) and 798 cm<sup>-1</sup> (CH<sub>3</sub> rocking in Si–CH<sub>3</sub>) [20]. For the pure PAA, the peak centered at 1713 cm<sup>-1</sup> was assigned to asymmetric stretching vibrations of –COOH groups, suggesting that most of the carboxylic acid groups were associated by intramolecular hydrogen bonding [21]. With the addition of NaOH to PAA during the mixing process, an additional small band at 1550 cm<sup>-1</sup> was attributed to –C=O asymmetric stretching vibrations of –COO<sup>-</sup> groups, indicating change in the molecular structure of the PAA chains in the rubber matrix [22]. It is assumed that, with the neutralization of NaOH, –COOH groups were converted into –COO<sup>-</sup> Na<sup>+</sup> and the broad peak of –C=O (from–COOH) at 1695 cm<sup>-1</sup> disappeared. The FTIR spectrum of the compatibilizer composite of PAA/PDMS with associated NaOH showed a weakened and narrowed absorption band at 1259 cm<sup>-1</sup> which is a characteristic of PDMS, and a new broad peak appeared at 1580 cm<sup>-1</sup>, which corresponds to the N–H bending vibration of amide groups formed between PAA and compatibilizer. This change confirms the formation of intermolecular bonds between rubber and SAP with incorporation of the compatibilizer.

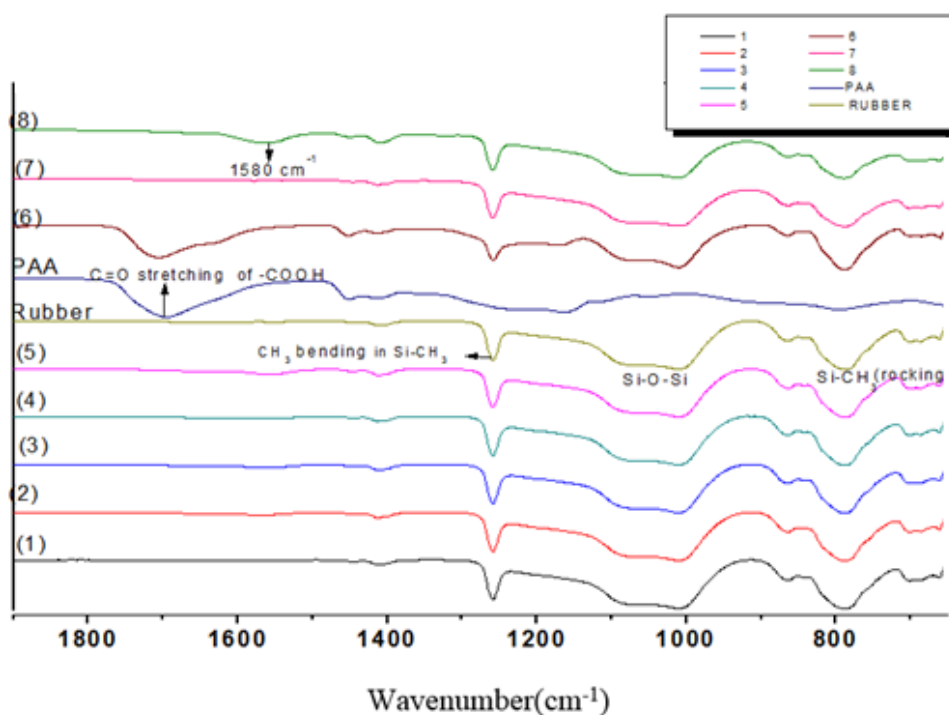


Figure 3.2 FTIR spectra of poly (acrylic acid), pure PDMS and their composites (refer to Table 3.1 for explanation of sample numbers)

### 3.4.2 Water swelling behaviour

Figure 3.3 shows the effect of PAA and NaOH on the WSR composites during soaking. With increasing soaking time, a slight increase in the swelling ratio of pure PAA in the rubber was observed to be about 31.5 % (sample 6). This means that the water molecules could only enter to WSR by means of diffusion and surface sorption and were prevented from being fully absorbed by the PAA resin inside the rubber. However, with NaOH in the mixture, the absorption ratio for WSRs (samples 1–5) changed significantly, indicating that water could penetrate the rubber and transfer between SAPs. As the FTIR results showed (Figure 3.2), the carboxylic groups of PAA interacted with the –OH group of NaOH. Therefore, partially neutralised PAA could disperse in the rubber and the swelling ratio increased. The amount of SAP played an important role in the degree of water absorption of the WSR composites [8].

With the increase of PAA concentration in the rubber, the swelling ratio increased. By adding 0.7 g of NaOH into PAA, the water swelling ratio increased compared with more PAA content added (from 3.0 to 4.0 g). However, the rapidest water absorption and the highest water swelling ratio of WSR occurred for the mass ratio of 2.5 g PAA and 0.5 g NaOH (sample 2). It may be assumed that most of the  $H^+$  ions of the  $-COOH$  groups in the PAA were replaced by  $Na^+$  in NaOH.

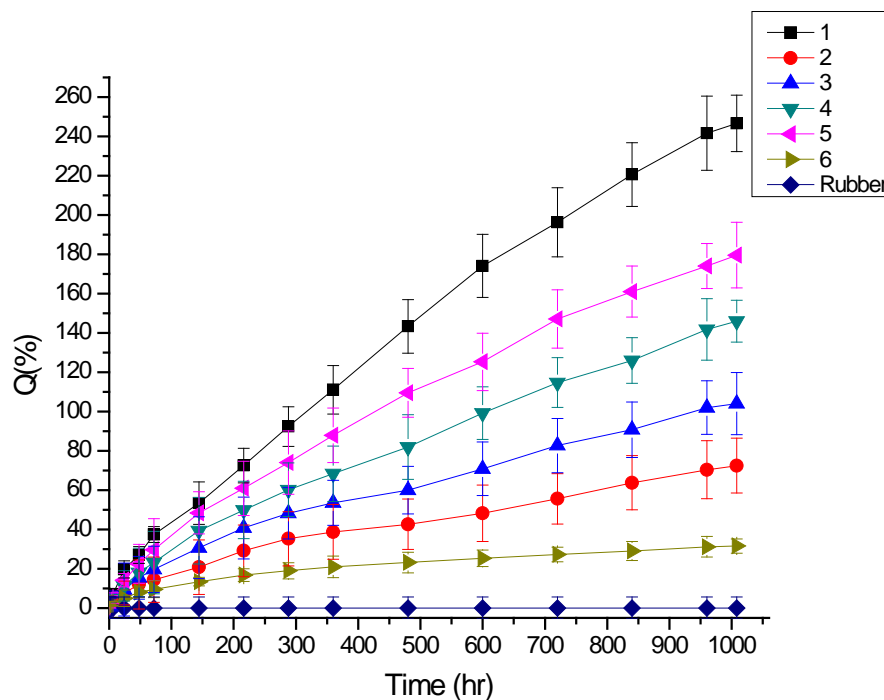


Figure 3.3 Water swellability of WSR composites

Figure 3.4 shows the effect of using compatibilizer with and without NaOH on the water swelling ratio of WSR. With the use of compatibilizer, the swelling rate accelerated twice. This can be explained as follows: the compatibilizer has hydrophobic and hydrophilic parts. The  $-Si$  part is compatible with PDMS and the  $-NH_3$  groups can react with PAA, which linking the PAA to the PDMS. Thus, interfacial tension between the two phases decreased (confirmed by characterization of the contact angles), and the cohesive force between them increased. As a result, the dispersion of PAA resin in the PDMS was improved and the water absorption abilities were enhanced. It can also

be seen from Figure 3.4 that, with the addition of NaOH and compatibilizer, the swelling rate increased sharply. For example, the swelling rate in 1000 h for PAA/rubber (sample 6) was 31.5 %, whereas for PAA/rubber with compatibilizer (sample 7) the swelling rate was 60.21 %. For PAA/rubber with NaOH (sample 1), due to effective neutralization, a sharp growth in swelling rate (246.65 %) was observed and finally, when both compatibilizer and NaOH (sample 8) in proper portions were used, the increment in water swelling rate reached 503.8 %. These results show that the combination of neutralisation of PAA and the compatibilization process had a synergetic effect in the composite.

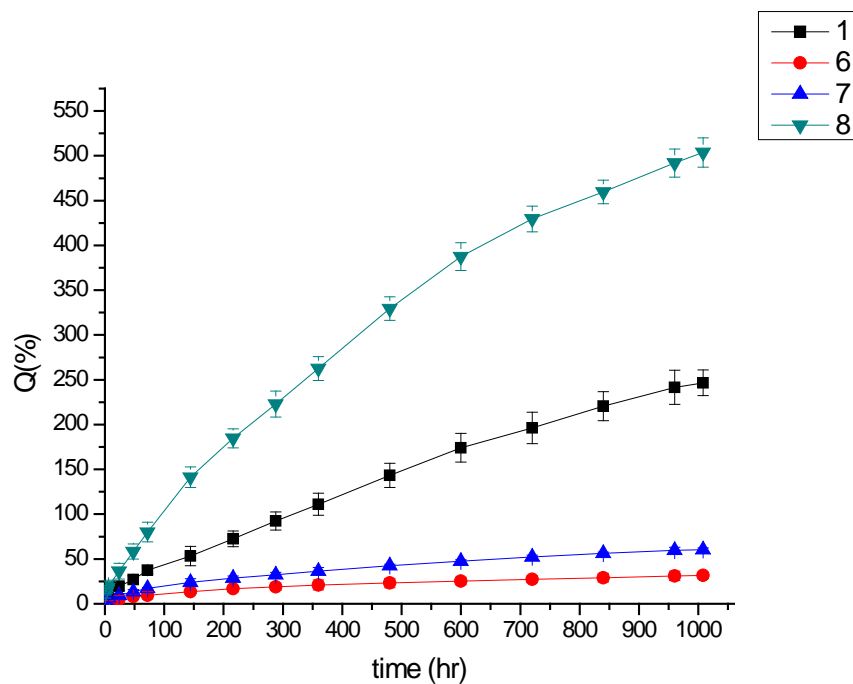


Figure 3.4 Water swellability of WSR with and without compatibilizer and NaOH

To investigate the second and third water swelling properties (Q2 and Q3) of WSR, the optimum WSR was chosen (sample 1: rubber with 2.5 g PAA and 0.5 g NaOH). This composite had the highest water swelling ratio on the first immersion. As shown in Figure 3.5, the effect of PAA on water swelling ability on the second immersion was similar to that on the first, indicating that a large amount of PAA still remained in the rubber and could absorb water. However, compared with

the first water swelling phenomenon, due to the loss of a small amount of PAA resin, the swelling rate was marginally lower for each of the second and third immersions in water.

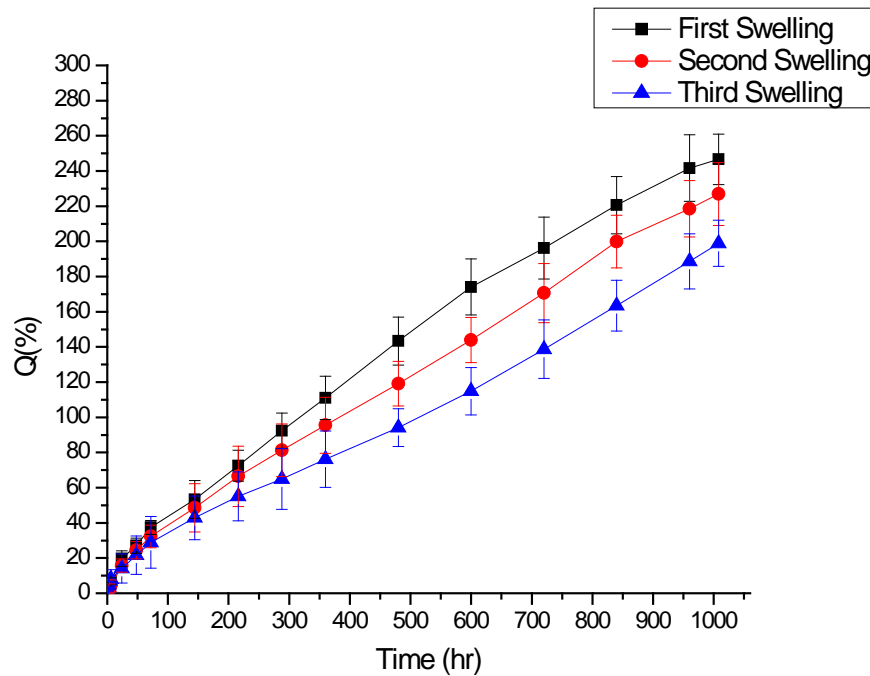


Figure 3.5 Water swellability of WSR for first, second and third dry swellings for sample 1

### 3.4.3 Morphological study

Figure 3.6 shows the SEM morphology of the fractured surfaces of WSR with different composition ratios of SAP and NaOH after 1000 h of soaking in water. In the micrographs, some spheres can be clearly seen that correspond to the PAA particles. The higher the loading of PAA, the more the agglomeration appeared in the surface after long immersion in water, as shown in Figure 3.6 a–e. The interfacial tension between hydrophilic PAA with a polar nature and nonpolar hydrophobic PDMS was high, and their adhesion was relatively low, indicating uneven distribution of PAA within the rubber matrix [18]. Figure 3.6 e) reveals that, with the addition of more NaOH, more PAA was neutralised and therefore less agglomeration was observed. The existence of some voids and weak boundary layers is probably attributable to incomplete wettability or bonding between the rubber matrix and the PAA, which may occur during the fabrication process.

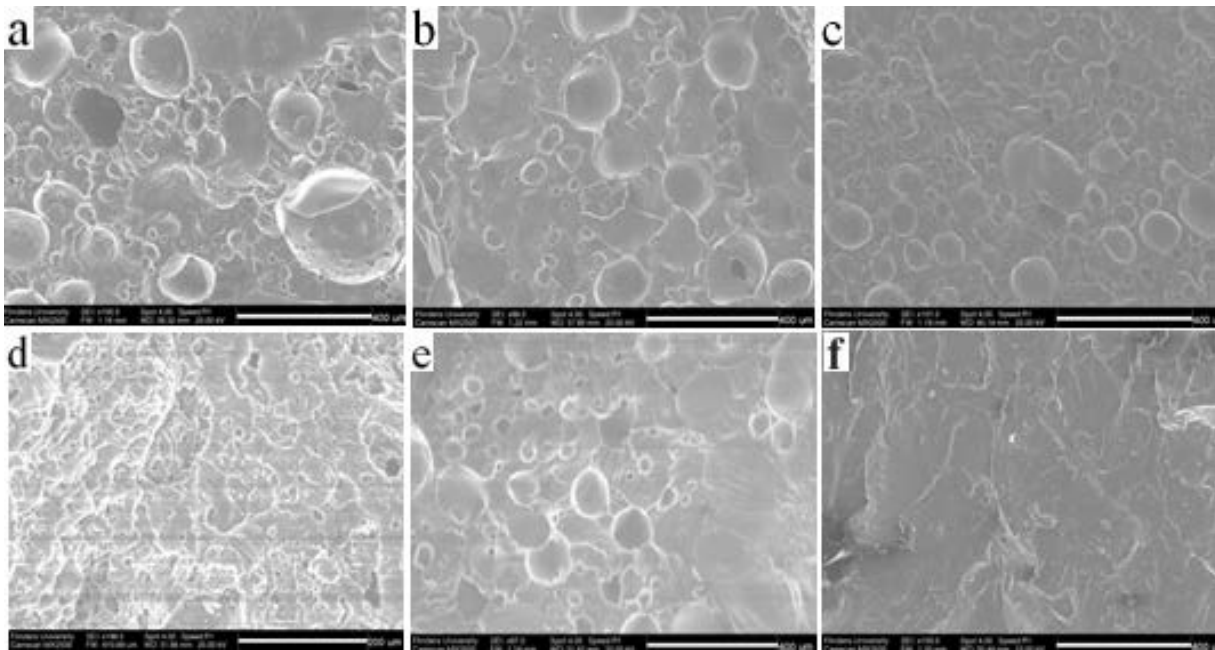


Figure 3.6 SEM micrographs of fractured surfaces of a–e samples 1–5 and f pure rubber after immersion in water for 1000 h

Figure 3.7 shows SEM micrographs of WSR with various contents of compatibilizer and NaOH. It can be seen that the compatibilizer is distributed evenly in the interface between PAA and rubber and no agglomeration is observed. The presence of small cracks on the fractured surface of samples indicates that, with the use of the compatibilizer, the rubber and PAA were linked with the  $-NH_3$  groups attached to the PAA and the  $-Si$  part attached to the PDMS. With that structure, the adhesion between the PAA and PDMS increased. These cracks could diffuse the surface tension between matrix and PAA, and, as a result, the PAA did not readily separate from the rubber matrix.

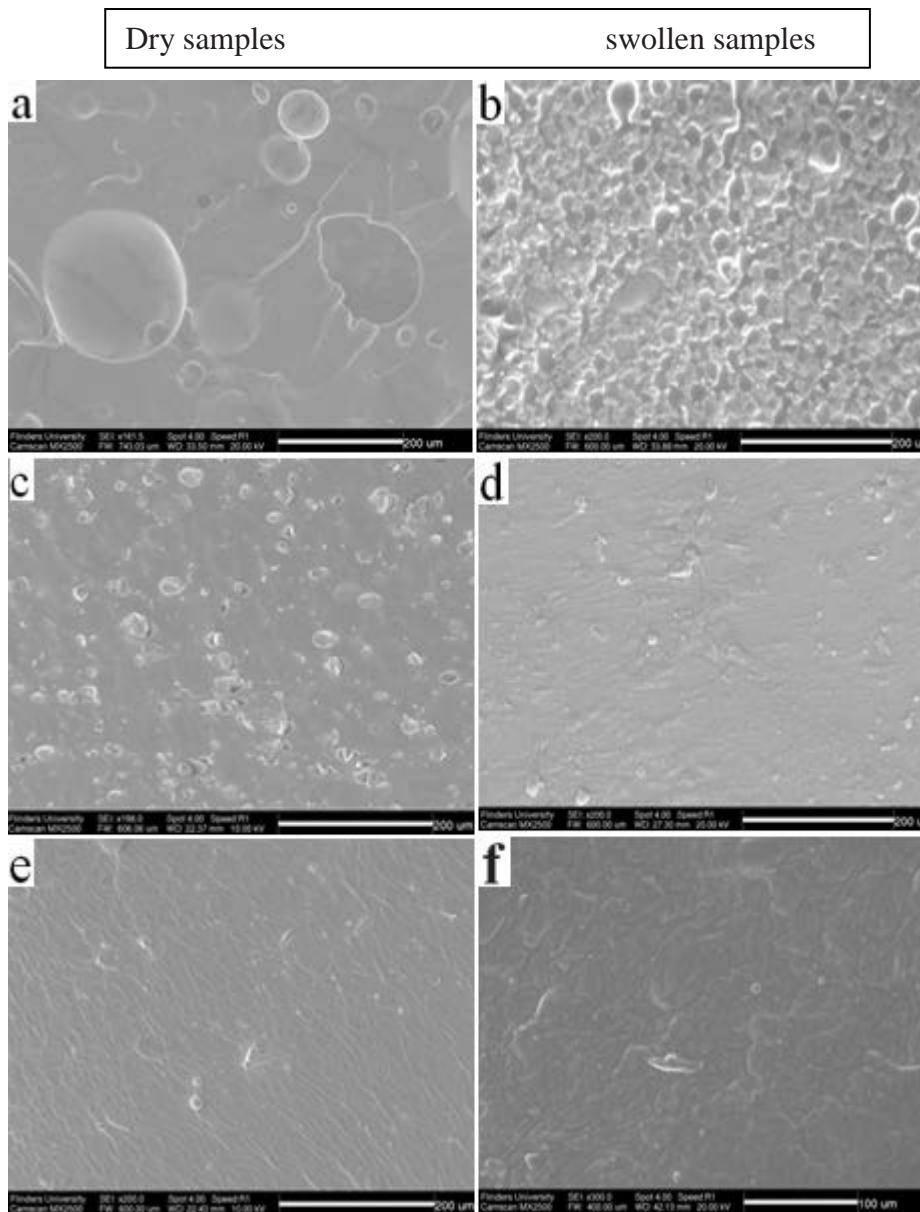


Figure 3.7 SEM micrographs of fractured surfaces of sample 6 (SAP/rubber), 7 (SAP/ rubber/ compatibilizer) and 8 (SAP/rubber/ compatibilizer/NaOH) in a dry and b swelling states (after 1000 h of soaking in water)

### 3.4.4 Contact angle

Figure 3.8 shows images of a water droplet on the surface of PAA, rubber and their composites after the first minute. As can be seen from the shape of the water droplet for pure PAA (Figure 3.8 a), the water contact angle decreased significantly during the first second of contact with water, as expected due to its high hydrophilicity. However, for the pure rubber (Figure 3.8 h), the water contact angle is much big due to its high hydrophobicity. While for the rest of the composites,

except sample 6 (PAA/rubber), the contact angles are similar, as shown in Figure 3.9. This means that the surface tension remains constant for all samples (samples 1–5), if only composition ratio changes. Without neutraliser, however (sample 6), the contact angle increased dramatically, indicating that the neutralizer also had the ability to minimise the interfacial tension between PDMS and PAA.

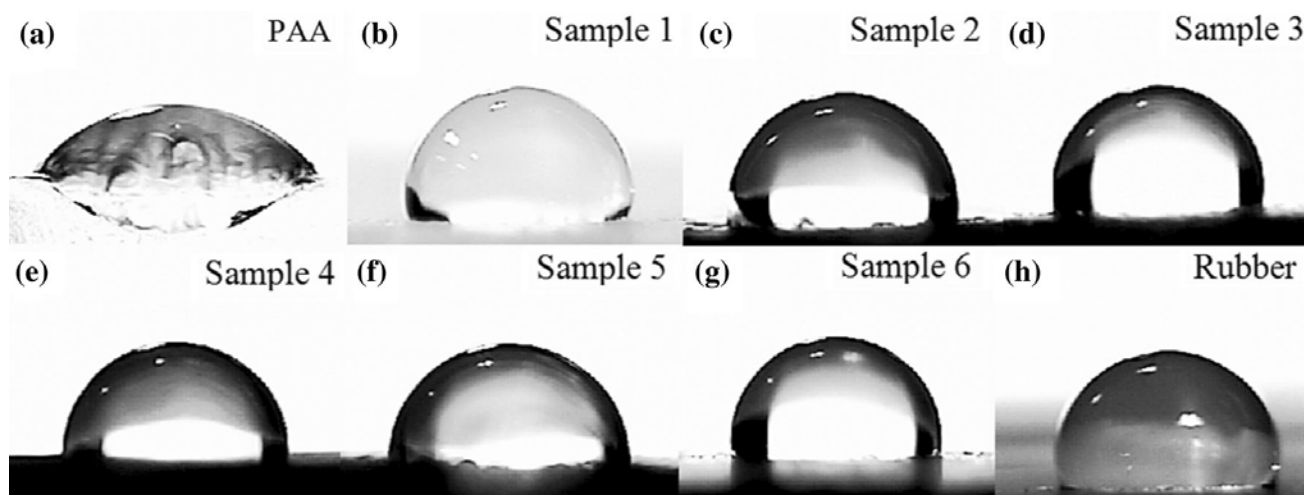


Figure 3.8 Optical images of water droplets on pure PAA, pure rubber and all composites

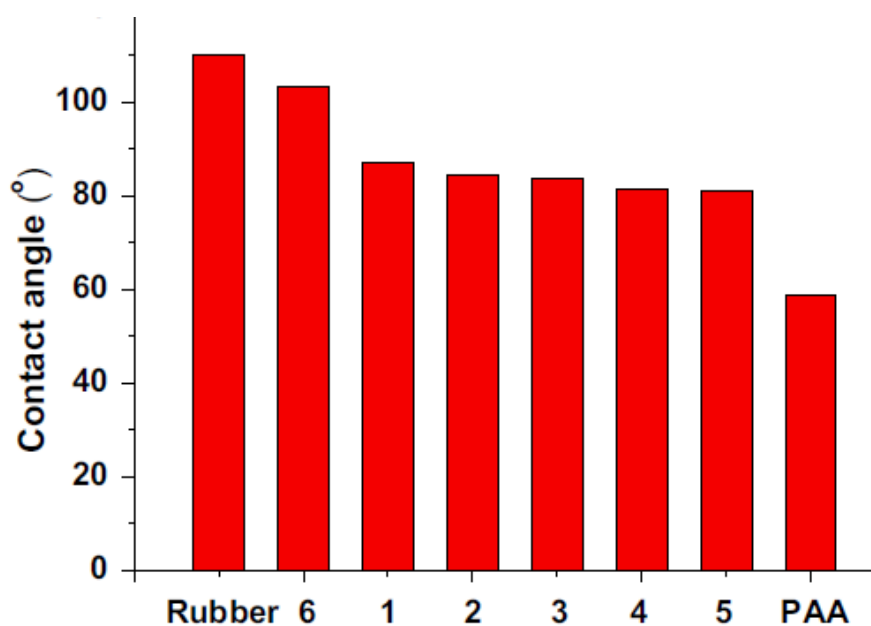


Figure 3.9 Effect of using PAA on contact angle of rubber with all composites

### 3.4.5 Mechanical properties

The results of tensile measurements such as tensile strength at break (TB) and elongation at break (EB) of rubber and all investigated composites before and after swelling in water are summarized together in Table 3.2. With an increase in SAP content, the TB and EB of the rubber each decreased due to an increase in flaws in the vulcanization of the rubber [8]. With an increase in the PAA concentration, more flaws in the rubber could be found and TB showed greater reduction. Moreover, rubber was replaced with a lower elastic material (PAA) that made WSR a brittle network with interconnections of distinctive domains, and the elongation of the samples showed considerable reduction. Increasing the duration of immersion caused a decreasing trend in EB and TB, which is attributed to the swelled hydrophilic components of the WSR composites. In the swollen samples, water served as a plasticiser and weakened the intermolecular forces between rubber chains, thus, the higher the amount of swelling, the lower the mechanical strength [17].

The mechanical properties of samples modified with KH550 and NaOH before and after water swelling. Incorporation of the compatibilizer increased both TB and EB. This is because, using the compatibilizer, the interfacial tension between the rubber and PAA decreased and the cohesive force between the two phases increased, reasoning that is supported by the SEM results (Figure 3.7). With an increase in the immersion time, the mechanical properties of the modified WSRs showed the same trend for the same reason as those in unmodified samples, that is, decreases in the mechanical properties due to action of water as a plasticiser.

Table 3.2 Tensile properties of WSR before and after immersion in water

Sample	Before immersing		100-h immersion		1000-h immersion	
	TB (MPa)	EB (%)	TB (MPa)	EB (%)	TB (MPa)	EB (%)
Rubber	17.9±0.33	197.8±32.0	—	—	—	—
1	1.31±0.42	125.9±25.0	1.05±0.18	126.3±25.4	0.46±0.30	112.3±31.0
2	1.11± 0.27	142.8±35.8	0.69±0.20	125.1±24.9	0.48±0.13	114.2±27.0
3	1.61± 0.50	147.7±43.8	1.07±0.26	141.2±30.0	0.25±0.16	103.6±46.0
4	1.14±0.18	144.7±23.5	0.64±0.19	119.1±31.0	0.50±0.19	109.2±23.0
6	6.62±0.07	191.7±18.0	4.42±0.37	161.4±27.0	2.22±0.97	157.42±31.0
7	2.12±0.35	166.6±21.9	1.98±0.39	162.0±30.5	1.61±0.36	166.0±22.0
8	2.29±0.27	171.5±32.6	0.46±0.24	107.0±29.2	0.09±0.42	66.3±27.0

### 3.5 Conclusions

PAA can react with PDMS by using of NaOH as a neutralizer of PAA and aminopropyltriethoxysilane as a compatibilizer between PAA and PDMS. A suitable PAA loading facilitated higher water absorbency but also caused a significant reduction in TB and EB. The use of a compatibilizer was demonstrated to be an effective solution for mixing immiscible blends of PAA and PDMS. Modified WSRs produced a markedly greater increase in water absorbency than found in unmodified WSRs. The mechanical properties before and after water swelling were improved in the modified samples. Morphological observation of the fracture surface of WSR before and after water swelling indicated that in compatibilized WSR, the interfacial tension and cohesive force between the rubber and the SAP decreased and increased, respectively. However, as we discussed earlier, SAPs won't disperse well in hydrophobic rubber even by using compatibilizer and neutralizer, resulting to the poor interfaces to the rubber and therefore, the swelling ability is ultimately lost. Next chapter represents a method to improve the water absorption properties and stability of WSR by using electrospun multi-scaled hybrid fiber mats of crosslinked poly (acrylic acid) (PAA) nanocomposite as water channels. The idea behind this is that the electrospun fibers

acted as internal multi-scale water channels to bridge isolated PAA particles wrapped in hydrophobic rubber together and link the internal PAAs with the composite surface to enhance the short- and long-term water swelling ability of WSR. The effects and mechanisms of those fibers on enhancing water swelling properties of WSR are discussed.

### 3.6 References

1. Wu, J., Lin, J., Li, G. and Wei, C., 2001. Influence of the COOH and COONa groups and crosslink density of poly (acrylic acid)/montmorillonite superabsorbent composite on water absorbency. *Polymer International*, 50(9), pp.1050-1053.
2. De Barra, E. and Hill, R., 1998. Influence of poly (acrylic acid) content on the fracture behaviour of glass polyalkenoate cements. *Journal of materials science*, 33(23), pp.5487-5497.
3. Mignon, A., Graulus, G.J., Snoeck, D., Martins, J., De Belie, N., Dubruel, P. and Van Vlierberghe, S., 2015. pH-sensitive superabsorbent polymers: a potential candidate material for self-healing concrete. *Journal of Materials Science*, 50(2), pp.970-979.
4. Hua, F. and Qian, M., 2001. Synthesis of self-crosslinking sodium polyacrylate hydrogel and water-absorbing mechanism. *Journal of materials science*, 36(3), pp.731-738.
5. Peng, R., Yu, Y., Chen, S., Yang, Y. and Tang, Y., 2014. Conductive nanocomposite hydrogels with self-healing property. *RSC Advances*, 4(66), pp.35149-35155.
6. Wang, G., Li, M. and Chen, X., 1997. Inverse suspension polymerization of sodium acrylate. *Journal of applied polymer science*, 65(4), pp.789-794.
7. Nakason, C., Nakaramontri, Y., Kaesaman, A., Kangwansukpamonkon, W. and Kiatkamjornwong, S., 2013. Synthesis and characterization of water swellable natural rubber vulcanizates. *European Polymer Journal*, 49(5), pp.1098-1110.

8. Saijun, D., Nakason, C., Kaesaman, A. and Klinpituksa, P., 2009. Water absorption and mechanical properties of water-swellaable natural rubber. *Sonklanakarin Journal of Science and Technology*, 31(5), pp.561-565.
9. Clarson, S.J. and Semlyen, J.A., 1993. *Siloxane polymers*. Prentice Hall..
10. Meng, E., Zhang, X. and Benard, W., 2011. Additive processes for polymeric materials. In *MEMS Materials and Processes Handbook* (pp. 193-271). Springer US.
11. Van Krevelen, D.W. and Hoftyzer, P.J., 1976. Permeation of polymers: the diffusive transport of gases, vapours and liquid in polymers. *Properties of Polymers, Elsevier, Amsterdam*, pp.403-425.
12. Arquint, P., Van der Wal, P.D., van der Schoot, B.H. and de Rooij, N.F., 1995, June. Flexible polysiloxane interconnection between two substrates for microsystem assembly. In *Solid-State Sensors and Actuators, 1995 and Eurosensors IX.. Transducers' 95. The 8th International Conference on* (Vol. 1, pp. 263-264). IEEE.
13. Antonisse, M.M., Engbersen, J.F. and Reinhoudt, D.N., 1995, June. Nitrate and bicarbonate selective CHEMFETs. In *Solid-State Sensors and Actuators, 1995 and Eurosensors IX.. Transducers' 95. The 8th International Conference on* (Vol. 1, pp. 867-869). IEEE.
14. Lötters, J.C., Olthuis, W., Veltink, P.H. and Bergveld, P., 1996. Polydimethylsiloxane as an elastic material applied in a capacitive accelerometer. *Journal of micromechanics and microengineering*, 6(1), pp.52-54.
15. Chu Z. 1996. Flexible package for a tactile sensor array. In: *Proceedings of 1996 National Sensor Conference*, Delft University Press, Delft, 121–124.
16. Wang, G., Li, M. and Chen, X., 1999. Effects of fillers on mechanical properties of a water-swellaable rubber. *Journal of applied polymer science*, 72(4), pp.577-584.

17. Zhang, Z., Zhang, G., Li, D., Liu, Z. and Chen, X., 1999. Chlorohydrin water-swelling rubber compatibilized by an amphiphilic graft copolymer. II. Effects of PVA-g-PBA and CPA on water-swelling behaviors. *Journal of applied polymer science*, 74(13), pp.3145-3152.
18. Wang, C., Zhang, G., Dong, Y., Chen, X. and Tan, H., 2002. Study on a water-swelling rubber compatibilized by amphiphilic block polymer based on poly (ethylene oxide) and poly (butyl acrylate). *Journal of applied polymer science*, 86(12), pp.3120-3125.
19. Magalhães, A.S.G., Almeida Neto, M.P., Bezerra, M.N., Ricardo, N.M. and Feitosa, J., 2012. Application of ftir in the determination of acrylate content in poly (sodium acrylate-co-acrylamide) superabsorbent hydrogels. *Química Nova*, 35(7), pp.1464-1467.
20. Lee, J., Kim, J., Kim, H., Bae, Y.M., Lee, K.H. and Cho, H.J., 2013. Effect of thermal treatment on the chemical resistance of polydimethylsiloxane for microfluidic devices. *Journal of Micromechanics and Microengineering*, 23(3), p.035007.
21. Guan, Y., Zhang, Y., Zhou, T. and Zhou, S., 2009. Stability of hydrogen-bonded hydroxypropylcellulose/poly (acrylic acid) microcapsules in aqueous solutions. *Soft Matter*, 5(4), pp.842-849.
22. Yu, Y., De Andrade, L.C.X., Fang, L., Ma, J., Zhang, W. and Tang, Y., 2015. Graphene oxide and hyperbranched polymer-toughened hydrogels with improved absorption properties and durability. *Journal of Materials Science*, 50(9), pp.3457-3466.

#### **4. [ELECTROSPUN MULTI-SCALE HYBRID NANOFIBER/NET WITH ENHANCED WATER SWELLING ABILITY IN RUBBER COMPOSITES<sup>1</sup>]**

In this chapter a study on electrospinning of various superabsorbent nanofibers of PAA with hyperbranched polymer (HB) and/or graphene oxide (GO) is carried out. Electrospun mats with hybrid fillers (HB and GO together) presence a spider web-like multi-scale structures that can enhance specific surface areas between these two and improve the water swelling ability of the nanofibers. These hybrid nanofiber mats of crosslinked poly (acrylic acid) (PAA) were then added to WSR. The effects and mechanisms of nanofibers on enhancing water swelling properties of WSR are discussed.

1. This work has been published in *Materials & Design*: Jinchao Zhao, Nazila Dehbari, Wei Han, Leping Huang, and Youhong Tang. "Electrospun multi-scale hybrid nanofiber/net with enhanced water swelling ability in rubber composites." *Materials & Design* 86:14-21 (2015). DOI: 10.1016/j.matdes.2015.07.105

## 4.1 Introduction

WSR with high elasticity, resilience, high toughness, and also high water swelling ability are widely used as sealing material [1, 2]. Synthesis of amphiphilic polymer is an important chemical modification method for the grafting of hydrophilic chains onto hydrophobic rubber, such as grafting co-polymerization of N, N-dimethylacrylamide onto natural rubber [3], grafting of poly(ethylene oxide) onto chlorosulphonated polyethylene and poly(ethylene oxide) onto butyl rubber [4, 5], but the chemical method is more complicated and more environmentally unfriendly than the physical method. In the physical method, common hydrophobic rubbers such as chloroprene rubber [6], chlorohydrin rubber [7], and natural rubber [8] have been mixed with various water-absorbent materials such as crosslinked forms of polyacrylate [9], poly(vinyl alcohol) [10], starch-acrylate copolymer [11] and some other fillers [2]. Water-absorbent materials known as superabsorbent polymers (SAP), which are kinds of hydrogel with three-dimensional (3D) network structures, possess a high degree of absorption and absorbing rate, as well as stability. However, as we observed in chapter 3, hydrophilic super water-absorbent resin do not disperse well in hydrophobic rubber, having very poor interfaces between them, so that the hydrophilic part can easily break off from rubber networks [12]. Thus swelling ability is ultimately lost, strength is remarkably decreased, and water is polluted as well. To overcome these problems, a silica coupling agent was used as a compatibilizer in our previous work [13] to increase the interactions between SAP and rubber. Improved swelling and mechanical properties were achieved. However, isolated SAPs were trapped within the rubber and water could not efficiently transfer between SAP particles in the rubber.

Previous studies [14, 15] have shown that by using even low nanofiber loadings in rubber composites, mechanical properties such as Young's modulus and tensile strength increased greatly. Because of the hydrophilic nature of the fibers they could act as internal water channels in

hydrophobic materials for superabsorbent nanocomposites and help to transfer water from the surface of the rubber matrix to hydrophilic SAP particles as well as between encapsulated SAP particles in the rubber matrix, enhancing the water swelling ability of WSR composites.

Electrospinning of ultrafine fibers ranging from submicron to nanometre size, with smaller pores and higher surface area than regular fibers, can be used in an enormous variety of applications [14, 16, 17]. In 2006, a two-dimensional (2D) spiderweb-like nanofiber/net (NFN) with ultrafine fiber diameter less than 20 nm was prepared by electrospinning/netting (ESN) [18, 19]. It exhibited extremely large specific surface area, high porosity, and large stacking density, providing optimal candidates for applications as sensor materials [20], biomedical wound dressing [21], and other significant applications [22, 23]. Ding *et al.* [18] were the first to find a procedure for generating novel 2D nanowebs in 3D fibrous mats by optimization of various processing parameters during electrospinning, but multi-scaled hybrid PAA NFN with enhanced properties has not yet been reported.

The present study is the first to report improved water absorption property and stability of WSR resulting from the use of electrospun multi-scaled hybrid NFN in 3D fibrous mats of crosslinked PAA functioning as water channels. Electrospinning of various superabsorbent SAP (PAA with hyper branched polymer and/or GO) 3D fibrous mats was performed. The effects and mechanisms of those fibers in enhancing the water swelling properties of WSR are discussed. This novel water channel system could be an effective method for enhancing the absorption property of WSR as well as for developing the feasibility of using the electrospun fine fibers in sealing material.

## 4.2 Experiments

### 4.2.1 Materials and Preparation of PAA and PAA hybrid solutions

Poly (acrylic acid) (PAA, average  $M_w \sim 450\,000\text{ g}\cdot\text{mol}^{-1}$ ), poly (acrylic acid) solution (average  $M_w \sim 250\,000\text{ g}\cdot\text{mol}^{-1}$ , 35 wt. % in  $\text{H}_2\text{O}$ ), ethylene glycol (EG, anhydrous, 99.8%), hyperbranched bis-MPA polyester-64-hydroxyl (HB), (3-Aminopropyl) triethoxysilane, sulfuric acid and ethanol were purchased from Sigma Aldrich Australia. Banana skin silicone rubber was provided by Barnes Products Pty Ltd, Australia. Graphene oxide (GO) was prepared by oxidizing graphite powder following a modified Hummers method and exfoliation of GO suspensions under bath ultrasonication [24-26]. All aqueous solutions were prepared using Milli-Q water ( $18.2\text{ M}\Omega\cdot\text{cm}$  at  $25\text{ }^\circ\text{C}$ ).

The PAA-EG solution was prepared according to previous work [18, 27]. In detail, 0.96 g EG was added to 100 g 6 wt% PAA/ethanol solutions as a crosslinking agent with concentration of 16 wt% relative to the PAA. After 24 h of mechanical mixing at ambient temperature, the PAA-EG electrospun solution was obtained. For the PAA-EG+HB solution, 0.96 g EG as a crosslinking agent with concentration of 16 wt% relative to the PAA and 0.9 g HB with concentration of 15 wt% relative to the PAA were added to 100 g 6 wt% PAA/ethanol solution. After 24 h of mechanical stirring at ambient temperature, the PAA-EG+HB electrospun solution was obtained. For the PAA-EG+GO solution, 0.03 g GO was dispersed in 5.97 g ethanol by ultrasonication by a LABEC mrc sonic-950wt at 950 w for 10 s. The prepared GO/ethanol solution was mixed with 6 g PAA and 88 g ethanol with GO concentration of 0.5 wt% relative to the PAA. 0.96 g EG was added to the PAA-GO solution as a crosslinking agent with concentration of 16 wt% relative to the PAA. The mixture was ultrasonicated for 30 min, followed by 24 h of mechanical mixing at ambient temperature, and the PAA-EG+GO electrospun solution was obtained.

For the PAA-EG+HB+GO solution, 0.03 g GO was dispersed in 5.97 g ethanol by ultrasonication by a LABEC mrc sonic-950wt at 950 w for 10 s. The prepared GO/ethanol solution was mixed with 6 g PAA and 88 g ethanol with GO concentration of 0.5 wt% relative to the PAA. 0.96 g EG as a crosslinking agent with concentration of 16 wt% relative to the PAA and 0.9 g HB with concentration of 15 wt% relative to the PAA were added to 100 g 6 wt% PAA/ethanol solution. The mixture was ultrasonicated for 30 min, followed by 24 h of mechanical mixing at ambient temperature, and the PAA-EG+HB+GO electrospun solution was obtained.

Once the electrospun solutions were obtained, sulfuric acid ( $1 \text{ mol}\cdot\text{L}^{-1}$ ) was added to the PAA and PAA hybrid solutions at a concentration of  $50 \text{ }\mu\text{L}\cdot\text{mL}^{-1}$  immediately before electrospinning processing.

#### **4.2.2 Preparation of PAA and PAA hybrid NFN mats**

The homogeneous PAA and PAA hybrid solutions were electrospun using an electrospinning machine (NaBond Technologies TL01, China). The parameters of the machine were optimized to obtain the best fibers without beads. Taking the PAA-HB-GO solution as an example, 20 mL PAA-EG+HB+GO solution was loaded into a hypodermic syringe (50 mL). A syringe pump was used to control the flow rate of 1.5 mL/h. The tip-to-collector distance and the applied voltage between the needle and the collector were set at 10 cm and 15 kV respectively to obtain a steady state condition. The x-axis moving speed of the needle and the drum speed were set at 3.5 mm/s and 200 rpm respectively to obtain a uniform fiber mat. An exhaust fan and a heater were used to control the temperature of the chamber at 35 °C, ensuring that the ethanol in the PAA-EG+HB+GO solution could volatilize at a proper speed. After settling, the PAA-EG+HB+GO solution was electrospun onto a silicon oil sprayed on aluminium foil that covered the drum. After 3 h

electrospinning process of the PAA-EG+HB+GO liquid, the freshly made PAA-EG+HB+GO NFN mats were crosslinked via heat treatment in a vacuum oven at 130 °C and a reduced pressure of 25 in Hg (84.7 kPa) for 30 min, and then cooled to room temperature. Thus 0.04 mm PAA-EG+HB+GO NFN mats were obtained. The preparation scheme of an electrospun PAA-EG+HB+GO NFN mat is shown in Figure 4.1 as an example.

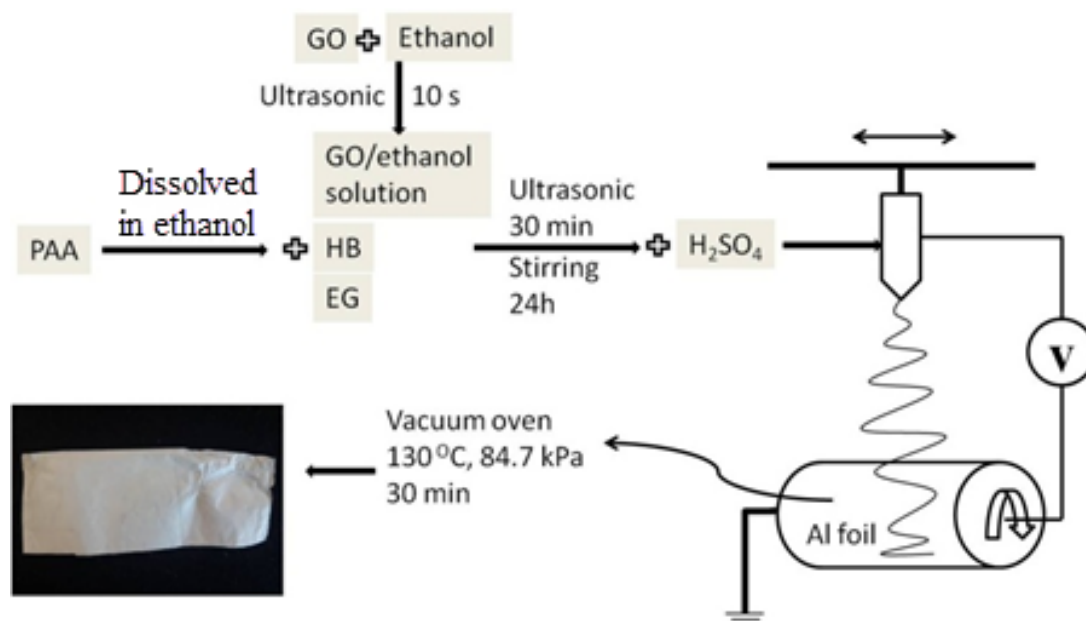


Figure 4.1 Preparation of electrospun PAA-HB-GO NFN mat

#### 4.2.3 Preparation of PAA hybrid NFN mat enhanced WSR composites

The as-prepared PAA and PAA hybrid NFN mat was added to the PAA/rubber composite to strengthen the properties of the WSR composites. The composites were prepared through a solution impregnation technique as shown in Figure 4.2. In detail, 12.5 g PAA was mixed with 2 g EG as a crosslinking agent, with 0.625 g 1 and 0.0625 g (3-Aminopropyl)triethoxysilane as compatibilizer. Then 20 g banana rubber part A was added into the prepared mixture. After 15 min stirring, the electrospun PAA or PAA hybrid NFN mat with 0.4 g and ~0.04 mm thickness was added, was cut

into  $0.5 \times 5 \text{ cm}^2$  strips. Then 20 g banana rubber part B was added and stirred for 10 min. The mixture was poured into  $10 \times 10 \text{ cm}^2$  plastic model boxes with 10 g in each. Following 24 h of curing at ambient temperature,  $\sim 15 \text{ mm}$  thickness PAA-EG+HB+GO NFN mat/PAA/rubber composite samples were obtained. For the control experiment, PAA/rubber composite (conventional WSR) was prepared under the same conditions.

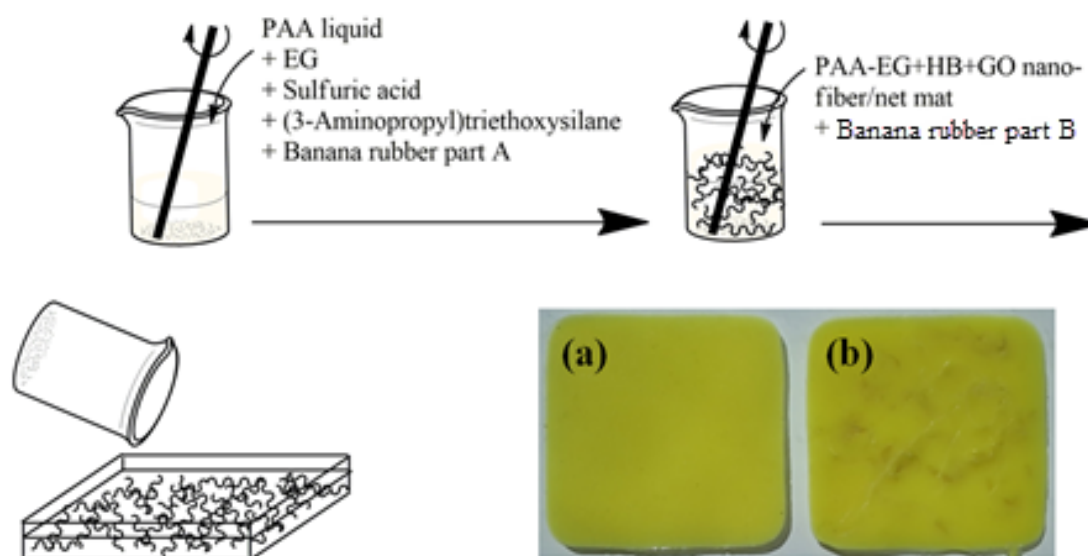


Figure 4.2 Scheme of composites preparation with (a) PAA/rubber composite and (b) PAA-HB-GO NFN mat/PAA/rubber composites

### 4.3 Characterizations

FTIR analysis of the hybrid fibers was performed using a PerkinElmer Spectrum 400 spectrometer equipped with an attenuated total reflectance (ATR, top plate type) accessory. Each sample ( $\sim 0.1 \text{ g}$ , dry) was mounted onto the central crystal of the ATR plate, and air was used as a background reference before each scan. FTIR spectra were then recorded using 64 scans from  $4000$  to  $550 \text{ cm}^{-1}$  with a resolution of  $4 \text{ cm}^{-1}$  in absorbance mode with background subtraction. Raman spectroscopic analysis of the GO and PAA hybrid NFN mats were performed on an Alpha 300RS

microscopy/spectroscopy instrument (Witec, Germany) using a 532 nm laser with a maximum power of <60 mW. Single spectra were recorded at an acquisition time of 10 s.

The surface morphology and the microstructure of all samples were investigated using a field-emission scanning electron microscope (FEI Inspect F50, US). Thermogravimetric analysis (TGA) was carried out using Q600 Simultaneous DSC/TG (TA Instruments, US). GO samples were heated from room temperature to 1000 °C at a rate of 20 °C·min<sup>-1</sup> in nitrogen. The composites were heated from room temperature to 500 °C at a rate of 20 °C·min<sup>-1</sup> in nitrogen. The surface area and pore volume were evaluated using nitrogen adsorption-desorption isotherms measured at 77 K on a TriStar II 3020 Micrometrics apparatus. The Brunauer-Emmett-Teller (BET) specific surface area was calculated using adsorption data at a relative pressure range of  $P/P_0 = 0.05-0.25$ . Pore size distribution was derived from the adsorption branch using the BJH method. The total pore volume was estimated from the amount adsorbed at a relative pressure ( $P/P_0$ ) of 0.99.

Water absorbency was tested by drying the samples in an oven at 100 °C for 24 h and weighed as  $m_0$ , followed by immersing weighed samples in an excess of Milli-Q water (500 mL) at 25 °C for 1 h to reach the swelling equilibrium. The swollen samples was then weighed as  $m_1$  until they were dripless. Subsequently the swollen samples were weighed as  $m_n$  at regular intervals. The absorbency was calculated as follows. Reported results represent the average values from five samples.

$$(m_n - m_0)/m_0$$

#### 4.4 Results and discussion

The desire for ever-higher specific surface area and porosity has encouraged researchers to improve electrospinning techniques [28]. In this work, the PAA and PAA hybrid NFN mats were prepared for high water absorption. The SEM images of PAA-EG, PAA-EG+HB, PAA-EG+GO and PAA-EG+HB+GO NFN mat are shown in Figure 4.3. The image of the PAA-EG NFN mat (Figure 4.3(a)) shows an interlinked 1D ultrafine fibrous mat formed from 700-800 nm diameter fibers with a small number of thinner fibers (< 100 nm) generated among the main fiber mat. With the addition of HB, spiderweb-like nanowebs were formed between the main electrospun fibers. Two types of fiber (nano and submicron sizes) arranged in a spiderweb-like structure were obtained (Figure 4.3(b)). SEM images of the mats showed that this network consisted of thin nanofibers with diameters of <100 nm and thick submicron fibers with diameters of about 700-800 nm, arranged in a spiderweb-like structure. Pirjo *et al.* [29] proved that high viscosity solutions produced sub-structures composed of smaller fibers between larger smooth fibers, forming the continuous web. As the profuse -OH groups in HB [30] could react with -COOH groups in the PAA during the crosslinking process (as proved by FTIR), the formation of a 2D structure in the hybrid mat could be attributed to the strong interfacial adhesion between HB and the PAA matrix which hinders the activity of PAA chains and increases the viscosity of the electrospun solution. From the image of the PAA-EG+GO NFN mat (Figure 4.3(c)), networks also form with the addition of GO. Pant *et al.* [31] suggested that the presence of a well-dispersed nano-conductor can increase the number of ions in the electrospinning solution.

A further increase of ions can initiate the splitting of sub-nanofibers from the main fibers and solidification with nanoparticles in the form of a spiderweb-like structure during electrospinning. With further addition of HB into the PAA-EG+GO system the viscosity is increased, augmenting the splitting of sub-nanofibers from the main fibers in the form of a

spiderweb-like structure during electrospinning (Figure 4.3(d)) [19, 31, 32]. We assume that the spiderweb-like structure increases the absorptivity of the fibrous mat due to its net-linked structure and ever-higher specific surface area and porosity.

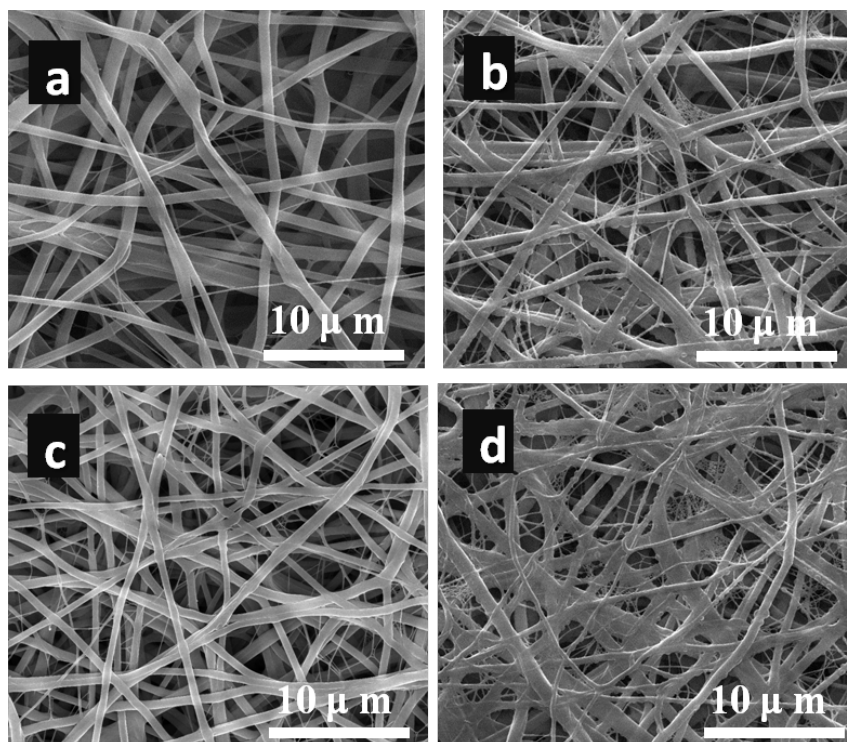


Figure 4.3 SEM images of (a) PAA-EG, (b) PAA-EG+HB, (c) PAA-EG+GO and (d) PAA-EG+HB+GO fibrous mats

The FTIR spectra of PAA, EG, HB, GO and PAA-EG, PAA-EG+HB, PAA-EG+GO and PAA-EG+HB+GO hybrid NFN mats are shown in Figure 4.4. In the FTIR spectrum of PAA, the peaks of O-H stretching of carboxylic group at  $3200-3700\text{ cm}^{-1}$ ,  $\text{-C=O}$  stretching of carboxylic group at  $1705\text{ cm}^{-1}$ ,  $\text{-COO}^-$  group at  $1452\text{ cm}^{-1}$ , C-O stretching intense doublet at  $1259\text{ cm}^{-1}$  are observed [33]. In the FTIR spectrum of EG, the peaks of O-H stretching of carboxylic group at  $3200-3700\text{ cm}^{-1}$ ,  $\text{-CH}_2\text{-}$  stretching at  $2937\text{ cm}^{-1}$ ,  $2873\text{ cm}^{-1}$ ,  $\text{-C-O(H)}$  stretching at  $1000-1260\text{ cm}^{-1}$  are observed [34]. In the FTIR spectrum of HB, the peaks of O-H stretching at  $3200-3700\text{ cm}^{-1}$ , the

peaks of C=O at  $1733\text{ cm}^{-1}$  and  $1459\text{ cm}^{-1}$  are associated with the symmetric COO<sup>-</sup> stretching and H-bonded ester C=O groups, respectively [35]. The peaks of O-C stretching ester groups and C-O(-OH) stretching hydroxyl are observed at  $1035$  and  $1131\text{ cm}^{-1}$ , respectively [35]. In the FTIR spectrum of GO, the peaks of  $2500\text{-}3400$  and  $1643\text{ cm}^{-1}$  are associated with the H-bonded stretching in C=O groups and C=O stretching, respectively [36].

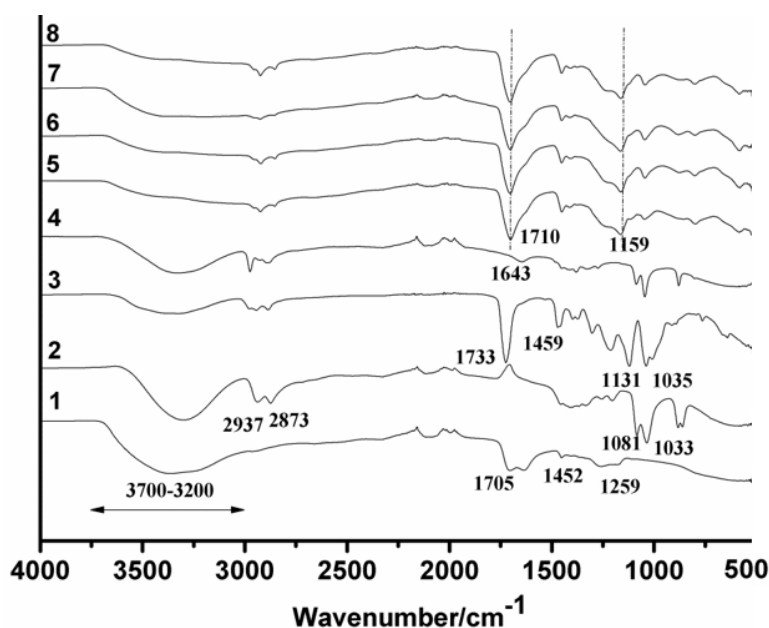


Figure 4.4 FTIR spectra of 1) PAA, 2) EG, 3) HB, 4) GO, 5) PAA-EG, 6) PAA-EG+HB, 7) PAA-EG+GO and 8) PAA-EG-HB+GO

When the PAA is crosslinked with EG, the strong O-H stretching of the carboxylic group at  $3200\text{-}3700\text{ cm}^{-1}$  changes to weak C=O stretching of ester at  $\sim 3450\text{ cm}^{-1}$ . The peaks of C=O stretching at  $\sim 1720\text{ cm}^{-1}$  and C-O-C stretching at  $1159\text{ cm}^{-1}$  also indicate the formation of ester. No significant difference is observed from the FTIR spectra of the PAA-EG, PAA-EG-HB, PAA-EG-GO and PAA-EG-HB-GO samples. There is no obvious O-H stretching at  $3200\text{-}3700\text{ cm}^{-1}$  in the spectra of PAA-EG-HB and PAA-EG-HB-GO, due to the cross linkage of the -COOH group in the

PAA with the profuse -OH groups in HB. In the PAA-EG-GO and PAA-EG-HB-GO samples, only a small amount (~0.5 wt%) of GO powder was added in the PAA structure and the major peaks of the GO overlap with those of the PAA-EG sample.

Raman spectra were used to prove the interactions between GO and PAA-EG matrix which could not be determined by FTIR. The Raman spectra of GO, PAA-EG, PAA-EG+GO and PAA-EG+HB+GO are shown in Figure 4.5. From the Raman spectrum of GO, the typical D and G peaks around 1357 and 1609  $\text{cm}^{-1}$  are derived from  $\text{sp}^3$  and  $\text{sp}^2$  carbon domains, respectively [37, 38]. No obvious Raman scattering is observed in the PAA-EG fibrous mat. But the D and G bands shift to higher frequencies for the PAA-EG+GO fibrous mat (1361 and 1617  $\text{cm}^{-1}$  respectively) and PAA-EG+HB+GO fibrous mat (1361 and 1621  $\text{cm}^{-1}$  respectively). The D/G ratios of GO, PAA-EG+GO and PAA-EG+HB+GO are 0.87, 1.21 and 1.19, respectively. As the blue-shifted (higher frequency) G bands reflect the influence of defects, and the intensity ratio of the D and G bands expresses the  $\text{sp}^2/\text{sp}^3$  carbon ratio, a measure of the extent of disorder [39, 40], the blue-shift and the increase of the intensity ratio of the D and G bands of the PAA-EG+GO and PAA-EG+HB+GO fibrous mats can be attributed to the formation of covalent bonds between GO and PAA chains [37].

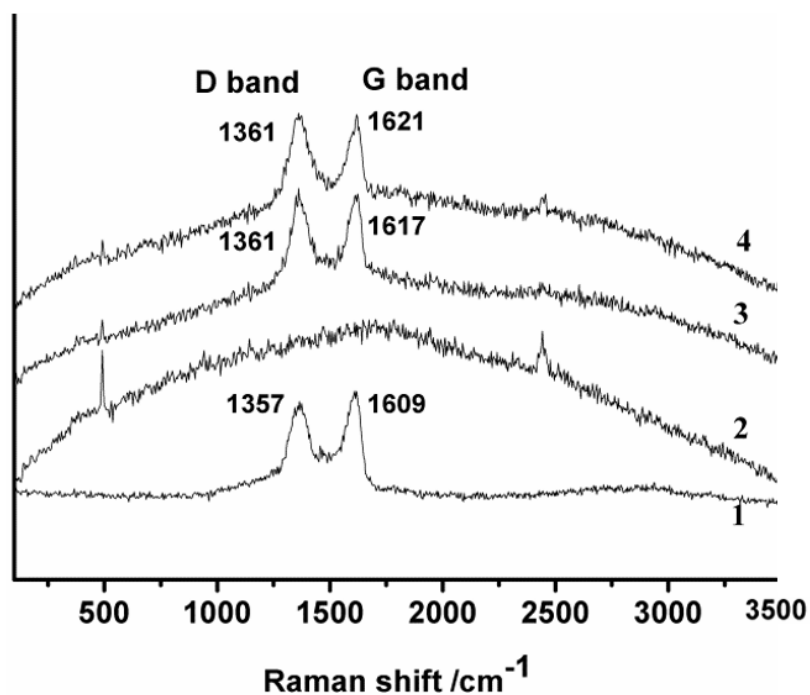


Figure 4.5 Raman spectra graph of 1) GO, 2) PAA-EG, 3) PAA-EG+GO and 4) PAA-EG+HB+GO

The interactions among PAA-EG, HB and GO were also proved by TGA testing. From Figure 4.6, two main weight loss regions are found in the PAA-EG and PAA-EG hybrid NFN mats. The first weight loss region (~150-270 °C) is assigned to the decomposition of the ester bond between PAA and EG. The significant weight loss in the second region (~270-500 °C) is assigned to the decomposition of polymer backbone and hydroxyethyl groups [41]. The decomposition temperatures increase in the order PAA-EG, PAA-EG+HB, PAA-EG+GO, and PAA-EG+HB+GO hybrid NFN mats, with the same weight loss in each of two main regions. Thus it can be concluded that the PAA-EG matrix with HB and GO incorporated has improved thermal stability. When HB is added into the PAA-EG, the profused -OH groups in HB [30] can react with -COOH groups in the PAA during the crosslinking process (as proved by FTIR), leading to strong interfacial adhesion between HB and the PAA matrix. The thermal stability of PAA-EG+HB increases because of the increased likelihood of formation of covalent bonding with the addition of HB. The addition of GO also increases the decomposition temperature of the PAA-EG matrix due to the confinement effect

of well-dispersed GO on the mobility of PAA-EG segmental chains [42]. The decomposition temperature of the PAA-EG+HB+GO is even higher than that of the PAA-EG+HB and PAA-EG+GO hybrid NFN mats due to the synergistic effects of GO and HB in the system [42].

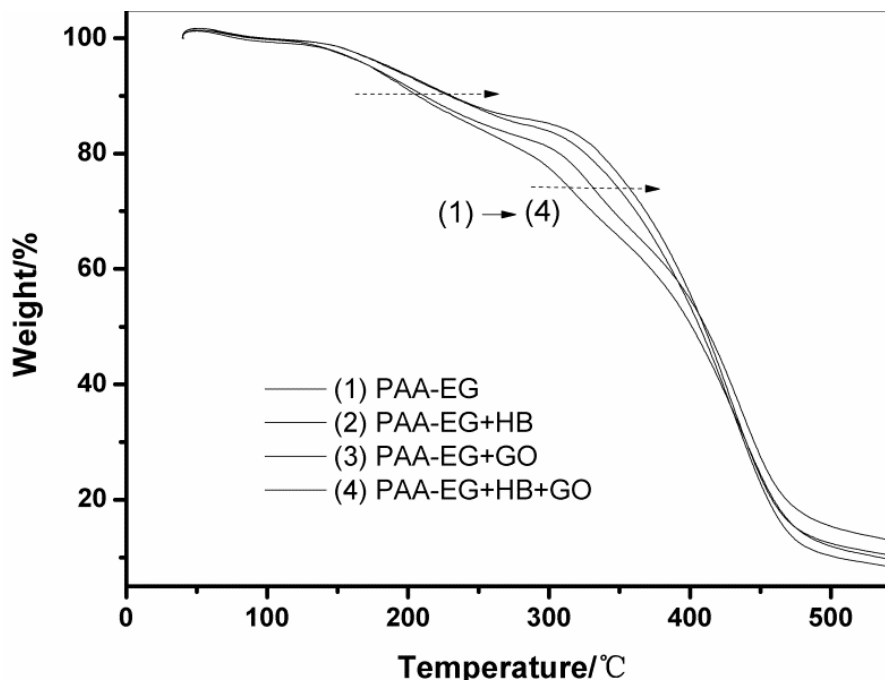


Figure 4.6 TGA curves of 1) PAA-EG, 2) PAA-EG+HB, 3) PAA-EG+GO and 4) PAA-EG+HB+GO fibrous mats

The specific surface area (SSA) shows a remarkable difference between the PAA and PAA hybrid NFN mats. The SSAs were  $7.03 \text{ m}^2\cdot\text{g}^{-1}$  for the PAA-EG and  $40.98$ ,  $12.87$ , and  $79.27 \text{ m}^2\cdot\text{g}^{-1}$  for the PAA-EG+HB, PAA-EG+GO, and PAA-EG+GO+HB, respectively (Table 4.1). This contributes to the spiderweb-like nanowebs formed between the main electrospun fibers in PAA-EG+HB, PAA-EG+GO, PAA-EG +GO+HB hybrid NFN mats (Figure 4.3(b and d)). The addition of HB and GO is highly effective for inducing the splitting of sub-nanofibers from the main fibers, which obviously increases the absorptiveness of the fibrous mats.

Table 4.1 BET specific surface area of PAA and PAA hybrid NFN mats

Sample	PAA-EG	PAA-EG +HB	PAA-EG+GO	PAA-EG+GO+HB
Specific surface area ( $\text{m}^2\cdot\text{g}^{-1}$ )	7.03	40.98	12.87	79.27

The water absorption properties of PAA-EG, PAA-EG+HB, PAA-EG+GO, and PAA EG+HB+GO hybrid NFN mats were investigated by immersing the hybrid NFN mats in Milli-Q water and the results are shown in Figure 4.7. The water absorption of all samples increased with the increase of time, occurring rapidly at the beginning (0-6 h) (Figure 4.7(a)). The PAA-EG sample shows a 59.1% increase from its initial weight. With the introduction of HB and GO, the water absorption capacity of the PAA-EG+HB, PAA-EG+GO, and PAA-EG+HB+GO increased by 72.6%, 66.2%, and 76.6%, respectively, 1.23, 1.12, and 1.30 times higher than that of the PAA-EG sample. After 24 h immersion, the water absorption of PAA-EG increases slowly, but there is still obvious increase in the water absorption capacity of the PAA-EG hybrid fibrous mats with incorporation of HB or GO. The water absorption of the PAA-EG fibrous mat is 121% higher than its original weight after 48 h immersion. For the hybrid mats, the water absorption of PAA-EG+HB, PAA-EG+GO, and PAA-EG+HB+GO reaches 158%, 199%, and 208%, 1.31, 1.64, and 1.72 times higher than that of the PAA-EG sample.

The increased water absorption of the materials incorporating HB and/or GO may be due to two main reasons. First, the spiderweb structure formed in the hybrid mat with the addition of HB and GO (Figure 4.7(c)) has a high aspect ratio as proved by BET test (Table 4.1), which can greatly increase absorption [43]. Second, the increased water absorption of the materials incorporating HB or GO may be due to the good dispersion of functionalized hydrophilic particles (-OH groups in

HB, -COOH, and -OH groups in GO) in the PAA structure acting as ‘water channels’ to enhance water distribution in the hydrogel structure [37, 44].

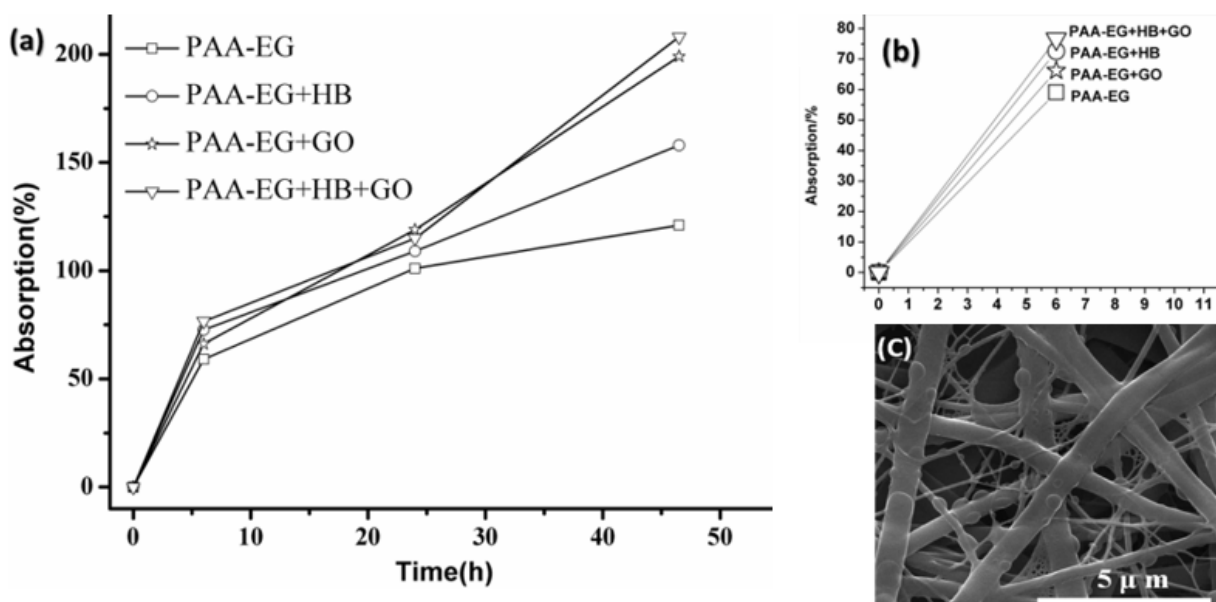


Figure 4.7 (a) Water absorption properties of PAA-EG, PAA-EG+HB, PAA-EG+GO and PAA-EG+HB+GO fibrous mats, (b) Water absorption properties of PAA-EG, PAA-EG+HB, PAA-EG+GO and PAA-EG+HB+GO fibrous mats in 6 h, (c) SEM image of PAA-EG+HB+GO fibrous mat

Application fields based on the use of electrospun fibers have steadily extended in recent years, now including composite reinforcement, filtration, biomedical applications, protective clothing, sensors, and so on [45-47]. From the high water absorption capacity of PAA-EG and its hybrid fibrous mat, the water absorption ability of WSR is further improved by introducing this fibrous mat as water channels. The current convenient physical mixing method for the preparation of WSR entails the major problem of phase separation because of the distinction between

hydrophobic rubber and hydrophilic SAP, such that the two phases in the blend system are not compatible, the SAP cannot disperse well in rubber and it easily drops out of rubber networks [48, 49]. In this work, the PAA was *in-situ* crosslinked with EG during the rubber curing process, and the silica coupling agent was used to improve the dispersion of PAA in the WSR. Multi-scale hybrid fibrous mats were selected and added into the WSR to further enhance its water swelling ability. The water absorption of five composites was investigated. As shown in Figure 4.8, the water absorption of the five samples increased rapidly at the beginning. The conventional WSR (PAA-EG) increased 2.96% in 24 h. With the addition of the fibrous mats, the water absorption of WSR+PAA-EG, WSR+PAA-EG+HB, WSR+PAA-EG+GO, and WSR+PAA-EG+HB+GO composites increased 3.31, 3.07, 3.23, and 3.11% respectively, which were higher than that of original WSR.

The water absorption rates of the composites increased with incorporation of the fibrous mats. After the 1000 h water immersion test, the water absorption of the five composites reached a balance value. The conventional WSR and the WSR+PAA-EG+HB+GO composites were ~1.5 times larger than before absorbing water (Figure 4.8(c)). It has been proved that if WSR is immersed in water, the hydrophilic component within it absorbs water and an expansion force is exerted. The greater the amount of absorbed water, the higher the expansion forces. When the expansion force reaches the balance value restriction of the elastomer, an equilibrium of swelling is achieved [49].

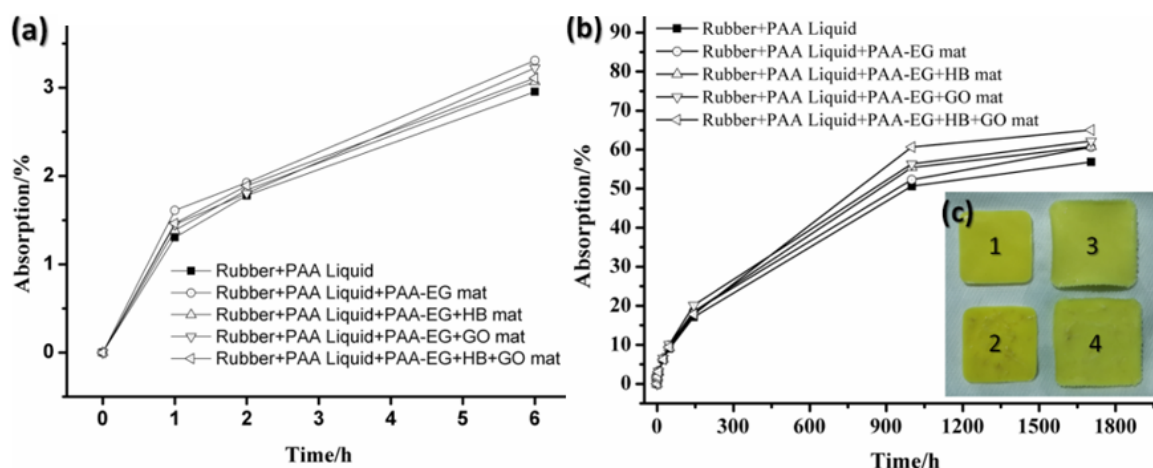


Figure 4.8 Water absorption ability of five composites in (a) 0-6 h and (b) 0-1800 h, and (c) photos of the conventional WSR (1) before and (3) after absorbing water for 1000 h, and WSR+PAA-EG+HB+GO (2) before and (4) after absorbing water for 1000 h

The water absorption of the original WSR increased 56.84% in 1800 h and the water absorption of the WSR+PAA-EG, WSR+PAA-EG+HB, WSR+PAA-EG+GO, and WSR+PAA-EG+HB+GO composites increased 60.65, 60.79, 62.21, and 65.04% respectively, being 3.81, 3.95, 5.37, and 8.2% higher than that of original WSR. The fibrous mats acting as water channels could rapidly induce water into the rubber and improve the water absorption due to the high absorption properties of the composites. Moreover, by bonding to SAP particles, the mats also prevented migration of SAP from the rubber. As a result, better water swelling ability was achieved, as shown in the schematics (Figure 4.9).

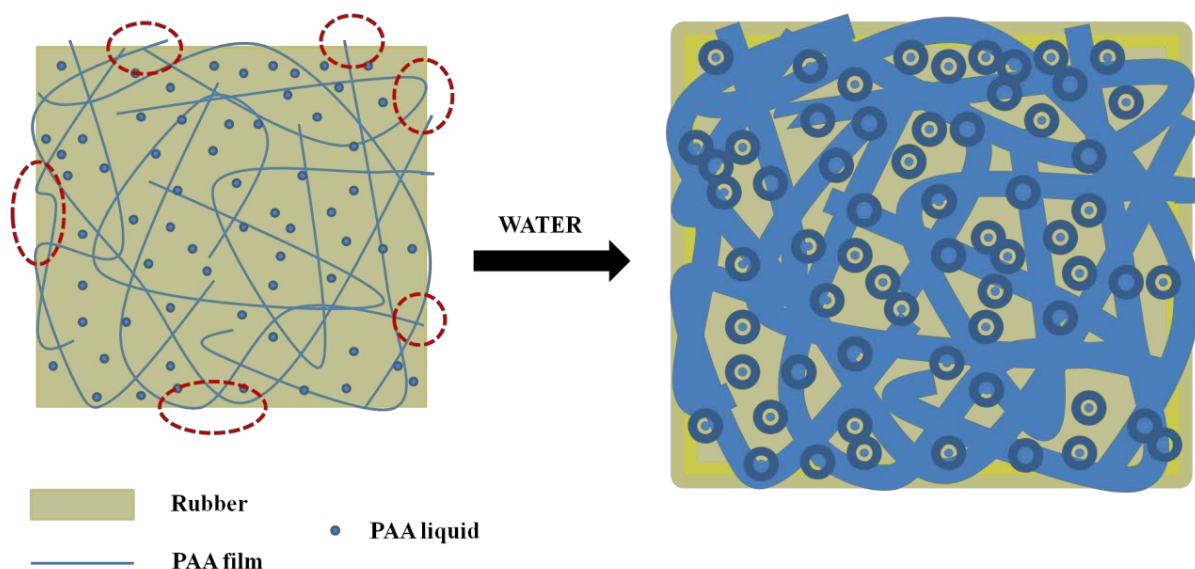


Figure 4.9 Schematics of water channel in WSR containing electrospun NFN mat

#### 4.5 Conclusions

Superabsorbent SAP fiber mats with hyperbranched polymer and/or graphene oxide having multi-scaled structure fibers were electrospun. The mats with fibers of nano- and submicro-diameter had enhanced water swelling abilities (swelling rate and swelling ratio). When hyperbranched polymer and graphene oxide were added, the hybrid mats showed synergistic effects on water swelling ability, due to the formation of spiderweb-like multi-scale structures and increased specific surface areas. The electrospun fiber mats were added into conventional rubber by simple physical mixing and the rubber composites showed considerable enhancement of water swelling ability, mainly due to the water channels built by the multi-scaled fiber mats to link the isolated superabsorbent particles together within the hydrophobic rubber matrix. The rubber composite containing hybrid fillers (hyperbranched polymer and graphene oxide) showed the highest water swelling ability (both short- and long-term) compared to the other rubber composites. The proposed enhancement mechanisms are illustrated as well. In next stage, highly elastic styrene-butadiene-

styrene (SBS) nanofibers with high tensile strength seems to be an effective choice to strengthen mechanical properties of WSR due to its miscibility with rubber.

#### 4.6 References

1. Wang, G., Li, M. and Chen, X., 1998. Preparation and water-absorbent properties of a water-swellaable rubber. *Journal of applied polymer science*, 68(8), pp.1219-1225.
2. Wang, G., Li, M. and Chen, X., 1999. Effects of fillers on mechanical properties of a water-swellaable rubber. *Journal of applied polymer science*, 72(4), pp.577-584.
3. Razzak, M.T., Otsuhata, K., Tabata, Y., Ohashi, F. and Takeuchi, A., 1988. Modification of natural rubber tubes for biomaterials I. Radiation-induced grafting of N, N-dimethyl acrylamide onto natural rubber tubes. *Journal of applied polymer science*, 36(3), pp.645-653.
4. Xie, Z., Li, M., Chen, X., Hu, H. and Li, S., 1996. Studies on water-swellaable elastomer. I. Synthesis and characterization of amphiphilic polymer. *Journal of applied polymer science*, 61(3), pp.495-499.
5. Yamashita, S., Kodama, K., Ikeda, Y. and Kohjiya, S., 1993. Chemical modification of butyl rubber. I. Synthesis and properties of poly (ethylene oxide)-grafted butyl rubber. *Journal of Polymer Science Part A: Polymer Chemistry*, 31(10), pp.2437-2444.
6. Song, S.S., Qi, H.B. and Wu, Y.P., 2011. Preparation and properties of water-absorbent composites of chloroprene rubber, starch, and sodium acrylate. *Polymers for Advanced Technologies*, 22(12), pp.1778-1785.

7. Zhang, G., Zhang, Z., Xie, F., Hu, X., Luo, X. and Chen, X., 2000. Chlorohydrin water swellable rubber compatibilized by an amphiphilic graft copolymer. I. Synthesis and characterization of compatibilizer PVA-g-PBA. *Journal of applied polymer science*, 75(8), pp.977-986.
8. Nakason, C., Nakaramontri, Y., Kaesaman, A., Kangwansukpamonkon, W. and Kiatkamjornwong, S., 2013. Synthesis and characterization of water swellable natural rubber vulcanizates. *European Polymer Journal*, 49(5), pp.1098-1110.
9. Li, S., Lang, F., Du, F. and Wang, Z., 2014. Water-swellable thermoplastic vulcanizates based on ethylene–vinyl acetate copolymer/chlorinated polyethylene/cross-linked sodium polyacrylate/nitrile butadiene rubber blends. *Journal of Thermoplastic Composite Materials*, 27(8), pp.1112-1126.
10. Amnuaypanich, S., Patthana, J. and Phinyocheep, P., 2009. Mixed matrix membranes prepared from natural rubber/poly (vinyl alcohol) semi-interpenetrating polymer network (NR/PVA semi-IPN) incorporating with zeolite 4A for the pervaporation dehydration of water–ethanol mixtures. *Chemical Engineering Science*, 64(23), pp.4908-4918.
11. Tao, L., Jing-Xin, L. and Xin-Yuan, L., 2007. Preparation and properties of volume expansion type blends of plasticized polyvinyl chloride/starch graft polyacrylate sodium. *Polymer-Plastics Technology and Engineering*, 46(6), pp.569-573.
12. Zhang, Z., Zhang, G., Li, D., Liu, Z. and Chen, X., 1999. Chlorohydrin water-swellable rubber compatibilized by an amphiphilic graft copolymer. II. Effects of PVA-g-PBA and CPA on water-swelling behaviors. *Journal of applied polymer science*, 74(13), pp.3145-3152.

13. Dehbari, N., Zhao, J., Peng, R. and Tang, Y., 2015. Neutralisation and compatibilisation effects on novel water-swellaable rubber composites. *Journal of Materials Science*, 50(15), pp.5157-5164.
14. Subbiah, T., Bhat, G.S., Tock, R.W., Parameswaran, S. and Ramkumar, S.S., 2005. Electrospinning of nanofibers. *Journal of Applied Polymer Science*, 96(2), pp.557-569.
15. Kim, J.S. and Reneker, D.H., 1999. Mechanical properties of composites using ultrafine electrospun fibers. *Polymer composites*, 20(1), pp.124-131.
16. Huang, Z.M., Zhang, Y.Z., Kotaki, M. and Ramakrishna, S., 2003. A review on polymer nanofibers by electrospinning and their applications in nanocomposites. *Composites science and technology*, 63(15), pp.2223-2253.
17. Pillay, V., Dott, C., Choonara, Y.E., Tyagi, C., Tomar, L., Kumar, P., du Toit, L.C. and Ndesendo, V.M., 2013. A review of the effect of processing variables on the fabrication of electrospun nanofibers for drug delivery applications. *Journal of Nanomaterials*, 2013.
18. Ding, B., Li, C., Miyauchi, Y., Kuwaki, O. and Shiratori, S., 2006. Formation of novel 2D polymer nanowebs via electrospinning. *Nanotechnology*, 17(15), p.3685.
19. Wang, X., Ding, B., Sun, G., Wang, M. and Yu, J., 2013. Electro-spinning/netting: a strategy for the fabrication of three-dimensional polymer nano-fiber/nets. *Progress in Materials Science*, 58(8), pp.1173-1243.
20. Ding, B., Wang, X., Yu, J. and Wang, M., 2011. Polyamide 6 composite nano-fiber/net functionalized by polyethyleneimine on quartz crystal microbalance for highly sensitive formaldehyde sensors. *Journal of Materials Chemistry*, 21(34), pp.12784-12792.

21. Panthi, G., Barakat, N.A., Risal, P., Yousef, A., Pant, B., Unnithan, A.R. and Kim, H.Y., 2013. Preparation and characterization of nylon-6/gelatin composite nanofibers via electrospinning for biomedical applications. *Fibers and Polymers*, 14(5), pp.718-723.
22. Hassan, M.S., Amna, T., Sheikh, F.A., Al-Deyab, S.S., Choi, K.E., Hwang, I.H. and Khil, M.S., 2013. Bimetallic Zn/Ag doped polyurethane spider net composite nanofibers: a novel multipurpose electrospun mat. *Ceramics International*, 39(3), pp.2503-2510.
23. Abdal-Hay, A., Mousa, H.M., Khan, A., Vanegas, P. and Lim, J.H., 2014. TiO<sub>2</sub> nanorods coated onto nylon 6 nanofibers using hydrothermal treatment with improved mechanical properties. *Colloids and Surfaces A: Physicochemical and Engineering Aspects*, 457, pp.275-281.
24. Cao, A., Liu, Z., Chu, S., Wu, M., Ye, Z., Cai, Z., Chang, Y., Wang, S., Gong, Q. and Liu, Y., 2010. A Facile One-step Method to Produce Graphene–CdS Quantum Dot Nanocomposites as Promising Optoelectronic Materials. *Advanced materials*, 22(1), pp.103-106.
25. Kovtyukhova, N.I., Ollivier, P.J., Martin, B.R., Mallouk, T.E., Chizhik, S.A., Buzaneva, E.V. and Gorchinskiy, A.D., 1999. Layer-by-layer assembly of ultrathin composite films from micron-sized graphite oxide sheets and polycations. *Chemistry of Materials*, 11(3), pp.771-778.
26. Yang, Y.K., He, C.E., He, W.J., Yu, L.J., Peng, R.G., Xie, X.L., Wang, X.B. and Mai, Y.W., 2011. Reduction of silver nanoparticles onto graphene oxide nanosheets with N, N-dimethylformamide and SERS activities of GO/Ag composites. *Journal of Nanoparticle Research*, 13(10), p.5571.

27. Meng, L., Klinkajon, W., Harkin, S., Supaphol, P. and Wnek, G.E., 2015. Electrospun crosslinked poly (acrylic acid) fiber constructs: towards a synthetic model of the cortical layer of nerve. *Polymer International*, 64(1), pp.42-48.
28. Ding, B., Wang, M., Wang, X., Yu, J. and Sun, G., 2010. Electrospun nanomaterials for ultrasensitive sensors. *Materials Today*, 13(11), pp.16-27.
29. Heikkilä, P. and Harlin, A., 2008. Parameter study of electrospinning of polyamide-6. *European Polymer Journal*, 44(10), pp.3067-3079.
30. Adrjanowicz, K., Kaminski, K., Dulski, M., Jasiurkowska-Delaporte, M., Kolodziejczyk, K., Jarek, M., Bartkowiak, G., Hawelek, L., Jurga, S. and Paluch, M., 2014. Dynamic glass transition and electrical conductivity behavior dominated by proton hopping mechanism studied in the family of hyperbranched bis-MPA polyesters. *Macromolecules*, 47(16), pp.5798-5807.
31. Pant, H.R., Bajgai, M.P., Nam, K.T., Seo, Y.A., Pandeya, D.R., Hong, S.T. and Kim, H.Y., 2011. Electrospun nylon-6 spider-net like nanofiber mat containing TiO<sub>2</sub> nanoparticles: a multifunctional nanocomposite textile material. *Journal of hazardous materials*, 185(1), pp.124-130.
32. Dong, Y., Mosaval, T., Haroosh, H.J., Umer, R., Takagi, H. and Lau, K.T., 2014. The potential use of electrospun polylactic acid nanofibers as alternative reinforcements in an epoxy composite system. *Journal of Polymer Science Part B: Polymer Physics*, 52(9), pp.618-623.
33. Shaikh, J.S., Pawar, R.C., Moholkar, A.V., Kim, J.H. and Patil, P.S., 2011. CuO-PAA hybrid films: Chemical synthesis and supercapacitor behavior. *Applied surface science*, 257(9), pp.4389-4397.

34. Zhang, J., Zhang, P., Ma, K., Han, F., Chen, G. and Wei, X., 2008. Hydrogen bonding interactions between ethylene glycol and water: density, excess molar volume, and spectral study. *Science in China Series B: Chemistry*, 51(5), pp.420-426.
35. Žagar, E. and Grdadolnik, J., 2003. An infrared spectroscopic study of H-bond network in hyperbranched polyester polyol. *Journal of molecular structure*, 658(3), pp.143-152.
36. Lin, J., Tang, Q., Wu, J. and Hao, S., 2007. The synthesis and electrical conductivity of a polyacrylate/graphite hydrogel. *Reactive and Functional Polymers*, 67(4), pp.275-281.
37. Peng, R., Yu, Y., Chen, S., Yang, Y. and Tang, Y., 2014. Conductive nanocomposite hydrogels with self-healing property. *RSC Advances*, 4(66), pp.35149-35155.
38. Kim, Y.K. and Min, D.H., 2012. Preparation of the hybrid film of poly (allylamine hydrochloride)-functionalized graphene oxide and gold nanoparticle and its application for laser-induced desorption/ionization of small molecules. *Langmuir*, 28(9), pp.4453-4458.
39. Fang, M., Wang, K., Lu, H., Yang, Y. and Nutt, S., 2009. Covalent polymer functionalization of graphene nanosheets and mechanical properties of composites. *Journal of Materials Chemistry*, 19(38), pp.7098-7105.
40. Bose, S., Kuila, T., Uddin, M.E., Kim, N.H., Lau, A.K. and Lee, J.H., 2010. In-situ synthesis and characterization of electrically conductive polypyrrole/graphene nanocomposites. *Polymer*, 51(25), pp.5921-5928.
41. Chen, S., Wu, G., Liu, Y. and Long, D., 2006. Preparation of poly (acrylic acid) grafted multiwalled carbon nanotubes by a two-step irradiation technique. *Macromolecules*, 39(1), pp.330-334.
42. Zhao, J.C., Du, F.P., Zhou, X.P., Cui, W., Wang, X.M., Zhu, H., Xie, X.L. and Mai, Y.W., 2011. Thermal conductive and electrical properties of polyurethane/hyperbranched poly

- (urea-urethane)-grafted multi-walled carbon nanotube composites. *Composites Part B: Engineering*, 42(8), pp.2111-2116.
43. Pant, H.R., Bajgai, M.P., Yi, C., Nirmala, R., Nam, K.T., Baek, W.I. and Kim, H.Y., 2010. Effect of successive electrospinning and the strength of hydrogen bond on the morphology of electrospun nylon-6 nanofibers. *Colloids and Surfaces A: Physicochemical and Engineering Aspects*, 370(1), pp.87-94.
44. Yu, Y., De Andrade, L.C.X., Fang, L., Ma, J., Zhang, W. and Tang, Y., 2015. Graphene oxide and hyperbranched polymer-toughened hydrogels with improved absorption properties and durability. *Journal of Materials Science*, 50(9), pp.3457-3466.
45. Huang, Z.M., Zhang, Y.Z., Kotaki, M. and Ramakrishna, S., 2003. A review on polymer nanofibers by electrospinning and their applications in nanocomposites. *Composites science and technology*, 63(15), pp.2223-2253.
46. Coleman, J.N., Khan, U., Blau, W.J. and Gun'ko, Y.K., 2006. Small but strong: a review of the mechanical properties of carbon nanotube-polymer composites. *Carbon*, 44(9), pp.1624-1652.
47. Pham, Q.P., Sharma, U. and Mikos, A.G., 2006. Electrospinning of polymeric nanofibers for tissue engineering applications: a review. *Tissue engineering*, 12(5), pp.1197-1211.
48. Zhang, Z., Zhang, G., Zhang, Y., Wang, Z., Yu, D., Hu, X., Hu, C. and Tang, X., 2004. Mechanical properties, water swelling behavior, and morphology of swellable rubber compatibilized by PVA-g-PBA. *Polymer Engineering & Science*, 44(1), pp.72-78.
49. Zhang, Y., He, P., Zou, Q. and He, B., 2004. Preparation and properties of water-swellaible elastomer. *Journal of applied polymer science*, 93(4), pp.1719-1723.

## **5. [ENHANCING WATER SWELLING ABILITY AND MECHANICAL PROPERTIES OF WATER SWELLABLE RUBBER BY PAA/SBS NANOFIBER MATS<sup>1</sup>]**

This chapter regards to the experimental work used to improve water swelling ability of WSR as well as mechanical strength and extensibility. By using double needle electrospinning technique to nanofiber mats of PAA, SBS and PAA/SBS have been prepared, characterized, tested and then added to WSR. The mechanisms of the nanofiber mats in enhancing the mechanical and water swelling properties of WSR are also discussed here.

1. This work has been published in Journal of Applied Polymer Science: Nazila Dehbari, Javad Tavakoli, Jinchao Zhao, and Youhong Tang. "Enhancing water swelling ability and mechanical properties of water-swellaable rubber by PAA/SBS nanofiber mats." Journal of Applied Polymer Science 133, no. 47 (2016) DOI: 10.1002/app.44213.

## 5.1 Introduction

WSRs are classified into rubber parts with high resilience, elasticity, toughness and stretchability and water absorption parts with super water absorption ability at the same time [1,2]. In terms of their ability to absorb and retain water, these kind of new materials are generally used for sealing applications as well as food and biomedical industries [3-7]. WSRs are normally prepared by multicomponent blending of a rubber matrix, superabsorbent polymers (SAP) and other hydrophilic/hydrophobic fillers through physical mixing, mechanical blending or chemical surface grafting. Chemical methods are less environmental friendly, complicated and expensive in comparison with other methods [2, 8-11].

Poor WSR's mechanical property is the major problem that limits their application, while affected diversely by swelling stability. With regard to the high hydrophilic polar characterization of SAPs, which is in contrast with the hydrophobic nonpolar properties of the rubber, SAP particles' aggregation as well as poor interface property and nonhomogeneous dispersion, often lead to remarkable poor mechanical properties, instability of water-swelling characterization and long-term water retention [1, 9, 12, 13]. Therefore, miscibility of SAP and rubber, with respect to promote mechanical properties, needs to be improved.

Introducing a compatibilizer is one of the immediate effective methods to enhance dispersion of two immiscible components that can react with both hydrophobic rubber matrix and hydrophilic SAPs [14]. In our previous research it was shown that using (3-aminopropyl)-triethoxysilane as a compatibilizer has a great impact on physical properties of WSR composites [15]. However, trapped SAPs within the rubber matrix had remained isolated. In previous chapter, with further experiments, we observed that poly (acrylic acid) (PAA) nanofibers in WSR composites were able to produce feasible connections between SAPs known as water channel [16], hence water had transferred between SAPs efficiently. Furthermore, introducing nanofibers/mats

into WSR composites shows a significant improvement in mechanical properties of WSR that depends on nanofibers types [17-20]. Among nanofibers, highly elastic poly (styrene-butadiene-styrene) (SBS) nanofibers with high tensile strength are known to be a good choice for WSRs' mechanical properties enhancement [21-24]. It seems that hydrophobic properties of rubber matrix and SBS nanofibers leads to appropriate composite's constituents miscibility and results in a better stress distribution.

Herein, contribution of SBS and PAA nanofibers, produced by double needle electrospinning method, on mechanical and swelling properties improvement of WSRs composites was investigated. The aim of this chapter was two folds: firstly, to understand how WSRs' mechanical properties may subjected to changes by introducing different types of nanofibers (PAA, SBS and PAA/SBS). The second, an investigation into the role of those nanofibers on swelling properties (first and second swelling) of WSR composites.

## **5.2 Experiments**

### **5.2.1 Materials and Sample preparation**

Poly acrylic acid particles (PAA, average  $M_w \sim 450\,000\text{ g}\cdot\text{mol}^{-1}$ ), poly (acrylic acid) solution (average  $M_w \sim 250\,000\text{ g}\cdot\text{mol}^{-1}$ ), ethylene glycol (EG) (anhydrous, 99.8%), sulfuric acid, dimethylformamide (DMF), tetrahydrofuran (THF), (3-Aminopropyl)-triethoxysilane used as a compatibilizer were purchased from Sigma Aldrich. Styrene-butadiene-styrene triblock copolymer (SBS) granules is supplied by ueyang Bailing Huaxing Chemicals Co., Ltd. (Yueyang, China) (average  $M_w \sim 300,000\text{ g/mol}$ ), and banana skin silicone rubber was purchased from Barnes products Pty Ltd, Australia. All chemicals used without any purification. All aqueous solutions were prepared using Milli-Q water at 25 °C.

The PAA solution was prepared according to previous work [25, 26]. For the SBS solution, 12 g of SBS was dissolved in the mixed solution of 13.67 g DMF and 41 g of THF with stirring. Solution electrospinning was performed by a fully automatic equipment (NaBond Technologies TL01, China) consisting of a syringe-flat tip needle and a high voltage supply. In order to obtain the best nanofibers without beads, PAA and SBS solutions were electrospun with two needles at the voltage of 15 KV, feeding rate of  $1.5 \text{ mLh}^{-1}$  on the aluminium foil covered cylindrical collector with tip-to-collector distance of 10 cm. The x-axis moving speed of the needle and the drum speed were set at 3.5 mm/s and 200 rpm respectively. The whole electrospinning process lasted for about 2 hrs for both solutions.

The obtained PAA and SBS nanofibers used in the WSR composite to strengthen its physical and mechanical properties. The composites were prepared through a solution impregnation technique as shown in Figure 5.1. In detail, 12.5 g PAA was mixed with 2 g EG (crosslinking agent), with 0.625 g sulfuric acid (dehydration agent) and 0.0625 g (3-aminopropyl)-triethoxysilane (compatibilizer) before addition to 20 g of rubber's part A. final mixture was prepared by adding 20 g of rubber's part B to solution while stirring for 10 min before moulding. Prepared PAA, SBS and PAA/SBS nanofibers with thickness of 0.04 mm with different ratio cut into  $0.5 \times 5 \text{ cm}^2$  strips were added to the final solution. The ratio of PAA nanofibers were kept constant in all composites to investigate the role of SBS nanofibers inside the composite (1% wt PAA nanofiber and 2% wt PAA/SBS nanofiber, respectively). Following 24 hrs of curing at ambient temperature, WSR composites consisting PAA, SBS and PAA/SBS nanofiber were obtained. For the control experiment, conventional WSR composite was prepared under the same conditions.

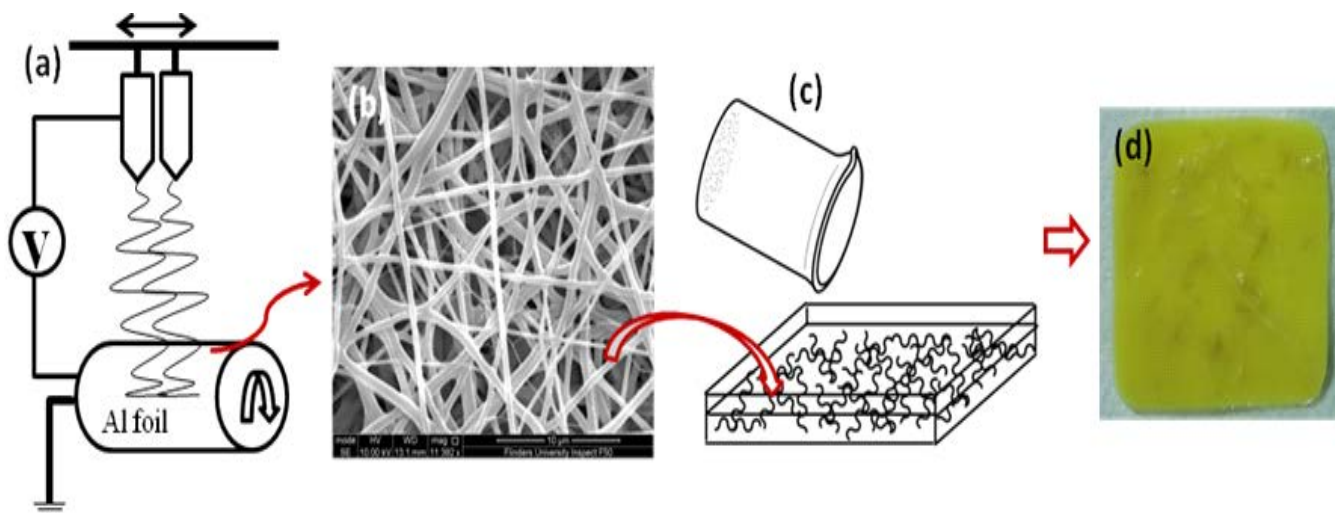


Figure 5.1 Steps of preparation of WSR enhanced with PAA/SBS nanofiber mats (a) the electrospinning machine with two needles setting, (b) the SEM image of the PAA/SBS nanofibers, (c) mixing of PAA/SBS nanofibers with WSR, and (d) the cured composite of WSR+PAA/SBS nanofibers

### 5.2.2 Characterizations

The surface morphology and distribution of the electrospun PAA and SBS nanofibers and all composite samples before and after swelling were characterized using scanning electron microscopy (FEI Inspect F50, US). Prior of using SEM, the K575X sputter coater was used for deposition of a very thin platinum film (~2 nm) on the surface of all samples. The average diameter of nanofibers obtained from SEM was measured by an image J software and compared with diameter of nanofibers inside the composite before and after swelling for further investigation. The surface wettability, surface tension and contact angle measurements of nanofibers and all composites were carried out with a Sinterface machine. The mechanical properties including, elongation at breaking point, ultimate strength and extensibility of nanofibers and composites before and after immersing in water were measured by Instron (USA). All reported mechanical results represent average values from three samples with the same dimensions, the force-stretch

curves are reported due to the large deformation occurred in the samples. Swelling behaviours of WSR composites were tested by measuring the initial weight of the dry samples ( $m_0$ ) and subsequently after they were immersed in Milli-Q water (500 mL) at 25 °C from 1 hr to several days. The swollen sample was then weighed at regular intervals ( $m_1$ ). The reported results represent the average values from three samples. Before measuring the weight of the swollen samples, the excess surface water was removed by filter papers. The swelling ratio was calculated using the following equation:

$$\frac{m_1 - m_0}{m_0} \times 100$$

To investigate the effect of PAA nanofibers inside WSR matrix, repeating swelling test was also performed. Each sample was dried at 70 °C until it achieved a constant weight. Then, they were again immersed in water at room temperature. At a specified time, they were taken out and the excess moisture on the surface was removed. The swelling ratio was calculated using the following equation:

$$\frac{m_3 - m_2}{m_2} \times 100$$

where,  $m_2$  and  $m_3$  were the weights of a sample before and after the second water swelling, respectively. To make sure ultrafine PAA nanofibers remained into composites after swelling experiment, all samples are dried, weighted, and compared with initial weight.

## 5.3 Results and discussion

### 5.3.1 Morphology

SEM images of PAA, SBS, and PAA/SBS nanofiber mats and WSR including PAA/SBS nanofibers (WSR+PAA/SBS) before and after swelling are shown in Figure 5.2. The average

diameter of PAA and SBS is about 0.65 and 0.96  $\mu\text{m}$ , respectively (Figure 5.2 a and b). The image of the PAA/SBS nanofiber mat (Figure 5.2 c) indicates that an interlinked structure composed of SBS and PAA nanofiber mats was prepared. The use of double needle electrospinning was effective for creating an entangled network consisting of two different types of fiber with sizes ranging from submicron to nanometre. Arrangement of these fibers resulted in the formation of a spider web-like structure [27–29] that increased the hydrophilicity and specific surface area while also affecting porosity. Figure 5.2 d) shows a WSR composite with randomly distributed PAA/SBS nanofibers in the dry state. After immersion in water, PAA nanofibers showed a slight increase in diameter (0.93  $\mu\text{m}$  in average) and an increase in their tendency to take up water. Unsurprisingly, the size of SBS nanofibers that were embedded in rubber matrix remained unchanged from that of SBS nanofibers in the dry state.

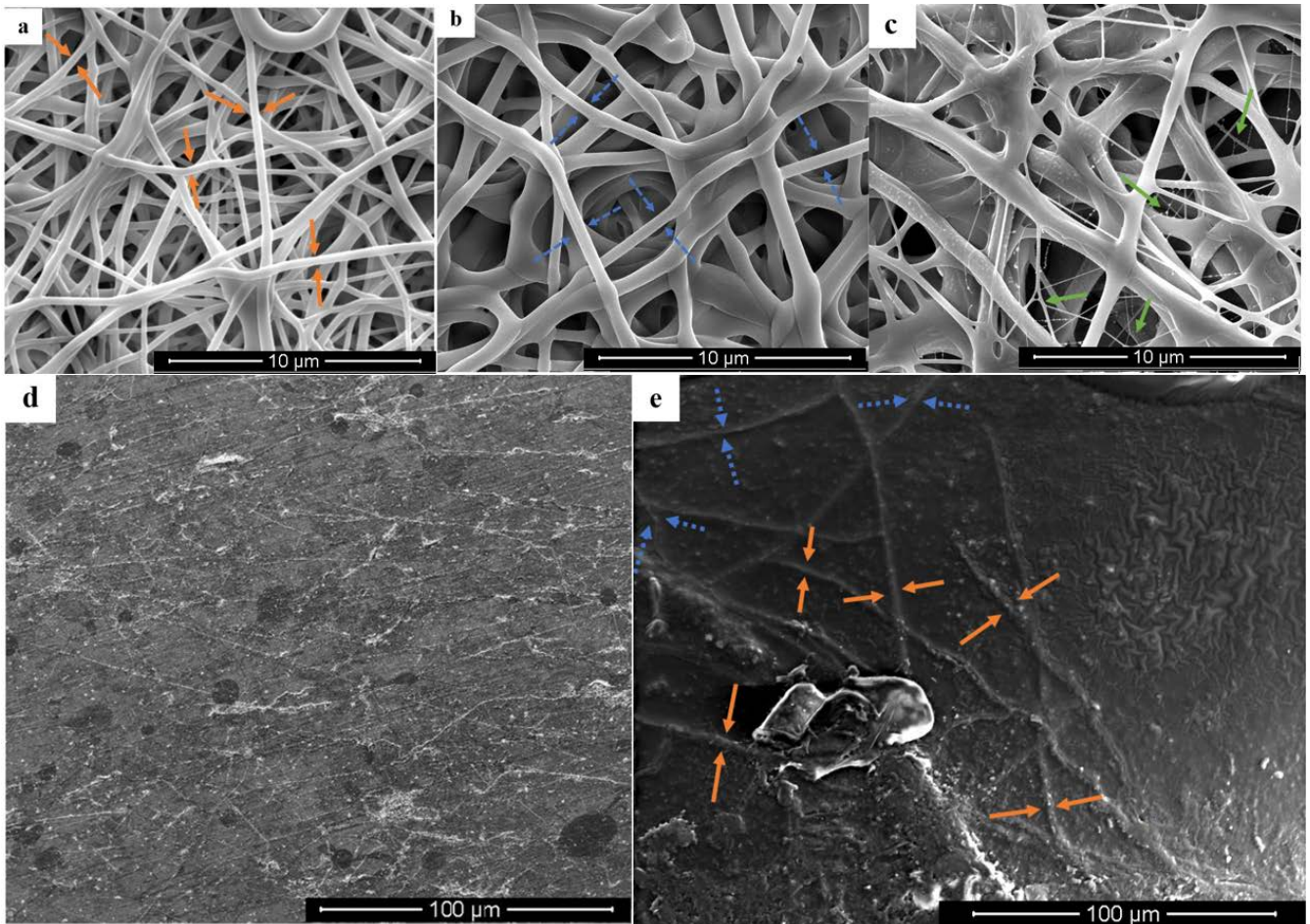


Figure 5.2 SEM micrographs of (a) PAA nanofibers with average diameter of 0.65  $\mu\text{m}$  (solid orange arrows), (b) SBS nanofibers with average diameter of 0.95  $\mu\text{m}$  (dashed blue arrows), (c) PAA/SBS nanofibers with some spider web-like structures (solid green arrows), and WSR+PAA/SBS composites (d) before and (e) after swelling, the bold channels representing PAA nanofibers that have absorbed water (solid orange arrows)

### 5.3.2 Contact angle of nanofiber mats

As was shown in Figure 5.3, the surface hydrophilicity of the SBS nanofiber mat (Figure 5.3 a) is very different from that of the PAA/SBS nanofiber mat (Figure 5.3 b). A significant decrease in contact angle in the PAA/SBS nanofiber mat, from  $117^\circ$  in Figure 5.3 a) to  $73^\circ$  in Figure 5.3 b) after a drop of water has been put on the surface for 30 s, indicates that the addition of PAA nanofibers to SBS nanofibers increased surface hydrophilicity. Therefore, enhancement of the

hydrophilicity of SBS nanofibers may change the bulk properties while increasing the water uptake capability of the WSR+PAA/SBS composite.

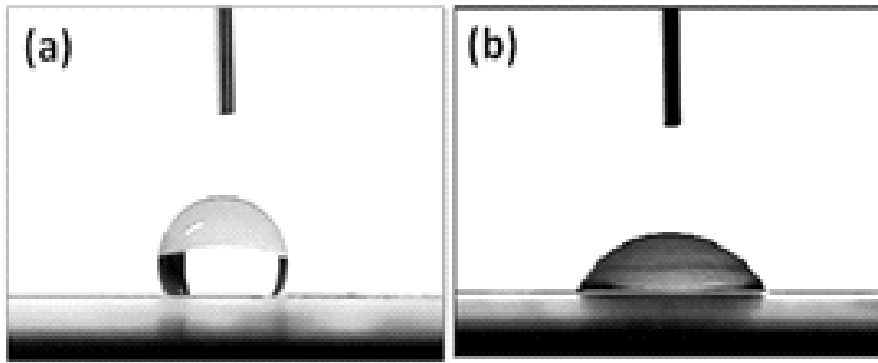


Figure 5.3 Contact angle images of (a) SBS nanofiber mat and (b) PAA/SBS nanofiber mat 30 s after a drop of water was put on the surface

### 5.3.3 Mechanical properties of nanofiber mats and composites

Figure 5.4 shows the mechanical behaviours of PAA, SBS, and PAA/SBS nanofibers in the dry state. The average elongation as well as average force at the breaking point are significantly enhanced in the PAA/SBS nanofiber mats in comparison with the PAA nanofiber mats. The mechanical contribution of super-elastic SBS nanofibers to the brittle PAA nanofiber structure—shown in SEM images to be like spider web networks with mechanical interlocking between two types of nanofibers—resulted in a better distribution of stress across the mats. This led to 15 and 7 times greater stretchability and breaking force for SBS/PAA nanofiber mats, compared to the values found for PAA nanofiber mats, respectively.

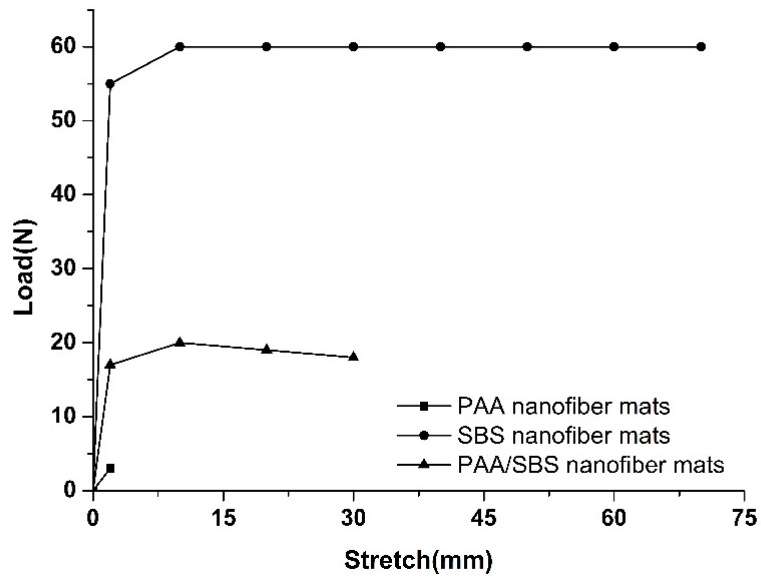


Figure 5.4 Force-stretch curves of PAA, SBS and PAA/SBS nanofiber mats

Figure 5.5 shows the load–stretch curves of composites with PAA, SBS, and PAA/SBS nanofiber mats before and after immersion in water for 1 week. A similar trend for WSR+PAA, WSR/SBS and WSR+PAA/SBS nanofiber composites was observed when compared to the trends of the nanofibers alone. In Figure 5.5 a), it can be seen that the breaking force of WSR with PAA nanofibers at the specific elongation of 20 mm increases from 4.0 N (for the conventional WSR composite) to 7.5 N. With the introduction of PAA nanofibers into WSR, however, the elongation at break decreases from 50 to 20 mm. The addition of SBS nanofiber mats to the WSR composite enhances the mechanical properties markedly from those in the dry state. Both force and elongation to break for WSR+SBS composite reaches the maximum value, i.e., 35 N and 60 mm. However, the WSR+SBS composite does not display enhanced water-swellaable ability, due to the hydrophobic characteristic of SBS. For the WSR+PAA/SBS nanofiber composite, the breaking force was twice as high as that of WSR alone, with a slight decrease in stretchability.

Figure 5.5 b) shows the mechanical properties of WSR with PAA, SBS and PAA/SBS nanofiber mats after immersing in water for 1 week. As it is appeared swelling has adverse effect on mechanical properties of WSR composites, as the elongation and force at breaking point decrease for all samples with respect to the dry state. Mechanical properties of WSR+PAA nanofiber mats and WSR+SBS nanofiber mats decrease by about 20% to 30% compared with that of WSR, however, by introducing SBS/PAA nanofiber mats into WSR, it smooths such a decrease to less than 5%.

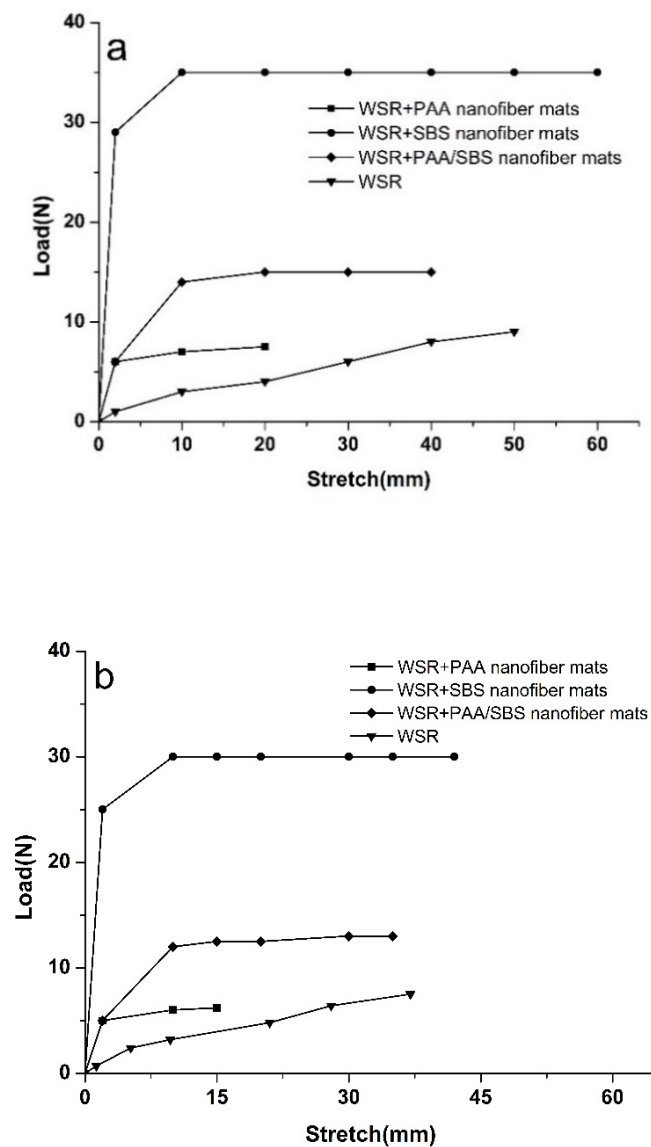


Figure 5.5 Force-stretch curves of composites with PAA, SBS and PAA/SBS nanofibers before (a) and (b) after immersing in water

Mechanical properties of PAA, SBS and PAA/SBS reinforced WSR composites before and after swelling are summarised in Table 5.1.

Table 5.1 Mechanical properties of PAA, SBS and PAA/SBS reinforced WSR composites

Sample	WSR+PAA nanofiber	WSR+SBS nanofiber	WSR+PAA/SBS nanofiber
Before swelling			
Elongation at break (mm)	20	60	40
Breaking force (N)	7.5	35	15
After swelling			
Elongation at break (mm)	15	44	37
Breaking force (N)	5.8	30	13

### 5.3.4 Swelling ratio of composites

The water absorption properties of samples for first and second swellings in water are shown in Figures 5.6 and 5.7. As we can see, initial swelling ratio of all composites for both first and second immersions in water was extremely high. In later stage, increasing of swelling ratio as a function of time become slower than that of the initial stage [30-31]. However, they did not reach to an equilibrium state after 650 hrs for both first and second immersing in water as shown in Figure 5.6.

The swelling properties of WSR improved with incorporation of PAA and PAA/SBS nanofiber mats into WSR (Figure 5.6 a). PAA constituent of PAA/SBS nanofiber mats plays an important role on absorbing water from the surface into the bulk by introducing water channels in the WSR composite.

This is consistent with our previous results [16]. As it was reported in Figure 5.6 b), all samples exhibit less swelling ratio in second swelling after 650 hrs, however, WSR+ PAA/SBS nanofiber mats composite experiences greater swelling ratio (about 40% ) at initial stage of swelling (first 6 hrs) for second swelling in comparison with that of the first swelling, as shown in Figure

5.7. Introducing of SBS/PAA nanofiber mats into WSR have great effect on second swelling at nano-level by increasing hydrophilicity of the bulk and surface of WSR. On the other hand, it is most probable to assume that those nanofibers may randomly connect SAPs to each other that lead to increasing swelling ratio in second swelling. The conventional WSR shows the same trend and amount of swelling ratio in both first and second swelling tests, so by introducing PAA/SBS nanofiber mats into WSR, water absorption rate in the initial stage has been enhanced especially in the repeated swelling periods.

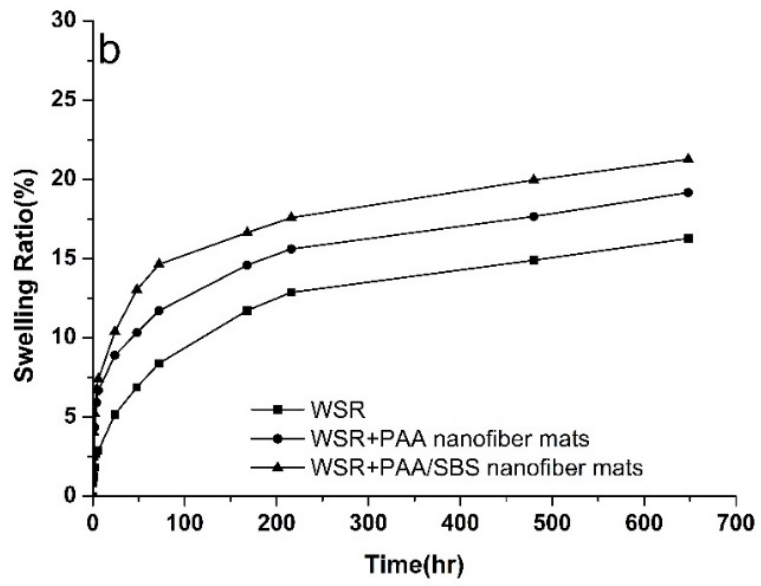
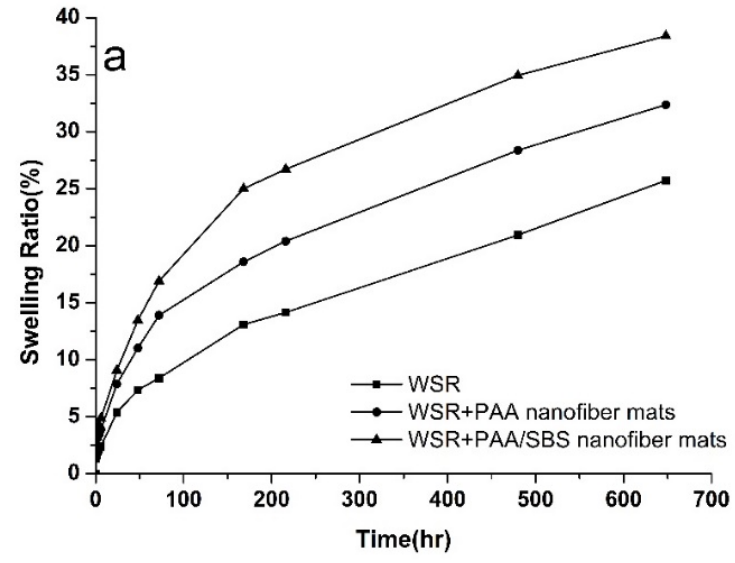


Figure 5.6 Water swellability of composites in (a) first and (b) second swellings to 650 hrs

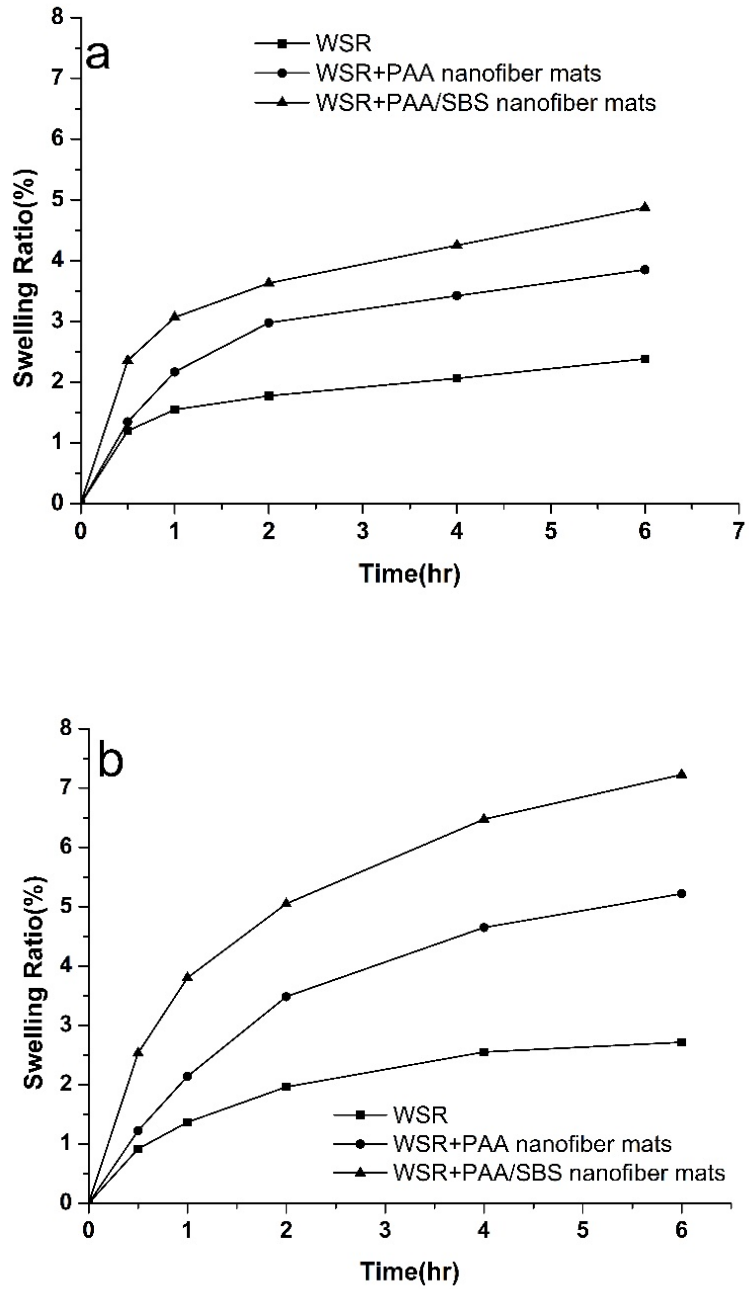


Figure 5.7 Water swellability of composites at (a) 1<sup>st</sup> and (b) 2<sup>nd</sup> absorbing periods for the first 6 hrs

#### 5.4 Mechanisms of enhanced swelling ratio and mechanical properties

The mechanical properties and swelling ratio of the WSR composites were significantly enhanced by the introduction of PAA/SBS nanofiber mats. Figure 5.8 depicts the proposed mechanism of nanofibers within the rubber after immersion in water, which was observed by SEM.

The PAA and SBS nanofibers in the PAA/SBS nanofiber mats entangled mechanically with each other to provide a spider web network within the matrix. These networks could act as the internal reinforcements to enhance the mechanical properties of WSR (similar to the enhancement in fiber-reinforced composites) even after the water absorption. Meanwhile, during the early stage of swelling those networks could induce water into the rubber more quickly and make random interconnections among discontinuous SAP particles. Therefore, the transfer of water from the surface to the bulk of the composite and between isolated SAPs trapped by the rubber matrix could occur more quickly than in conventional WSR, as shown in Figure 5.2 e. As a result, excellent water swelling ability and mechanical properties were achieved.

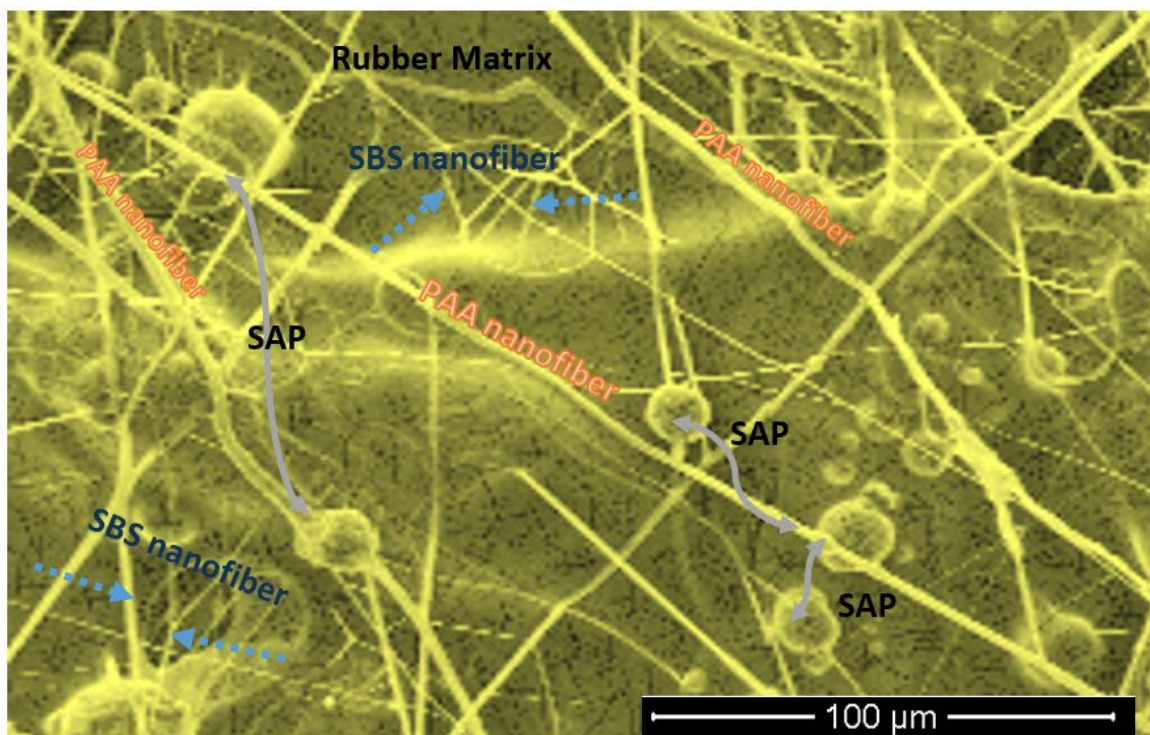


Figure 5.8 SEM images show the proposed mechanism of WSR containing PAA and SBS nanofiber mats after swelling (Dashed arrows with blue colour pointing SBS nanofibers)

## 5.5 Conclusions

In this chapter, electrospun nanofibers of PAA, SBS, and PAA/SBS were prepared by the electrospinning method. The resultant nanofibers were introduced to enhance the mechanical properties and water swellability of conventional WSR. In SEM images of PAA/SBS nanofiber mats, some spider web networks were observed with physical entanglements between nanofibers of PAA and SBS. The PAA constituent of PAA/SBS nanofiber mats could enhance the water absorption of the composite, while the mechanical properties of the WSR composite were improved by SBS nanofiber mats. The proposed mechanism was illustrated. The other possible solutions to enhance the mechanical properties of WSR, is first manipulating SAP structure (here PAA) by adding reinforcement agent to the original recipe during fabrication. In next chapter, the whole idea will be explained. The second idea is replacing PAA nanofiber with PVA nanofiber to enhance both swelling ability and mechanical properties at the same time which will be discussed in chapter 7.

## 5.6 References

1. Nakason, C., Nakaramontri, Y., Kaesaman, A., Kangwansukpamonkon, W. and Kiatkamjornwong, S., 2013. Synthesis and characterization of water swellable natural rubber vulcanizates. *European Polymer Journal*, 49(5), pp.1098-1110.
2. Wang, G., Li, M. and Chen, X., 1999. Effects of fillers on mechanical properties of a water-swallowable rubber. *Journal of applied polymer science*, 72(4), pp.577-584.
3. Wu, J., Lin, J., Li, G. and Wei, C., 2001. Influence of the COOH and COONa groups and crosslink density of poly (acrylic acid)/montmorillonite superabsorbent composite on water absorbency. *Polymer International*, 50(9), pp.1050-1053.
4. Mignon, A., Graulus, G.J., Snoeck, D., Martins, J., De Belie, N., Dubruel, P. and Van Vlierberghe, S., 2015. pH-sensitive superabsorbent polymers: a potential candidate material for self-healing concrete. *Journal of Materials Science*, 50(2), pp.970-979.

5. Yamashita, S., Kodama, K., Ikeda, Y. and Kohjiya, S., 1993. Chemical modification of butyl rubber. I. Synthesis and properties of poly (ethylene oxide)-grafted butyl rubber. *Journal of Polymer Science Part A: Polymer Chemistry*, 31(10), pp.2437-2444.
6. Saijun, D., Nakason, C., Kaesaman, A. and Klinpituksa, P., 2009. Water absorption and mechanical properties of water-swellaable natural rubber. *Sonklanakarin Journal of Science and Technology*, 31(5), p.561.
7. Hua, F. and Qian, M., 2001. Synthesis of self-crosslinking sodium polyacrylate hydrogel and water-absorbing mechanism. *Journal of materials science*, 36(3), pp.731-738.
8. Gong, J.P., Katsuyama, Y., Kurokawa, T. and Osada, Y., 2003. Double-Network Hydrogels with Extremely High Mechanical Strength. *Advanced Materials*, 15(14), pp.1155-1158.
9. Zhang, Z., Zhang, G., Li, D., Liu, Z. and Chen, X., 1999. Chlorohydrin water-swellaable rubber compatibilized by an amphiphilic graft copolymer. II. Effects of PVA-g-PBA and CPA on water-swelling behaviors. *Journal of applied polymer science*, 74(13), pp.3145-3152.
10. Meng, E., Zhang, X. and Benard, W., 2011. Additive processes for polymeric materials. In *MEMS Materials and Processes Handbook* (pp. 193-271). Springer US.
11. Amnuaypanich, S., Patthana, J. and Phinyocheep, P., 2009. Mixed matrix membranes prepared from natural rubber/poly (vinyl alcohol) semi-interpenetrating polymer network (NR/PVA semi-IPN) incorporating with zeolite 4A for the pervaporation dehydration of water–ethanol mixtures. *Chemical Engineering Science*, 64(23), pp.4908-4918.
12. Magalhães, A.S.G., Almeida Neto, M.P., Bezerra, M.N., Ricardo, N.M. and Feitosa, J., 2012. Application of ftir in the determination of acrylate content in poly (sodium acrylate-co-acrylamide) superabsorbent hydrogels. *Química Nova*, 35(7), pp.1464-1467.

13. Wang, C., Zhang, G., Dong, Y., Chen, X. and Tan, H., 2002. Study on a water-swelling rubber compatibilized by amphiphilic block polymer based on poly (ethylene oxide) and poly (butyl acrylate). *Journal of applied polymer science*, 86(12), pp.3120-3125.
14. Utracki, L.A., 2002. Compatibilization of polymer blends. *The Canadian Journal of Chemical Engineering*, 80(6), pp.1008-1016.
15. Dehbari, N., Zhao, J., Peng, R. and Tang, Y., 2015. Neutralisation and compatibilisation effects on novel water-swelling rubber composites. *Journal of Materials Science*, 50(15), pp.5157-5164.
16. Zhao, J., Dehbari, N., Han, W., Huang, L. and Tang, Y., 2015. Electrospun multi-scale hybrid nanofiber/net with enhanced water swelling ability in rubber composites. *Materials & Design*, 86, pp.14-21.
17. Chen, C.H. and Cheng, S., 1967. Mechanical properties of fiber reinforced composites. *Journal of Composite Materials*, 1(1), pp.30-41.
18. Mallick PK. 1988. Book review: fiber-reinforced composites: Materials, manufacturing, and design, Marcel Dekker, Inc., New York, 469 pages.
19. Huang, Z.M., Zhang, Y.Z., Kotaki, M. and Ramakrishna, S., 2003. A review on polymer nanofibers by electrospinning and their applications in nanocomposites. *Composites science and technology*, 63(15), pp.2223-2253.
20. Coleman, J.N., Khan, U., Blau, W.J. and Gun'ko, Y.K., 2006. Small but strong: a review of the mechanical properties of carbon nanotube–polymer composites. *Carbon*, 44(9), pp.1624-1652.
21. Subbiah, T., Bhat, G.S., Tock, R.W., Parameswaran, S. and Ramkumar, S.S., 2005. Electrospinning of nanofibers. *Journal of Applied Polymer Science*, 96(2), pp.557-569.

22. Kim, J.S. and Reneker, D.H., 1999. Mechanical properties of composites using ultrafine electrospun fibers. *Polymer composites*, 20(1), pp.124-131.
23. Park, M., Im, J., Shin, M., Min, Y., Park, J., Cho, H., Park, S., Shim, M.B., Jeon, S., Chung, D.Y. and Bae, J., 2012. Highly stretchable electric circuits from a composite material of silver nanoparticles and elastomeric fibres. *Nature nanotechnology*, 7(12), pp.803-809.
24. Borba, P.M., Tedesco, A. and Lenz, D.M., 2014. Effect of reinforcement nanoparticles addition on mechanical properties of SBS/Curauá fiber composites. *Materials Research*, 17(2), pp.412-419.
25. Ding, B., Li, C., Miyauchi, Y., Kuwaki, O. and Shiratori, S., 2006. Formation of novel 2D polymer nanowebs via electrospinning. *Nanotechnology*, 17(15), p.3685..
26. Meng, L., Klinkajon, W., Harkin, S., Supaphol, P. and Wnek, G.E., 2015. Electrospun crosslinked poly (acrylic acid) fiber constructs: towards a synthetic model of the cortical layer of nerve. *Polymer International*, 64(1), pp.42-48.
27. Wang, X., Ding, B., Sun, G., Wang, M. and Yu, J., 2013. Electro-spinning/netting: a strategy for the fabrication of three-dimensional polymer nano-fiber/nets. *Progress in Materials Science*, 58(8), pp.1173-1243.
28. Pant, H.R., Bajgai, M.P., Nam, K.T., Seo, Y.A., Pandeya, D.R., Hong, S.T. and Kim, H.Y., 2011. Electrospun nylon-6 spider-net like nanofiber mat containing TiO<sub>2</sub> nanoparticles: a multifunctional nanocomposite textile material. *Journal of hazardous materials*, 185(1), pp.124-130.
29. Heikkilä, P. and Harlin, A., 2008. Parameter study of electrospinning of polyamide-6. *European Polymer Journal*, 44(10), pp.3067-3079.

- 30 Zhang, Z., Zhang, G., Zhang, Y., Wang, Z., Yu, D., Hu, X., Hu, C. and Tang, X., 2004. Mechanical properties, water swelling behavior, and morphology of swellable rubber compatibilized by PVA-g-PBA. *Polymer Engineering & Science*, 44(1), pp.72-78.
31. Zhang, Y., He, P., Zou, Q. and He, B., 2004. Preparation and properties of water-swella-ble elastomer. *Journal of applied polymer science*, 93(4), pp.1719-1723.

## 6. [IN SITU POLYMERIZED HYPERBRANCHED POLYMER REINFORCED POLY (ACRYLIC ACID) HYDROGELS<sup>1</sup>]

One of the treatments to enhance performance characteristics of the SAPs (especially in terms of mechanical stability), is using reinforcement agent. In this chapter by in situ polymerization of hyperbranched polymer with acrylic acid monomers, the physical and mechanical properties of PAA hydrogel is evaluated. By the incorporation of HB into the PAA hydrogels, the mechanical test results shows a significant enhancement, alongside with simultaneous increase of water uptake capability.

1. This work has been published in Materials Chemistry Frontiers: Nazila Dehbari, Javad Tavakoli, Simranjeet Singh Khatri, Youhong Tang” *In situ* polymerized hyperbranched polymer reinforced poly (acrylic acid) hydrogels”. Materials Chemistry Frontiers, 2017. DOI:10.1039/C7QM00028F

## 6.1 Introduction

As we discussed in Chapter 5, the potential use of poly (acrylic acid) (PAA) and styrene–butadiene–styrene (SBS) triblock copolymer nanofibers to reinforce composites was investigated. To overcome the low mechanical strength of PAA, there are several feasible ways. Here, we mainly focused on reinforcing SAP hydrogel structures. Hydrogels are three-dimensional cross-linked, water-swollen and hydrophilic polymer whose properties are highly dependent on environmental conditions [1-3]. As an enviro-sensitive material, hydrogels have been widely used for industrial and biomedical applications due to their unique structure and capabilities [4-6]. The properties of a specific hydrogel are extremely important in selecting which materials are suitable for a given application. The suitability of a hydrogel for a given application depends on the mechanical properties that are affected by environmental conditions such as temperature, pH level and ionic strength, both magnetic and electric field as well as the monomer type and crosslinking agents [7-9].

Among various types of hydrogels, poly acrylate polymers such as poly acrylic acid (PAA) with distinctive absorptivity properties have most versatile structure to enhance their practical utility in everyday life such as filtration, water remediation, diapers and hygiene products, cosmetics, wound dressings, medical waste solidification and metal ion removal [10-14]. During extensive studies that have been performed on evaluation of different properties of PAA hydrogels, such as swelling [15], adhesion [16], diffusion [17], physico-chemical [18] and mechanical [19], it was revealed that the most concerning issue about this type of hydrogels is their poor mechanical properties [11, 20-22]. Poor mechanical properties of PAA hydrogels, which is extremely relates to their subsequence to large swelling volume change, count as a great weakness in adopting for high-tech applications and has limited their specific applications [23, 24]. Typically, PAA hydrogels exhibit low young modulus ( $< 200$  KPa), low fracture energy ( $< 20$  Jm<sup>-2</sup>) and possess low tensile

strength ( $< 0.2$  MPa) [25, 26]. Therefore improving PAA hydrogels' mechanical properties via toughening methods by mixing different types of crosslinked polymer or introducing energy-dissipating mechanisms is highly focused [27-29]. Various methods of producing multi-functional cross-linked hydrogel [30], nano-composite hydrogels [31], hybrid interpenetrating networks [32], slip-link network [33] and homogenous hydrogel [34] that were introduced to toughen PAA hydrogels have been shown to improve the mechanical properties. To the best of our knowledge, toughening hydrogels using chemical methods may limit its biomedical application as unreacted components diversely affect the biocompatibility [35, 36]. On the other hand although other methods were reported to enhance mechanical properties of the hydrogels, some inherent disadvantageous like weak-self recovery and poor fatigue resistance still existed [29]. Contribution of hyper-branched polymers on hydrogels' toughening -performed physically- leads to an unconventional assemblies and complex structures with responsive properties [37, 38].

Recently hyper-branched polymers (HB), one of the most extensively used nanoparticles, with the structure of highly branched tree-like dendritic material containing numerous  $-OH$  end groups has been used for hydrogels' mechanical properties [39-41]. In crosslinked hydrogel with HB macromolecule, the polymeric chains are held together by directional discrete supramolecular binding sites to enhance the mechanical properties of resultant composite [42, 43]. These evidences suggesting a potential of using HB polymers as a reinforcement agent in PAA based hydrogels [44, 45].

The aim of this study is toughening of PAA hydrogel with combination of covalent and physical crosslinking to improve the properties of hydrogels by introducing HB polymers without sacrificing the swelling ratio of final product through an easy process, cost effective, with an

environmental friendly method. The structural-property relation of hydrogels have been evaluated and a possible mechanism has also been proposed.

## 6.2 Material preparation and characterisations

Acrylic acid monomer (AA), hyperbranched bis-MPA polyester-64-hydroxyl (HB), ammonium persulfate (APS) as an initiator and N, N'-Methylenebis (acrylamide) (MBA) as a crosslinking agent were purchased from Sigma Aldrich (Australia) and used in analytical grade without any further purification. Sodium hydroxide (NaOH) was supplied from Chem-Supply (Australia). All aqueous solutions were prepared using Milli-Q water at room temperature.

Synthesize of PAA-HB solution was followed by previous work [31]. Briefly, 3.7 g acrylic acid was dispersed in 3.5 cm<sup>3</sup> distilled water at 5 °C. A 0.45 g cm<sup>-3</sup> NaOH solution was prepared by dissolving 1.63 g sodium hydroxide powder in 3.62 g distilled water followed by cooling in an ice-water bath for 10 min. NaOH solution was then added into the acrylic acid solution dropwise with magnetic stirring at 5 °C for 20 min. Ultimately, 0.025 g MBA and 0.08 g APS powder were added into the mixture following by shaking vigorously to ensure homogeneity by an IKA Vortex 3 shaker. The mixture was poured into a glass mould and placed in an oven at pre-set temperature of 60 °C for 10 min, while heating continued for next 20 min with the temperature increased from 60 to 80 °C at a rate of 1 °C min<sup>-1</sup>. After the overall heating duration of 30 min, prepared hydrogels were cooled to the room temperature for 2 h, as remained at oven. The synthesized PAA samples were peeled off from the mould and stored in sealed bags at 4 °C for testing. For the PAA-HB sample, 3.5 cm<sup>3</sup> distilled water was mixed with 0.6 g HB powder and 3.7 g acrylic acid was added into the suspension which was then shaken vigorously by an IKA Vortex 3 shaker. The rest of the procedure was the same as above.

To investigate the possible interaction between the PAA and HB in the hybrid samples, Fourier transform infrared (FTIR) spectroscopy (PerkinElmer Spectrum 400 spectrometer equipped with an attenuated total reflectance (ATR, top-plate type) was performed in terms of their functional groups. Each sample was mounted in turn onto the central crystal of the ATR plate, and air was used as a background reference before each scan. FTIR spectra were then recorded using 64 scans from 4000 to 550  $\text{cm}^{-1}$  with a resolution of 4  $\text{cm}^{-1}$  in absorbance mode with background subtraction.

The thermal behaviour of the hydrogels was studied using differential scanning calorimeter (DSC) (TA instruments, USA). Samples were heated in a sealed aluminium crucible with another empty aluminium crucible as a reference, over the temperature range of -30 °C to 300 °C at a rate of 10 °C/ min in  $\text{N}_2$  atmosphere.

The surface morphology of the PAA and PAA-HB hydrogels was characterized using scanning electron microscopy (SEM) (CamScan MX2500). Dried specimens were mounted on aluminium stubs with double adhesive tape, then sputter coated with platinum at 2 nm thickness. High voltage was set at 10 kV and the distance from the sample to the beam source was kept constant for all tests performed. To investigate distribution of HB particles in PAA hydrogel, a transmission electron microscope (TEM) (Philips CM200, the Netherlands) was employed. For preparation of the TEM specimens, all the hydrogel samples were completely dried in a vacuum oven overnight at 50 °C. Then, the samples were ultramicrotomed using glass knives on an ultra-cut microtome (Leica Ultra cut-R ultra-microtome, Germany) to produce thin sections with a nominal thickness of 100 nm.

The swelling behaviour of the PAA and PAA-HB samples was tested by measuring the initial weight of the dry samples and subsequently the weight after they had been immersed in distilled water until equilibrium. Each test was repeated three times. Before measurement of the weight of the swollen samples, excess surface water was removed by filter paper. The swelling ratio was calculated using the equation:

$$\frac{m_t - m_0}{m_0} \times 100 \quad (1)$$

where  $m_0$  and  $m_t$  are the weight of sample in the initial dry and the swollen state, respectively.

Also swelling kinetics of PAA and PAA-HB hydrogels were conducted in solutions of different pH (2, 7 and 10), attuned by solving sodium hydroxide and hydrochloric acid in deionized water. The dynamic swelling kinetics of both samples were explored by soaking and alternating them between solutions of pH 10 and pH 2 every two hours, 3 times.

The mechanical properties of PAA and PAA-HB were measured for intact and notch-induced samples, using an Instron universal testing machine. All the samples were cut into a square shape with the dimensions 3.0 mm×3.0 mm. Each sample's thickness was measured as  $2.00 \pm 0.01$  mm at five different points using a digital calliper. Notches with the depths of 3.0, 5.0, 8.0, 11.0 and 14.0 mm were introduced to the middle of the samples, using a laser cut machine. All samples (intact and notch-induced) were secured by sandpaper and superglue at both ends and the initial length of the samples was set at 5 mm. The tests were conducted at room temperature with strain rate of 50 mm/min. All mechanical test results were the mean of at least five measurements. For dynamic testing, a PAA-HB sample was loaded to a certain stretch of  $\lambda=4$  and unloaded to zero (first loading), after which the test was repeated at time intervals of 10 s, 10 min, 1 h and 24 h

(second loading). Between the first and second loadings, all samples were wrapped in a polyethylene bag and stored at 4 °C.

A univariate ANOVA with Bonferroni post-hoc was conducted (IBM SPSS Statistics for Windows, Version 22.0. Armonk, NY: IBM Corp.), having dependent variables of ultimate strength, elongation at break and toughness and fixed factors of composition (PAA and PAA/HB) using an alpha of 0.05.

## 6.3 Results and discussion

### 6.3.1 Molecular interactions within hydrogels

FTIR spectra of HB powder and hydrogels of PAA and PAA-HB are shown in Figure 6.1. The observed peaks at  $1728\text{ cm}^{-1}$  and  $1440\text{ cm}^{-1}$  are ascribed to H-bonded ester C=O groups and COO<sup>-</sup> stretching of HB polymer, Figure 6.1a) [31]. The characteristic absorption peaks of C–O(–OH) stretching hydroxyl and O–C stretching ester groups occur at  $1041\text{ cm}^{-1}$  and  $1121\text{ cm}^{-1}$ , respectively. For PAA hydrogel, peaks at  $1680$ ,  $1551$ , and  $1403\text{ cm}^{-1}$  are related to the –C=O asymmetric stretching of –COOH and COO<sup>-</sup> groups, and COO symmetric stretching of –COO<sup>-</sup> groups are, respectively [46, 47]. The stretching of –CH<sub>2</sub>– (asymmetric and symmetric) and bending of C–H were observed at  $2939$ ,  $2855$ , and  $1450\text{ cm}^{-1}$ , indicating the existence of a PAA main chain [48]. During the neutralization process of PAA by NaOH, –COOH groups of AA were partially converted into –COO<sup>-</sup> Na, which was confirmed by the FTIR result (Figure 6.1b). In PAA-HB sample (Figure 6.1c), with the addition of HB into the PAA structure, compared to the PAA curves, new absorption peaks due to C–O(–OH) hydroxyl and O–C ester groups of HB occurred at  $1041$  and  $1121\text{ cm}^{-1}$ , attributing to the polymer binder [49]. These characteristic absorption peaks provide evidence for the successful preparation of PAA-HB hydrogel.

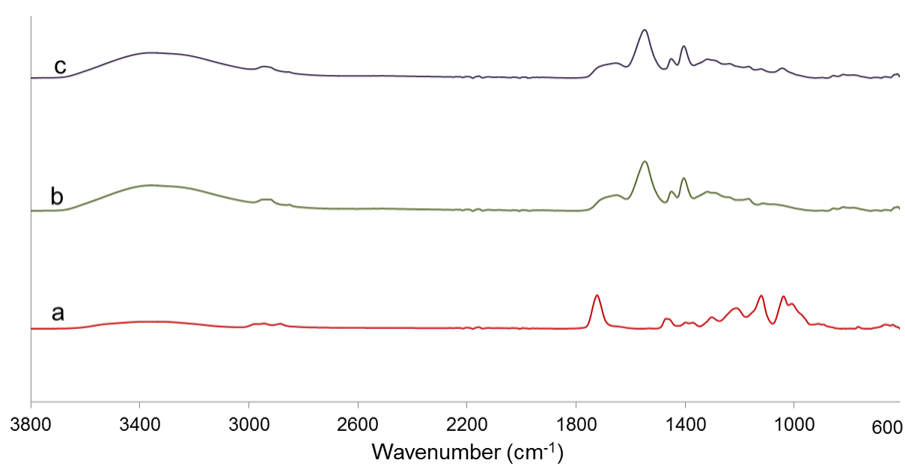


Figure 6.1 FTIR spectra of (a) HB powder, (b) PAA and (c) PAA-HB hydrogel

The molecular interaction of PAA and PAA-HB hydrogels was also investigated by DSC measurements from -50 to 75 °C, as shown in Figure 6.2. From the DSC curve, it can be seen that the addition of HB polymer into the PAA results in a reduction in the glass transition temperature ( $T_g$ ) from -0.63 to -7.43 °C. This phenomenon is attributed to the supramolecular structure of HB, which can cause physical entanglement between PAA network structures and increase the crystallinity of the final hydrogel as compared to those features in the PAA hydrogel. This result confirmed that the contribution of HB can cause the formation of PAA-based hybrid materials, in which mechanical and other properties could also be changed [4].

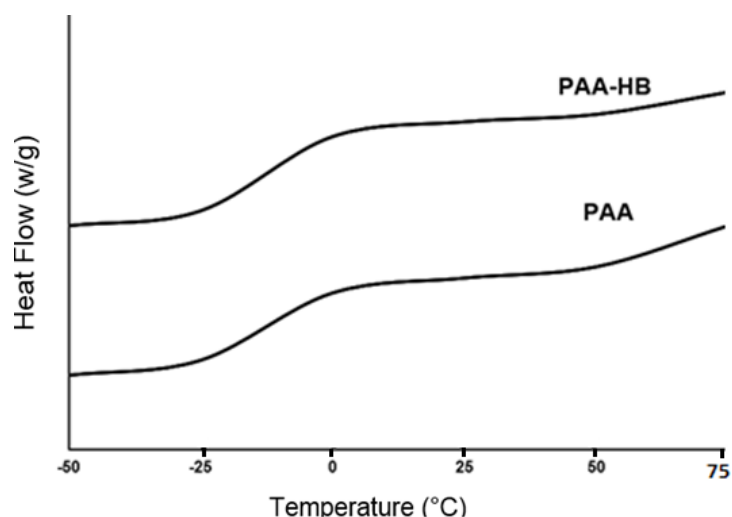


Figure 6.2 DSC curves of PAA and PAA hybrid samples

### 6.3.2 Morphological understanding

To confirm the interactions between the HB polymer and the PAA, the morphologies of the hydrogels were observed by SEM at different scales. The HB polymer binders were evenly distributed into the PAA structure, as shown in Figure 6.3. The rough surface of the PAA-HB also suggested good dispersion of the HB within the PAA. A change in surface morphology of the PAA-HB samples, as compared to the smooth surface of a PAA sample, is consistent with FTIR results that suggest the possibility of hyperbranched polymer contribution to the structural organization of PAA molecules. Also TEM images suggest good dispersion of HB inside the PAA, as shown below.

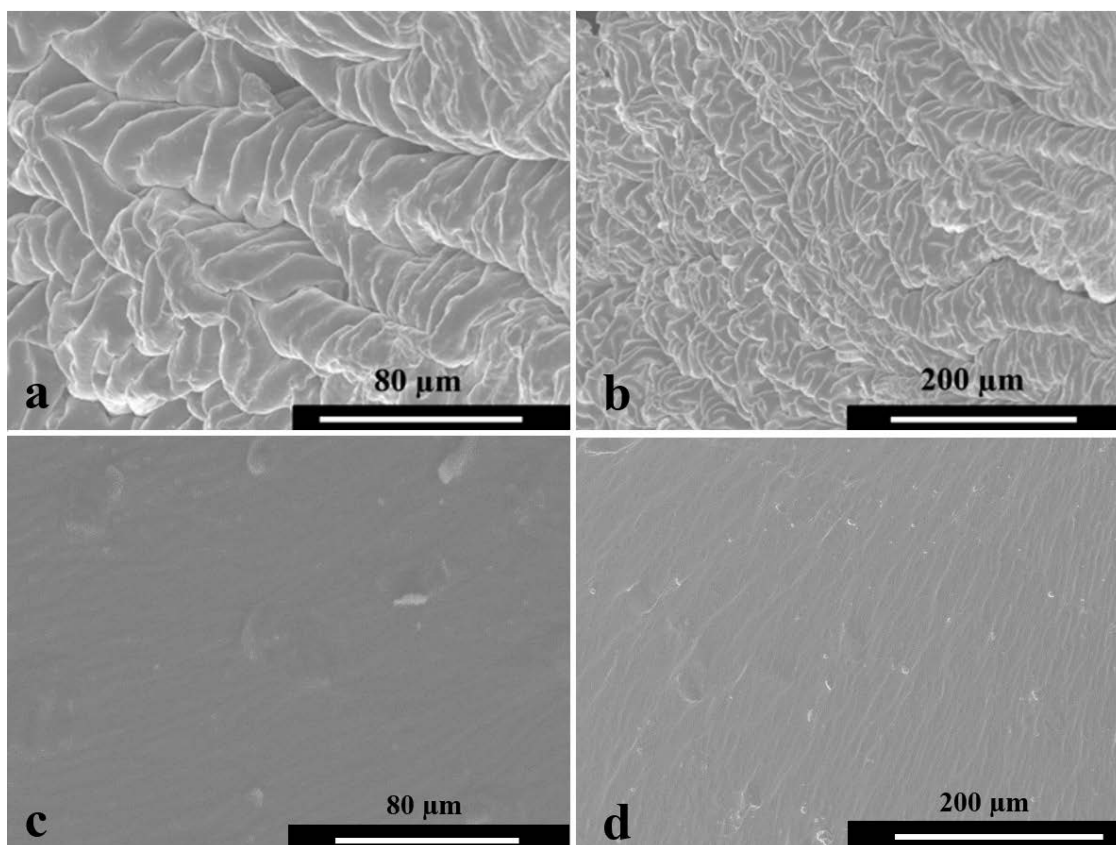


Figure 6.3 SEM images of (a) and (b) PAA-HB surfaces and (c) and (d) PAA surfaces two different magnifications of 80  $\mu\text{m}$  and 200  $\mu\text{m}$

TEM images of PAA-HB samples are shown in Figure 6.4. The aggregated nanospheres in the range of 10-200 nm in diameter are attributed to the HB polymer binders which are dispersed well in the PAA matrix. Due to the numerous hydroxyl groups at the ends of the HB, the particles tended to aggregate. Meanwhile, the hydrophilic character of these hydroxyl groups could help to enhance the compatibility of HB with PAA during in situ polymerisation [31].

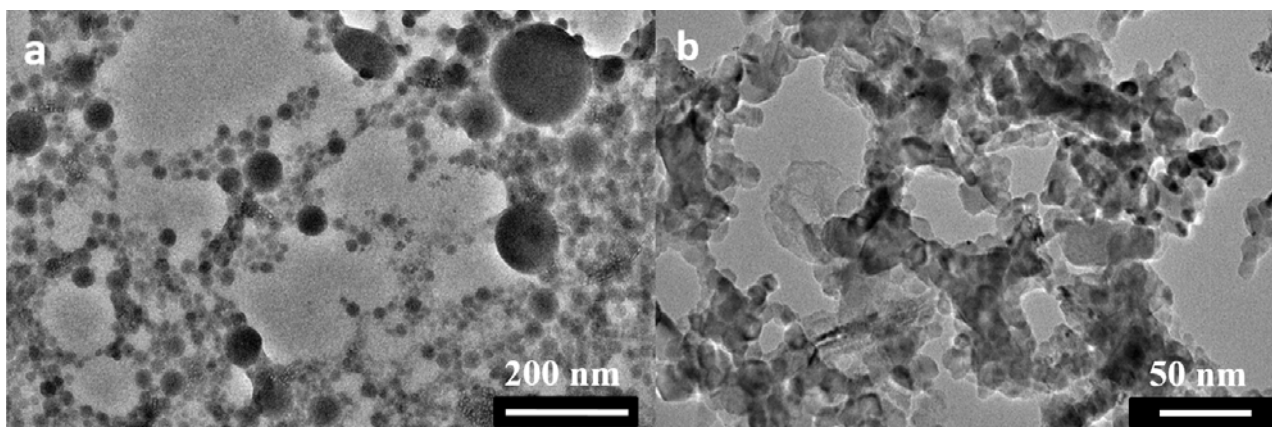


Figure 6.4 TEM images of PAA-HB hydrogel

### 6.3.3 Water swelling behaviours

The swelling behaviours of PAA and PAA-HB hydrogels immersed in water at 25°C are shown in Figure 6.5. The addition of HB into the PAA solution caused increased water uptake by the hydrogel. In the first 15 minutes, the water uptake of both hydrogels was extremely fast, following by constant increments, finally reaching equilibrium within 150 min. In the PAA sample, the swelling ratio (SR) at equilibrium stage was about 8.6 K% of its initial weight. With the introduction of HB, however, this amount was increased to a higher value of 9.6 K%, which was about 1.12 times higher than that of the PAA. This increase was attributed to the availability of a large number of hydrophilic hydroxyl groups in the HB particles, which could bind to water and increase the absorption capacity of the hydrogel. The slopes of SR versus immersion duration of both PAA and PAA-HB samples showed similar trends. Once the time exceeded 150 min, the SR of samples reached a plateau, indicating excellent water retention by the PAA and PAA-HB hydrogels.

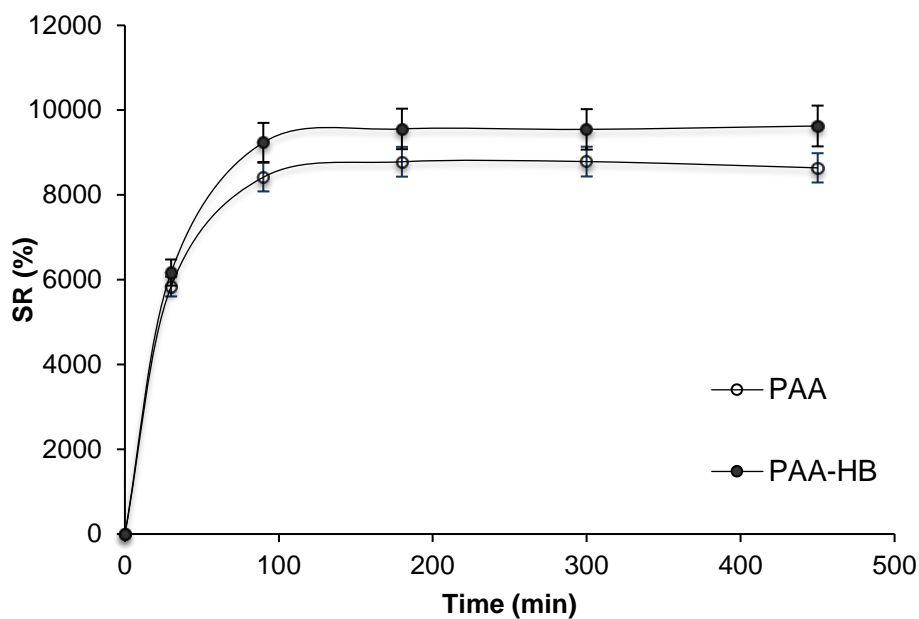


Figure 6.5 Swelling ratios of PAA and PAA-HB hydrogels immersed in water

### 6.3.4 Mechanical behaviours of hydrogels

The effects of adding HB to the PAA structure on the mechanical properties of the PAA-HB hydrogel are shown in Figure 6.6. As shown, the ultimate tensile strength of the PAA-HB hydrogel is improved by 130% ( $1.15 \pm 0.10$  MPa) compared to the PAA hydrogel with ultimate strength of approximately  $0.50 \pm 0.04$  MPa. Also, elongation at break is doubled, from  $340 \pm 12\%$  for PAA to  $650 \pm 35\%$  for PAA-HB. Thus, the fracture energy of the PAA-HB hydrogel, measured as  $4483 \pm 39$   $\text{KJm}^{-3}$ , is approximately four times greater than that of the PAA hydrogel, which was  $1020 \pm 29$   $\text{KJm}^{-3}$ .

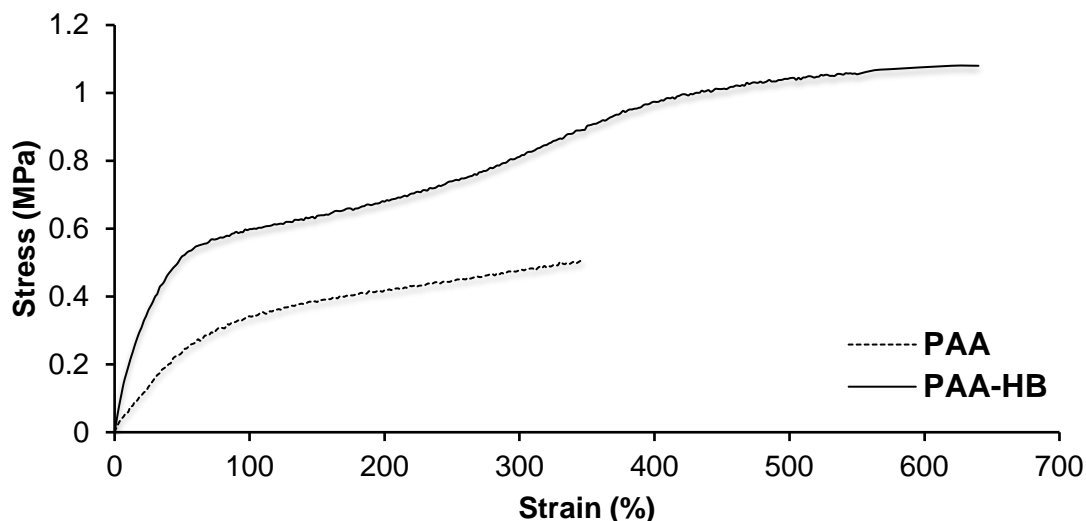


Figure 6.6 Mechanical properties of PAA and PAA-HB hydrogels

Stress-strain curves for the PAA-HB samples at different stretch ratios are presented in Figure 6.7. The stretch ratio ( $\lambda$ ) was defined as the ratio of final to initial length. As is evident, the stress-strain relationship for all stretch ratios is linear for strain less than 50%. As  $\lambda$  increases, the ultimate tensile stress and the corresponding strain both increase. Table 6.1 shows the change in ultimate stress, Young's modulus and toughness at different stretch ratios.

Table 6.1 Change in selected mechanical properties of PAA-HB at different stretch ratios

Mechanical properties	Unit	Stretch ratio ( $\lambda$ )				
		1	3	5	6	8
Ultimate stress	MPa	0.13±0.21	0.25±0.18	0.26±0.27	0.27±0.15	0.37±0.14
Young's modulus	MPa	2.21±0.18	2.55±0.12	2.55±0.08	2.55±0.16	2.55±0.21
Toughness	KJm <sup>-3</sup>	97±11	459±32	835±49	1094±69	2124±51

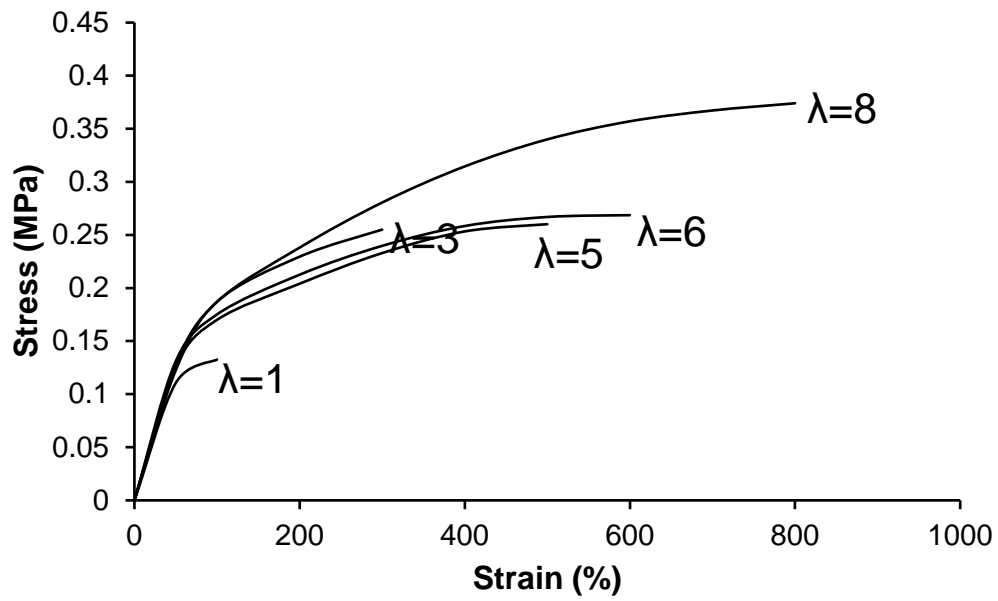
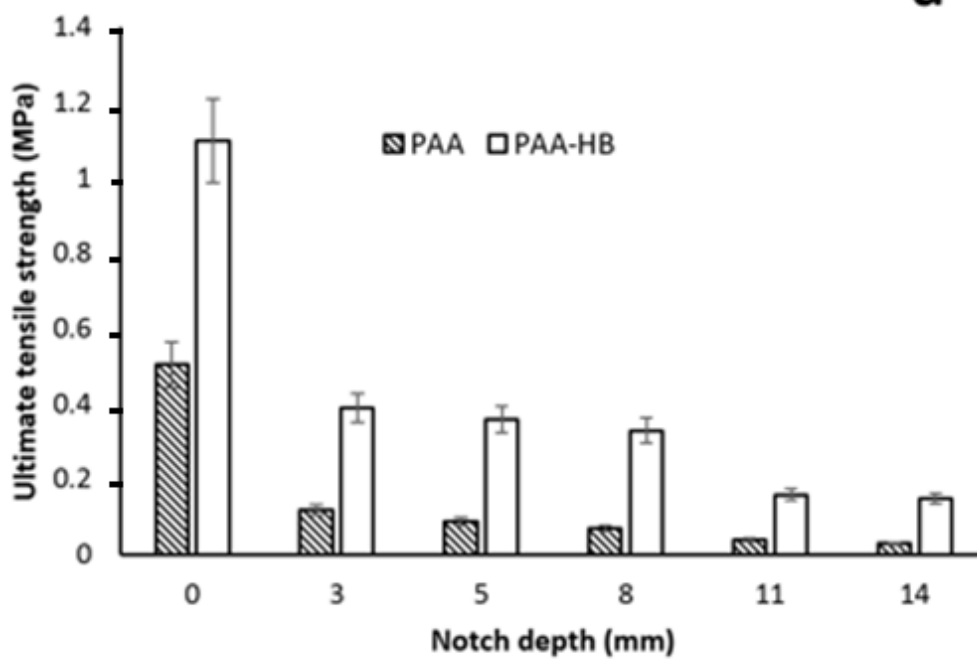
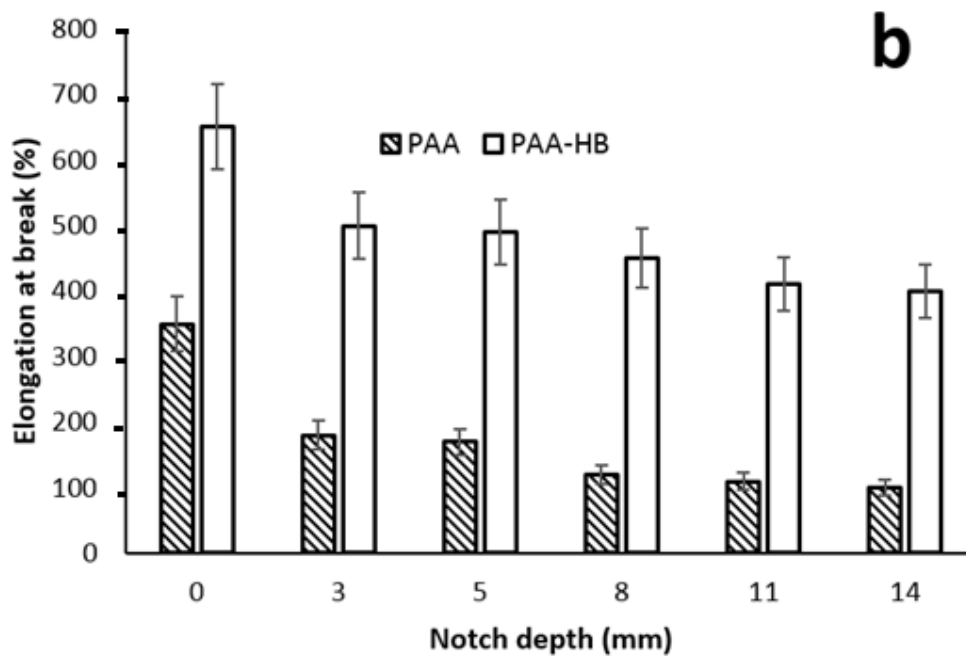


Figure 6.7 Stress-strain relationship for PAA-HB hydrogels at different stretch ratios

A comparison of the mechanical properties of PAA and PAA-HB at different notch depths and the stretchability of PAA-HB samples with selected notches of 0 and 14 mm is presented in Figure 6.8(a-d).

**a****b**

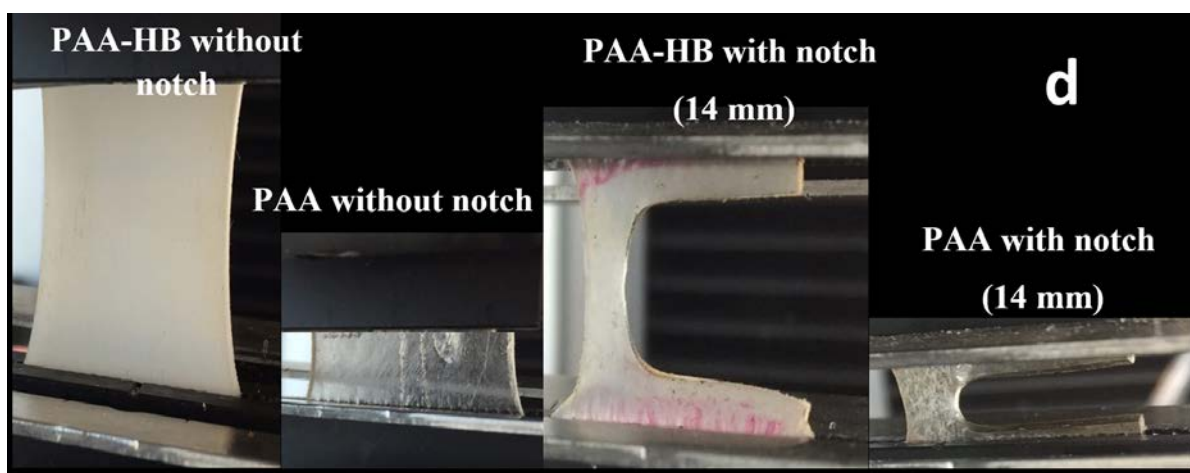
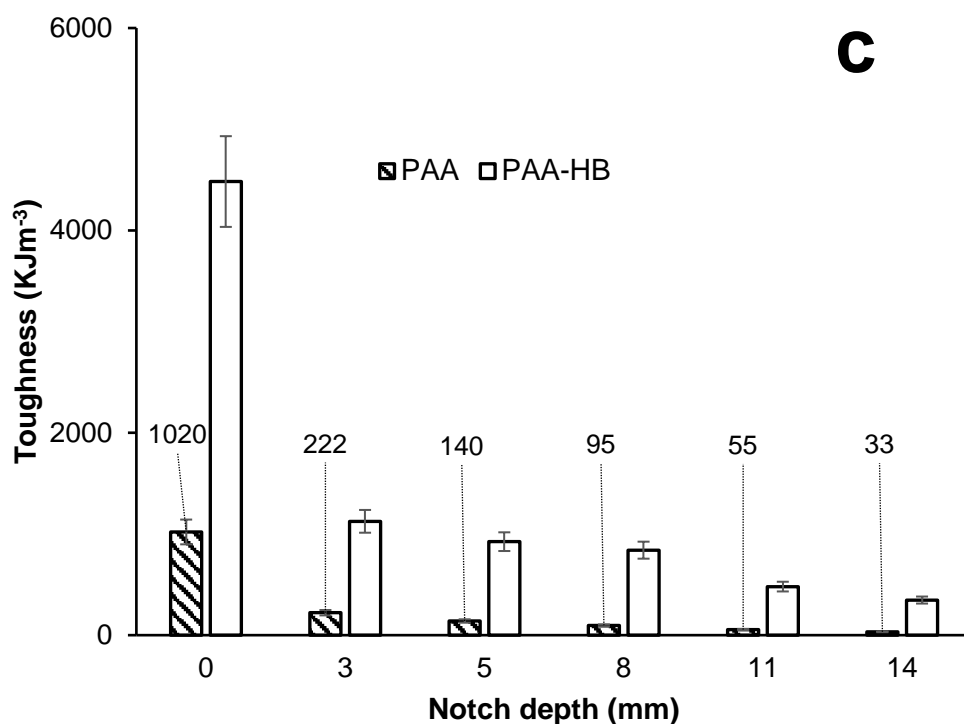


Figure 6.8 Comparison of mechanical properties of PAA with PAA-HB hydrogel for different notch depths. (a) Ultimate tensile strength, (b) elongation at break, (c) toughness and (d) stretchability

As shown, the unnotched samples display greater toughness, elongation at break and ultimate strength than the notched samples. Also the PAA-HB samples have significantly enhanced mechanical properties compared to the PAA samples. Surprisingly, the ultimate tensile strength for the PAA-HB samples with notch depths of 3, 5 and 8 mm remains constant at approximately  $0.10 \pm$

0.02 MPa. A similar trend is found for the samples with 11 and 14 mm notches, as shown Figure 6.8 (a). Generally, the elongation of the unnotched PAA-HB samples is about twice that of the intact PAA samples. The stretchability of the PAA-HB and PAA samples for different notch depths is about 20% and 50% lower than that of the corresponding intact samples, respectively, and remains constant for all notch depths, as shown in Figure 6.8 (b). Figure 6.8 (c) shows that both intact and notched PAA-HB samples with different depths have significant improvement in fracture toughness compared with the corresponding PAA samples. The PAA samples with notch depths greater than 5 mm have negligible toughness. Figure 6.8 (d) shows the stretchability of the intact sample (un-notched) versus the notched sample (14 mm) for both PAA and PAA-HB hydrogels.

Statistical analysis revealed that the overall effect of introducing different notches on the selected mechanical properties of stiffness, elongation at break and ultimate strength of both PAA and PAA-HB was significant ( $P < 0.01$ ). Due to the marked decrease in those mechanical properties of PAA after notch insertion, changes in notch depth showed no significant effect on the ultimate strength ( $P=0.99$ ), whereas in the PAA-HB samples, introducing a notch with depth greater than 11 mm resulted in a significant change in ultimate strength ( $p=0.004$ ). Meanwhile, it was found that a change in notch depth from 1 to 5 mm had a significant effect on the PAA samples' elongation at break ( $P=0.003$ ), but not when the notch was greater than 5 mm ( $P=1.00$ ). In contrast, the addition of HB into the PAA structure improved the elongation at break property. It was shown that the change was negligible for samples with notch depth difference less than 6 mm ( $P=0.593$ ). For PAA samples with notch depth greater than 2 mm, the change in fracture toughness was significant ( $P=0.021$ ). However, notches at least 6 mm or greater needed to be introduced to the PAA-HB samples to significantly affect toughness ( $P=0.004$ ).

Figure 6.9 shows the results of dynamic tests that were performed on intact PAA-HB samples. As shown, the hysteresis effect for the first loading to a stretch of  $\lambda=4$  and the subsequent unloading to zero is huge in comparison to that of samples with a second loading. The PAA-HB hydrogels dissipated energy effectively and their hysteresis loop reduced for the second loading at different time intervals after the first loading. It seems that the change in maximum stress at the stretch ratio of 4 was negligible for all second tests for a given sample, indicating the effect of hyperbranching on the mechanical properties of the PAA due to increasing physical interaction or internal friction.

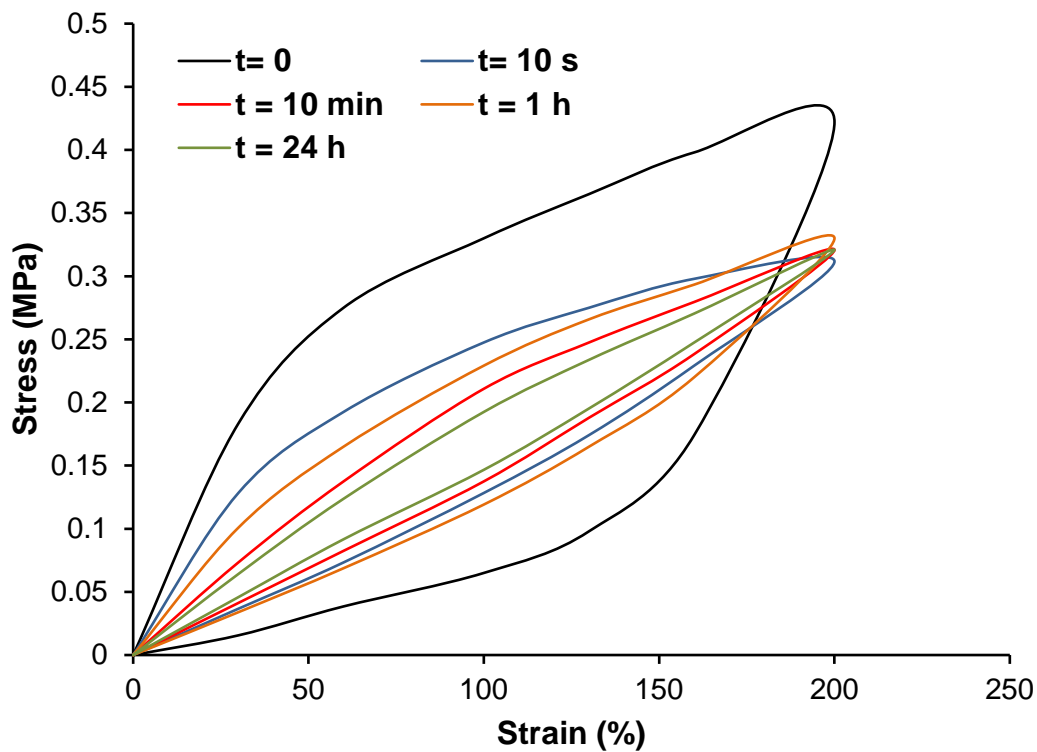


Figure 6.9 Hysteresis effect of loading to a certain stretch ( $\lambda=4$ ) and unloading to zero for first and second loadings with different time intervals. All dynamic tests were performed at  $50 \text{ mm}\cdot\text{min}^{-1}$  strain rate

## 6.4 Proposed mechanism

Hydrogels of PAA and PAA-HB were successfully synthesized through a one-step, cost-effective and environmentally friendly method. From the above investigations, the mechanism for the PAA-HB network structure can be proposed. Figure 6.10 illustrates the structure of PAA hydrogel including HB particles. Numerous -COOH groups of PAA result in the formation of hydrogen bonding. These hydrogen bond formations increase in the presence of water. On the other hand, HB experiences some physical entanglement in PAA networks due to its high molecular weight and star shape. Meanwhile, -OH groups of HB can effectively connect with -COOH groups of PAA, resulting in the formation of hydrogen bonding. After MBA and APS were added during in situ polymerisation, PAA networks were constructed tightly around the HB molecules. Therefore, PAA-HB hydrogels are expected to have higher mechanical properties compared to those of PAA hydrogels.

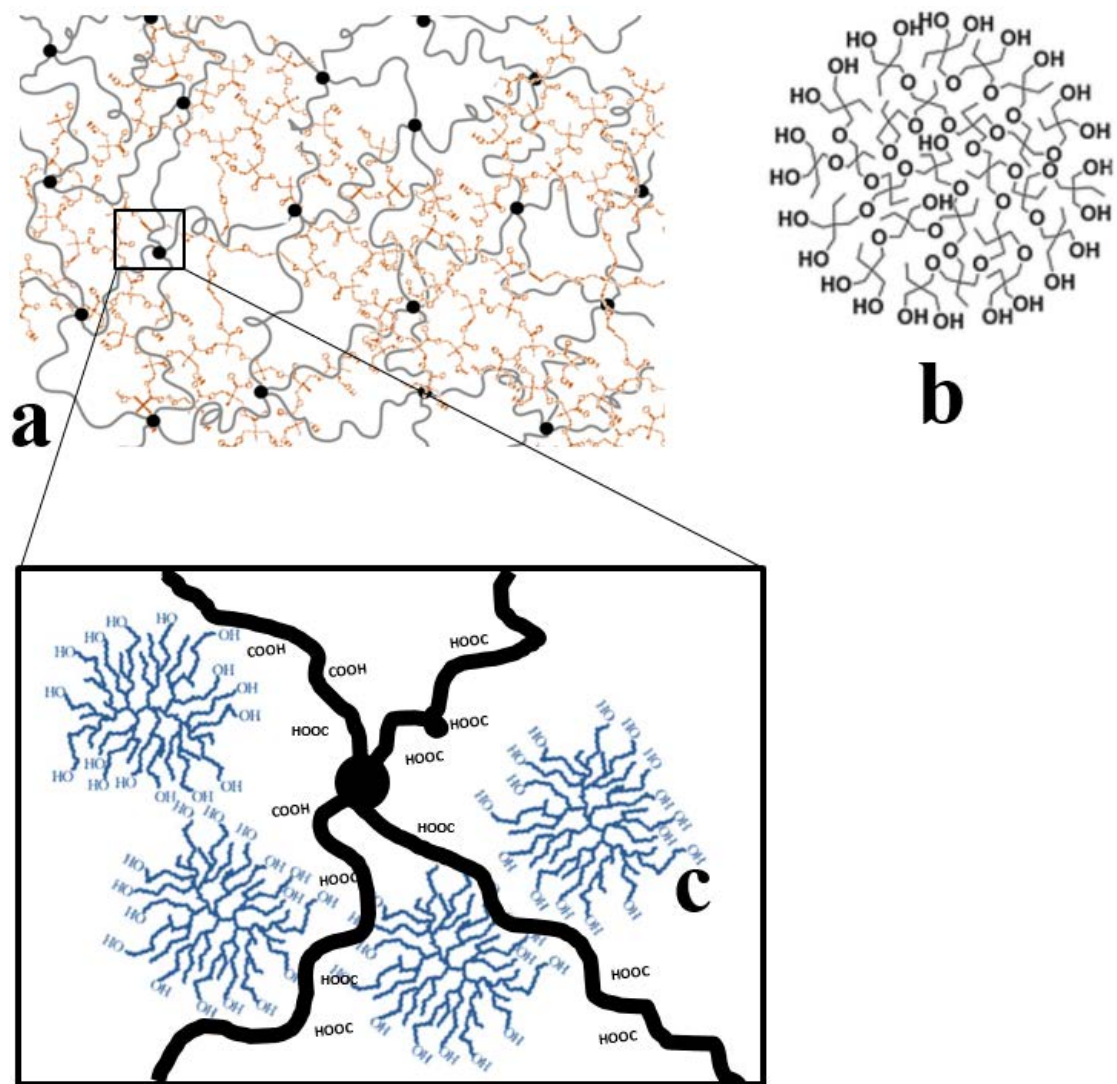


Figure 6.10 (a) Interpenetrating networks of PAA-HB, (b) schematic structure of a HB molecule, and (c) schematic illustration of possible physical interaction and hydrogen bond formation mechanism between PAA chains and HB molecules

To compare our study with other research studies relevant information is presented in Table 6.2, more details have to be noticed during the comparison as mechanical characterisation was performed under different conditions. As it can be seen from the table, different toughening agents/methods, i.e. graphene oxide, branched polymers, hyper-branched polymers, IPN, etc., may improve some mechanical properties while their negative effects on other properties, such as swelling ability need to be addressed.

Table 6.2 Different PAA hydrogel toughening methods with mechanical and swelling properties

Method	UTS (MPa)	EAB (%)	SR (%)	T (MJ/m <sup>3</sup> )	Ref
PAA hydrogel	0.07	115	300	0.5	[50]
	0.06	78	8000	N/A	[31]
Dually cross-linked single network	1	2000	1800	13.5	[50]
micellar copolymerization of acrylic acid	1.7	800	500	N/A	[51]
incorporation of silica nanoparticle and branched polymer	0.15	1200	250	N/A	[52]
PAA-chitosan IPN	6	10	70	N/A	[53]
PAA-PVA IPN	0.5	200	35	N/A	[54]
PAA-graphene oxide	0.03	300	100	N/A	[55]
	0.2	450	12000	N/A	[31]
PAA-Guar gum membrane	40	60	N/A	N/A	[56]
PAA- cellulose nanocomposite	0.35	400	350	N/A	[57]
PAA- hyper-branched nanocomposite	1.25	650	10000	2.124	Our Study

## 6.5 Sensor application

To investigate the possibility of utilizing the toughened PAA-HB hydrogel as a pH-sensitive sensor, its enviro-responsive and dynamic swelling properties were investigated here. Measuring the swelling ratio as a function of time in solutions at different pH values of 2, 7 and 10 revealed that the overall trend of swelling kinetic curves for PAA-HB samples are consistent with those without HB. Below the pKa, both PAA and PAA-HB samples swelled significantly less than those above the pKa ( $P = 0.041$ ). However, the increase of the pH value resulted in a higher swelling ratio

for PAA-HB samples compared to that of PAA samples (Figure 6.11a). As it is shown in Figure 6.11b, despite a negligible change in the equilibrium swelling ratio (ESR) for PAA and PAA-HB samples at pH = 3, increasing the pH value from 7 to 10 resulted in 10% and 23% ESR increases for PAAHB compared to those of PAA, respectively.

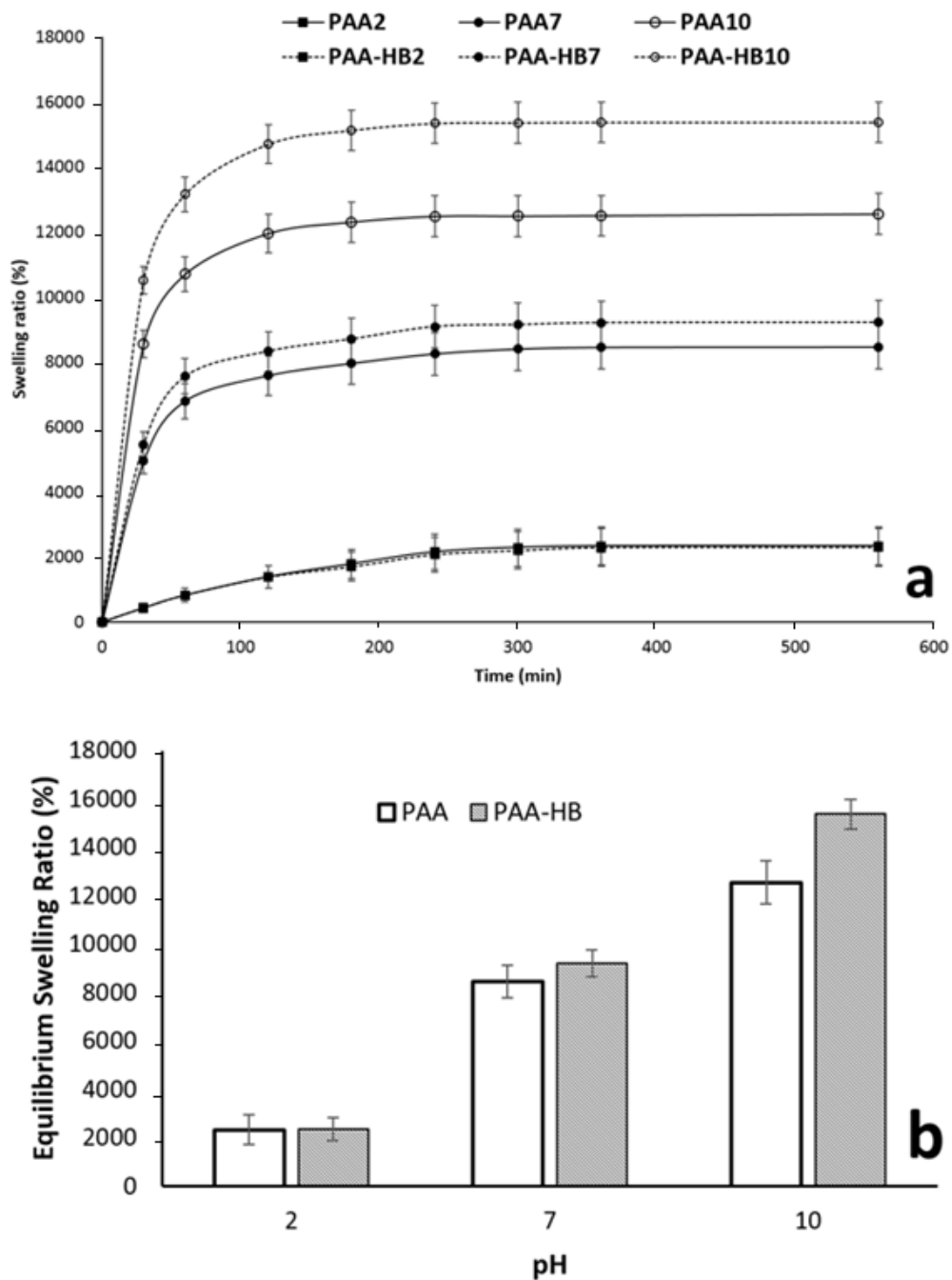


Figure 6.11 Effect of pH values on the (a) swelling kinetics and (b) equilibrium swelling ratio (ESR) of PAA and PAA-HB samples

Dynamic swelling behavior, with the pH value alternating between 2 and 10, was examined to confirm the reversibility of the swelling process and the ability of the samples to maintain their swelling capacity during cycling deformation. All cycles were performed in two hour intervals as swelling kinetics showed that samples approximately approached their equilibrium state after two hours. The ratio of samples' swelling ratio at pH 10 and 2 (mentioned as SR10/SR2 and called the reversibility factor (RF)) was calculated and compared for three cycles. As shown in Figure 6.12a, comparing the 2nd and 3rd cycles to the 1st cycle, changes in RF for PAA-HB samples were significantly lower than those of PAA samples ( $P = 0.046$ ). It means that differences between the swelling ratio at pH 10 and 2 were less for PAA-HB samples as compared to those of PAA samples. Meanwhile, after performing 3 cycles of dynamic swelling, PAA-HB samples were more structurally stable than PAA hydrogels. Deep cracks and dimensional instability were observed in PAA samples after the alternative swelling/deswelling process. HB addition provides improved mechanical properties to the hydrogel, enhances the pH sensitivity of PAA hydrogels and improves the swelling properties with a positive impact on dimensional stability.

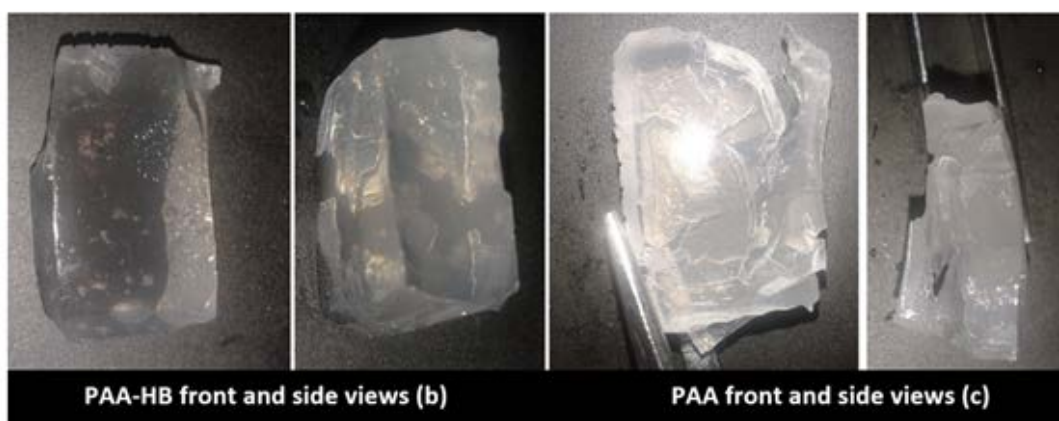
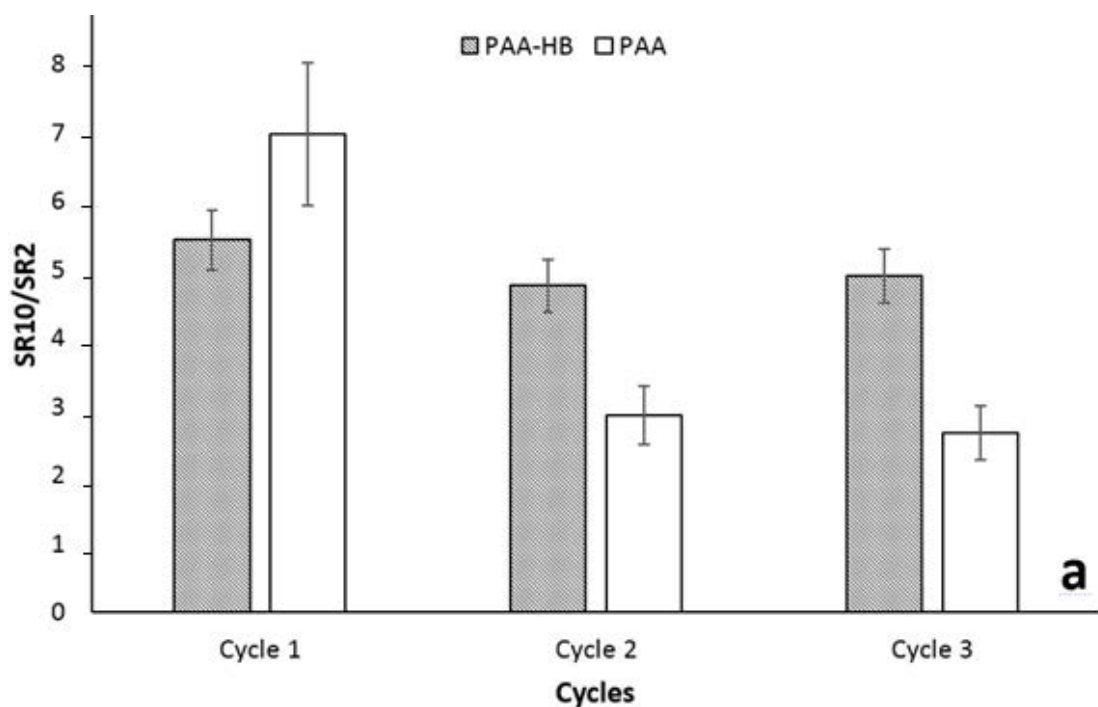


Figure 6.12 (a) Change in the SR10/SR2 ratio during three cycles of dynamic swelling revealed higher pH sensitivity of PAA-HB hydrogels compared to that of PAA samples. After 3 cycles, the better dimensional stability of (b) PAA-HB samples compared to that of (c) PAA samples was in general agreement with the enhanced mechanical properties from HB

## 6.6 Conclusions

To enhance the mechanical properties of PAA, hyperbranched polymers (HB) were employed by *in situ* polymerization with AA monomers. A hydrogel network was formed with the mechanical entanglement of HB into the PAA structure and a possible hydrogen bond between the active group of HB and  $-COOH$  groups of PAA. TEM results showed that spherical HB particles

were well dispersed in the PAA matrix, indicating the good compatibility of PAA with HB. Significant improvements in mechanical properties were achieved when the capability of water uptake was increased by approximately 20%. With the introduction of notches in the PAA and PAA-HB samples, the effects on selected mechanical properties were significant, but notches at least 6 mm or greater had to be introduced to significantly affect the toughness of the PAA-HB samples. It is worth mentioning the possibility of their application in sensors, where the simultaneous enviro-responsive and mechanical properties of hydrogels are important. Besides of developing this novel method to enhance the PAA hydrogel, in next chapter an alternative method would be substituting of PAA nanofibers with PVA with higher mechanical strength and high elasticity with respect to its hydrophilicity nature.

## 6.7 References

1. Brannon-Peppas, L. and Peppas, N.A., 1991. Equilibrium swelling behavior of pH-sensitive hydrogels. *Chemical Engineering Science*, 46(3), pp.715-722.
2. Jabbari, E., Tavakoli, J. and Sarvestani, A.S., 2007. Swelling characteristics of acrylic acid polyelectrolyte hydrogel in a dc electric field. *Smart Materials and Structures*, 16(5), p.1614.
3. Lin, Z., Mei, D., Chen, M., Wang, Y., Chen, X., Wang, Z., He, B., Zhang, H., Wang, X., Dai, W. and Yin, Y., 2015. A comparative study of thermo-sensitive hydrogels with water-insoluble paclitaxel in molecule, nanocrystal and microcrystal dispersions. *Nanoscale*, 7(36), pp.14838-14847.
4. Peng, R., Yu, Y., Chen, S., Yang, Y. and Tang, Y., 2014. Conductive nanocomposite hydrogels with self-healing property. *RSC Advances*, 4(66), pp.35149-35155.

5. Han, L., Lu, X., Wang, M., Gan, D., Deng, W., Wang, K., Fang, L., Liu, K., Chan, C.W., Tang, Y. and Weng, L.T., 2017. A Mussel-Inspired Conductive, Self-Adhesive, and Self-Healable Tough Hydrogel as Cell Stimulators and Implantable Bioelectronics. *Small*, 13(2).
6. Hamed, I., Özogul, F. and Regenstein, J.M., 2016. Industrial applications of crustacean by-products (chitin, chitosan, and chitooligosaccharides): A review. *Trends in Food Science & Technology*, 48, pp.40-50.
7. Eslahi, N., Abdorahim, M. and Simchi, A., 2016. Smart Polymeric Hydrogels for Cartilage Tissue Engineering: A Review on the Chemistry and Biological Functions. *Biomacromolecules*, 17(11), pp.3441-3463.
8. Wang, J., Kaplan, J.A., Colson, Y.L. and Grinstaff, M.W., 2017. Mechanoresponsive materials for drug delivery: harnessing forces for controlled release. *Advanced drug delivery reviews*, 108, pp.68-82.
9. Singhal, R. and Gupta, K., 2016. A Review: Tailor-made Hydrogel Structures (Classifications and Synthesis Parameters). *Polymer-Plastics Technology and Engineering*, 55(1), pp.54-70.
10. Lim, S.L., Tang, W.N.H., Ooi, C.W., Chan, E.S. and Tey, B.T., 2016. Rapid swelling and deswelling of semi-interpenetrating network poly (acrylic acid)/poly (aspartic acid) hydrogels prepared by freezing polymerization. *Journal of Applied Polymer Science*, 24(133), pp.n-a.
11. Zhong, M., Liu, Y.T., Liu, X.Y., Shi, F.K., Zhang, L.Q., Zhu, M.F. and Xie, X.M., 2016. Dually cross-linked single network poly (acrylic acid) hydrogels with superior mechanical properties and water absorbency. *Soft matter*, 12(24), pp.5420-5428.
12. Pal, A., Giri, A. and Bandyopadhyay, A., 2016. Influence of hydrodynamic size and zeta potential of a novel polyelectrolyte poly (acrylic acid) grafted guar gum for adsorption of Pb (II) from acidic waste water. *Journal of Environmental Chemical Engineering*, 4(2), pp.1731-1742.

13. Sharma, S., Dua, A. and Malik, A., 2016. Superabsorbent polymer gels based on polyaspartic acid and polyacrylic acid. *Journal of Material Sciences & Engineering*, 5, p.235.
14. Chen, Y., Zhang, Y., Wang, F., Meng, W., Yang, X., Li, P., Jiang, J., Tan, H. and Zheng, Y., 2016. Preparation of porous carboxymethyl chitosan grafted poly (acrylic acid) superabsorbent by solvent precipitation and its application as a hemostatic wound dressing. *Materials Science and Engineering: C*, 63, pp.18-29.
15. Elliott, J.E., Macdonald, M., Nie, J. and Bowman, C.N., 2004. Structure and swelling of poly (acrylic acid) hydrogels: effect of pH, ionic strength, and dilution on the crosslinked polymer structure. *Polymer*, 45(5), pp.1503-1510.
16. Peppas, N.A. and Sahlin, J.J., 1996. Hydrogels as mucoadhesive and bioadhesive materials: a review. *Biomaterials*, 17(16), pp.1553-1561.
17. Işık, B., 2004. Swelling behavior and determination of diffusion characteristics of acrylamide–acrylic acid hydrogels. *Journal of applied polymer science*, 91(2), pp.1289-1293.
18. Yin, M.J., Yao, M., Gao, S., Zhang, A.P., Tam, H.Y. and Wai, P.K.A., 2016. Rapid 3D patterning of poly (acrylic acid) ionic hydrogel for miniature pH sensors. *Advanced Materials*, 28(7), pp.1394-1399.
19. You, J., Xie, S., Cao, J., Ge, H., Xu, M., Zhang, L. and Zhou, J., 2016. Quaternized chitosan/poly (acrylic acid) polyelectrolyte complex hydrogels with tough, self-recovery, and tunable mechanical properties. *Macromolecules*, 49(3), pp.1049-1059.
20. Li, J., Su, Z., Ma, X., Xu, H., Shi, Z., Yin, J. and Jiang, X., 2017. In situ polymerization induced supramolecular hydrogels of chitosan and poly (acrylic acid-acrylamide) with high toughness. *Materials Chemistry Frontiers*, 1, pp. 310 - 318.

21. Yang, L.Q., Lu, L., Zhang, C.W. and Zhou, C.R., 2016. Highly stretchable and self-healing hydrogels based on poly (acrylic acid) and functional POSS. *Chinese Journal of Polymer Science*, 34(2), pp.185-194.
22. Haq, M.A., Su, Y. and Wang, D., 2017. Mechanical properties of PNIPAM based hydrogels: A review. *Materials Science and Engineering: C*, 70, pp.842-855.
23. He, G., Ke, W., Chen, X., Kong, Y., Zheng, H., Yin, Y. and Cai, W., 2017. Preparation and properties of quaternary ammonium chitosan-g-poly (acrylic acid-co-acrylamide) superabsorbent hydrogels. *Reactive and Functional Polymers*, 111, pp.14-21.
24. Haraguchi, K., 2011. Synthesis and properties of soft nanocomposite materials with novel organic/inorganic network structures. *Polymer journal*, 43(3), pp.223-241.
25. Anseth, K.S., Bowman, C.N. and Brannon-Peppas, L., 1996. Mechanical properties of hydrogels and their experimental determination. *Biomaterials*, 17(17), pp.1647-1657.
26. Kim, D. and Park, K., 2004. Swelling and mechanical properties of superporous hydrogels of poly (acrylamide-co-acrylic acid)/polyethylenimine interpenetrating polymer networks. *Polymer*, 45(1), pp.189-196.
27. Su, Q., Duan, L., Zou, M., Chen, X. and Gao, G.H., 2017. The tough allograft adhesive behavior between polyacrylamide and poly (acrylic acid) hydrophobic association hydrogels. *Materials Chemistry and Physics*, 193, pp.57-62.
28. Zeng, M., Feng, Z., Huang, Y., Liu, J., Ren, J., Xu, Q. and Fan, L., 2017. Chemical structure and remarkably enhanced mechanical properties of chitosan-graft-poly (acrylic acid)/polyacrylamide double-network hydrogels. *Polymer Bulletin*, 74(1), pp.55-74.
29. Liu, X., Duan, L. and Gao, G., 2017. Rapidly self-recoverable and fatigue-resistant hydrogels toughened by chemical crosslinking and hydrophobic association. *European Polymer Journal*, 89, pp.185-194.

30. Thoniyot, P., Tan, M.J., Karim, A.A., Young, D.J. and Loh, X.J., 2015. Nanoparticle–hydrogel composites: Concept, design, and applications of these promising, multi-functional materials. *Advanced Science*, 2(1-2).
31. Yu, Y., De Andrade, L.C.X., Fang, L., Ma, J., Zhang, W. and Tang, Y., 2015. Graphene oxide and hyperbranched polymer-toughened hydrogels with improved absorption properties and durability. *Journal of Materials Science*, 50(9), pp.3457-3466.
32. Naficy, S., Kawakami, S., Sadegholvaad, S., Wakisaka, M. and Spinks, G.M., 2013. Mechanical properties of interpenetrating polymer network hydrogels based on hybrid ionically and covalently crosslinked networks. *Journal of Applied Polymer Science*, 130(4), pp.2504-2513.
33. Naficy, S., Brown, H.R., Razal, J.M., Spinks, G.M. and Whitten, P.G., 2011. Progress toward robust polymer hydrogels. *Australian Journal of Chemistry*, 64(8), pp.1007-1025.
34. Cai, X., Tong, H., Shen, X., Chen, W., Yan, J. and Hu, J., 2009. Preparation and characterization of homogeneous chitosan–polylactic acid/hydroxyapatite nanocomposite for bone tissue engineering and evaluation of its mechanical properties. *Acta biomaterialia*, 5(7), pp.2693-2703.
35. Baker, M.I., Walsh, S.P., Schwartz, Z. and Boyan, B.D., 2012. A review of polyvinyl alcohol and its uses in cartilage and orthopedic applications. *Journal of Biomedical Materials Research Part B: Applied Biomaterials*, 100(5), pp.1451-1457.
36. Park, H. and Park, K., 1996. Biocompatibility issues of implantable drug delivery systems. *Pharmaceutical research*, 13(12), pp.1770-1776.
37. Schwab, E. and Mecking, S., 2005. Synthesis and properties of highly branched polycations with an aliphatic polyether scaffold. *Journal of Polymer Science Part A: Polymer Chemistry*, 43(19), pp.4609-4617.

38. Yuan, J., Soll, S., Drechsler, M., Müller, A.H. and Antonietti, M., 2011. Self-assembly of poly (ionic liquid) s: polymerization, mesostructure formation, and directional alignment in one step. *Journal of the American Chemical Society*, 133(44), pp.17556-17559.
39. Klymenko, A., Nicolai, T., Benyahia, L., Chassenieux, C., Colombani, O. and Nicol, E., 2014. Multiresponsive hydrogels formed by interpenetrated self-assembled polymer networks. *Macromolecules*, 47(23), pp.8386-8393.
40. Lena, J.B., Goroncy, A.K., Thevarajah, J.J., Maniego, A.R., Russell, G.T., Castignolles, P. and Gaborieau, M., 2017. Effect of transfer agent, temperature and initial monomer concentration on branching in poly (acrylic acid): A study by <sup>13</sup>C NMR spectroscopy and capillary electrophoresis. *Polymer*, 114, pp.209-220.
41. Castignolles, P., Graf, R., Parkinson, M., Wilhelm, M. and Gaborieau, M., 2009. Detection and quantification of branching in polyacrylates by size-exclusion chromatography (SEC) and melt-state <sup>13</sup>C NMR spectroscopy. *Polymer*, 50(11), pp.2373-2383.
42. Voorhaar, L. and Hoogenboom, R., 2016. Supramolecular polymer networks: hydrogels and bulk materials. *Chemical Society Reviews*, 45(14), pp.4013-4031.
43. Wang, X., Guo, X., Wang, H. and Guo, P., 2016. Effect of Linear-Hyperbranched Amphiphilic Phosphate Esters on Collagen Fibers. *Journal of agricultural and food chemistry*, 65(1), pp.104-116.
44. Kucharczyk, P., Zednik, J., Humpolicek, P., Capakova, Z. and Sedlarik, V., 2017. Versatile synthesis of comb-shaped poly (lactic acid) copolymers with poly (acrylic acid)-based backbones and carboxylic acid end groups. *Reactive and Functional Polymers*, 111, pp.79-87.
45. Xu, W., Ledin, P.A., Shevchenko, V.V. and Tsukruk, V.V., 2015. Architecture, assembly, and emerging applications of branched functional polyelectrolytes and poly (ionic liquid) s. *ACS applied materials & interfaces*, 7(23), pp.12570-12596.

46. Wang, J., Wang, W. and Wang, A., 2010. Synthesis, characterization and swelling behaviors of hydroxyethyl cellulose-g-poly (acrylic acid)/attapulgite superabsorbent composite. *Polymer Engineering & Science*, 50(5), pp.1019-1027.
47. Wang, W., Kang, Y. and Wang, A., 2013. One-step fabrication in aqueous solution of a granular alginate-based hydrogel for fast and efficient removal of heavy metal ions. *Journal of Polymer Research*, 20(3), pp.101-110.
48. Zhao, J., Dehbari, N., Han, W., Huang, L. and Tang, Y., 2015. Electrospun multi-scale hybrid nanofiber/net with enhanced water swelling ability in rubber composites. *Materials & Design*, 86, pp.14-21.
49. Zu, S.Z. and Han, B.H., 2009. Aqueous dispersion of graphene sheets stabilized by pluronic copolymers: formation of supramolecular hydrogel. *The Journal of Physical Chemistry C*, 113(31), pp.13651-13657.
50. Zhong, M., Liu, Y.T., Liu, X.Y., Shi, F.K., Zhang, L.Q., Zhu, M.F. and Xie, X.M., 2016. Dually cross-linked single network poly (acrylic acid) hydrogels with superior mechanical properties and water absorbency. *Soft matter*, 12(24), pp.5420-5428.
51. Gulyuz, U. and Okay, O., 2014. Self-healing poly (acrylic acid) hydrogels with shape memory behavior of high mechanical strength. *Macromolecules*, 47(19), pp.6889-6899.
52. Yang, J., Gong, C., Shi, F.K. and Xie, X.M., 2012. High strength of physical hydrogels based on poly (acrylic acid)-g-poly (ethylene glycol) methyl ether: role of chain architecture on hydrogel properties. *The Journal of Physical Chemistry B*, 116(39), pp.12038-12047.
53. Lee, J.W., Kim, S.Y., Kim, S.S., Lee, Y.M., Lee, K.H. and Kim, S.J., 1999. Synthesis and characteristics of interpenetrating polymer network hydrogel composed of chitosan and poly (acrylic acid). *Journal of Applied Polymer Science*, 73(1), pp.113-120.
54. Kim, S.Y., Shin, H.S., Lee, Y.M. and Jeong, C.N., 1999. Properties of electroresponsive poly (vinyl alcohol)/poly (acrylic acid) IPN hydrogels under an electric stimulus. *Journal of Applied Polymer Science*, 73(9), pp.1675-1683.

55. Shen, J., Yan, B., Li, T., Long, Y., Li, N. and Ye, M., 2012. Mechanical, thermal and swelling properties of poly (acrylic acid)–graphene oxide composite hydrogels. *Soft Matter*, 8(6), pp.1831-1836.
56. Huang, Y., Lu, J. and Xiao, C., 2007. Thermal and mechanical properties of cationic guar gum/poly (acrylic acid) hydrogel membranes. *Polymer degradation and stability*, 92(6), pp.1072-1081.
57. Yang, J., Han, C.R., Duan, J.F., Ma, M.G., Zhang, X.M., Xu, F., Sun, R.C. and Xie, X.M., 2012. Studies on the properties and formation mechanism of flexible nanocomposite hydrogels from cellulose nanocrystals and poly (acrylic acid). *Journal of Materials Chemistry*, 22(42), pp.22467-22480.

## **7. [IN SITU FORMED INTERNAL WATER CHANNELS IMPROVING WATER SWELLING AND MECHANICAL PROPERTIES OF WSR COMPOSITES<sup>1</sup>]**

In order to strengthen the stability of nanofibers in WSR, nanofibers of PVA and SBS are employed in conventional WSR in this chapter. With the replacement of PAA nanofiber with PVA nanofibers, considerable improvement in elasticity, strength, and water-swelling behaviour was observed. Furthermore, the secondary water-swelling behaviours of the WSR composite showed a remarkable increase in swelling rate as well as in mechanical properties.

1. This work has been published in Journal of Applied Polymer Science: Nazila Dehbari, Javad Tavakoli, Jinchao Zhao, Youhong Tang. "*In situ* formed internal water channels improving water swelling and mechanical properties of water swellable rubber composites." Journal of Applied Polymer Science 134, no. 9 (2017) DOI: 10.1002/app.44548.

## 7.1 Introduction

In Chapter 3, practical solutions were employed to reduce the extraction of SAPs from the rubber matrix of WSRs, such as using a compatibilizer to disperse SAPs well in the rubber phase and neutralizer to enhance the swelling properties [1]. By increasing the swelling ability of WSR the mechanical strength was decreased. To overcome this problem, nanofibers of various polymers were employed. WSR with electrospun nanofibers is a multicomponent product offering swell ability and elasticity similar to those of conventional WSR, while the electrospun nanofibers give the strength properties by reinforcing the composite [2-7].

In next stage, the introduction of nanofibers of PAA and SBS could enhance the properties of WSRs [8, 9]. The role of SBS nanofibers in swelling properties of WSR is negligible due to its hydrophobicity nature, while it has a great impact on mechanical properties of WSR because of its highly elasticity [10-13]. On the other hand, PAA nanofibers in WSR composites produced feasible connections between SAPs resulting in improvement of swelling properties. However, because of the low mechanical strength of PAA nanofibers, especially after water swelling, defects were introduced into the resultant composite, causing the mechanical properties to diminish again after swelling. To address this issue, we proposed two solutions: 1) reinforcing the PAA hydrogel structure by adding HB polymer which was discussed in Chapter 6, and 2) replacing PAA nanofiber with more feasible polymer with high mechanical strength to enhance the resultant WSR composite. Among various polymers, Poly (vinyl alcohol) (PVA) is a semi-crystalline hydrophilic polymer with high biocompatibility and no toxicity, and is usually used to improve materials that have poor physical properties [14-17]. Due to its ease in preparation as a bulk material, films or nanofibers, PVA has been considered for a wide range of applications. One of the main reasons for the attractiveness of PVA nanofibers is their high water permeability without sacrificing flexibility and toughness [18, 19]. Therefore, substituting PAA nanofibers by PVA nanofibers should be effective in enhancing the mechanical properties of WSRs.

In this chapter, WSRs with PVA and SBS nanofibers were investigated. The SBS nanofibers enhanced extensibility and the PVA nanofibers could be in situ dissolved in water to create empty water channels for transferring water between isolated SAPs particles without affecting mechanical strength. The swelling kinetics, contact angle, and mechanical properties of WSR were investigated as a function of PVA/SBS nanofibers with a proposed enhancement mechanism.

## **7.2 Experiments**

### **7.2.1 Materials and methods**

PVA solution (average Mw  $\sim 250,000 \text{ g}\cdot\text{mol}^{-1}$ ), ethylene glycol (EG) (anhydrous, 99.8%), sulfuric acid, mowiol (99.9% hydrolyzed), (3-aminopropyl)-triethoxysilane were obtained from Sigma Aldrich and banana skin silicone rubber was obtained from Barnes products Pty Ltd, Australia. SBS (average Mw  $\sim 300\,000 \text{ g}\cdot\text{mol}^{-1}$ ) was supplied by Yueyang Bailing Huaxing Chemicals Co., Ltd, China. Milli-Q water was used as the solvent to prepare PVA solution. All chemicals were used as received.

Separate homogenous solutions of SBS and PVA were prepared by gentle mechanical stirring at room temperature overnight prior to electrospinning. Ultrafine SBS and PVA nanofibers were prepared by an electrospinning method with optimized parameters of 1.5 mL/h flow rate, 200 rpm collector speed, 10 cm tip-to-collector distance and 15 KV of voltage for about 2 hrs. Then, the resultant nanofibers were added and the resultant composites showed enhanced water swelling ability. They were cut into  $0.5 \times 5 \text{ cm}^2$  strips and added to WSR composite [8]. The amount of PVA in WSR was 1%wt and kept constant (1%wt/1%wt, PVA/SBS) to the effect of SBS to be investigated. Each mold was filled with an equal weight of 10 g of composite. To control the experiment, WSRs without nanofibers were tested with the same condition. All the reported results represent average values from at least three samples.

### 7.2.2 Sample characterization

The water absorbency of WSR composites were determined by measuring the weight of samples before ( $m_0$ ) and after immersing ( $m_1$ ) in water (Milli-Q, 500 mL) at ambient temperature for 1 hr to several days at regular intervals. The excess surface water of the swollen samples was removed by filter papers prior of measuring. The swelling ratio was calculated using the following equation:

$$\frac{m_1 - m_0}{m_0} \times 100$$

where  $m_0$  was the initial dry weight and  $m_1$  was the weight of swollen samples.

Repeated immersion was tested to investigate the effect of both SAPs and electrospun PVA and SBS nanofibers within the matrix. Samples were dried at below 70 °C to reach a constant weight. Then they were again immersed in water at room temperature. At a specified time, they were taken out and the moisture on the surface was removed. The swelling ratio was calculated using the following equation:

$$\frac{m_3 - m_2}{m_2} \times 100$$

where,  $m_2$  and  $m_3$  were the weights of a sample before and after the second water swelling, respectively.

Surface wettability and surface energy of samples were determined by measuring the contact angle (Sinterface, Berlin, Germany) of WSR samples including PVA, SBS, and PVA/SBS nanofibers, using a drop of deionized (DI) water onto a plane solid surface of the corresponding composite. The contact angle measurement was performed at room temperature with about 50–60% relative humidity and the volume of droplet was about 0.4 mL. The Mechanical properties of

samples, including ultimate strength (Load), extensibility and stiffness, were measured by a universal mechanical test machine (Instron, Melbourne, Australia) and compared. Tensile tests were performed at strain rate of 5%/min at room temperature for WSR, WSR+PVA and WSR+PVA/SBS samples until failure in both dry and wet conditions. Samples after first and second swelling were taken out from the water after 350 h and gently blotted with tissue paper to remove excess water from the surface. Rectangular samples in similar dimensions (5 mm×10 mm×2 mm, L×W×T) were attached to the Instron gripper while were secured by sand paper and adhesive. All reported mechanical results represent average values from at least three samples. Because the samples had the same dimensions, the ultimate forces are reported here. The morphology of the electrospun PVA and SBS nanofibers, average nanofiber diameter, and distribution of the electrospun PVA/SBS nanofibers into composites was investigated using field-emission scanning electron microscopy (SEM FEI Inspect F50, Oregon, US) on samples sputtered with platinum.

### **7.3 Results and discussion**

#### **7.3.1 Swelling behaviour**

The swelling behaviour of the samples was characterized by measuring swelling ratio as a function of time for the first and second swelling occasions and the results are presented in Figure 7.1. An increment of swelling ratio was observed in all samples with an increase in time. Unlike the conventional WSR, WSR with nanofibers of PVA and SBS did not reach an equilibrium state after 350 h. With the introduction of PVA nanofibers to WSR, an enhancement of 100% was observed in swelling properties, with the swelling ratio increasing from 14% to 31%. This increase may have resulted from the fact that some parts of ultrafine PVA nanofibers could absorb water and in situ dissolved into water to introduce empty water channels. These newly formed channels could make random interconnections among isolated SAP particles to transfer water within the composite.

In the samples of WSR+PVA/SBS, the increment of swelling ratio (20%) was less than that of WSR/PVA nanofibers (31%), an outcome that was mainly related to the hydrophobic nature of SBS nanofibers. In the WSR/PVA and WSR+PVA/SBS hybrid composites, the water uptake ability was enhanced at the second swelling occasion in comparison with that found in the first swelling occasion from 31% to 39% and 20% to 26%, respectively. This outcome indicated that, at the measurement occasion for the second swelling behaviour, greater transport of water existed among SAPs through water channels created by PVA nanofibers. The conventional WSR had decreased swellability at the second swelling occasion, as similarly reported elsewhere [1, 8, 20]. Since there is no strong interfacial adhesion between hydrophobic elastomer and hydrophilic SAPs, some of SAPs migrate from the bulk into the surface. Therefore, swelling ratio of WSR was marginally lower in second swelling due to the loss of a small amount of SAPs.

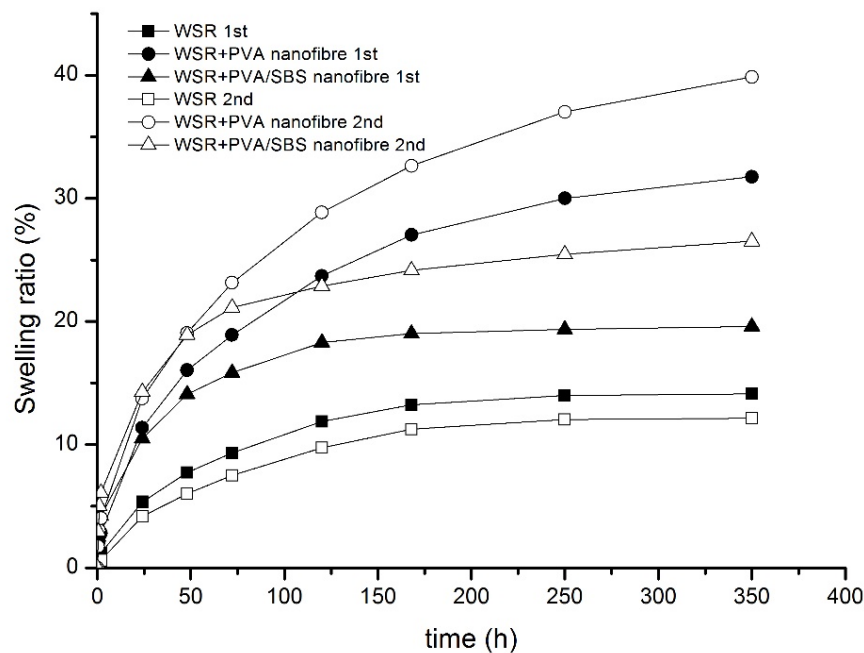


Figure 7.1 Effect of PVA and SBS nanofibers on 1<sup>st</sup> and 2<sup>nd</sup> occasion swelling properties of WSR samples

The initial swelling behaviours of WSR, WSR/PVA nanofiber, and WSR+PVA/SBS nanofiber composites for the first and second swelling measurement are compared in Figure 7.2. Significant variation in the initial swelling ratio (in the first 2 h) among all samples can be seen. The initial swelling ratio increased at the second swelling occasion in the WSR/PVA nanofiber and WSR+PVA/SBS nanofiber samples, indicating the contribution of PVA and SBS nanofibers in the WSR composite's swelling properties at first stage of immersion. This indicated the possibility of in situ formation of water channels by PVA nanofibers that could result in water transfer among SAP particles. However, in the conventional WSR samples, the initial swelling ratio decreased at the second swelling occasion.

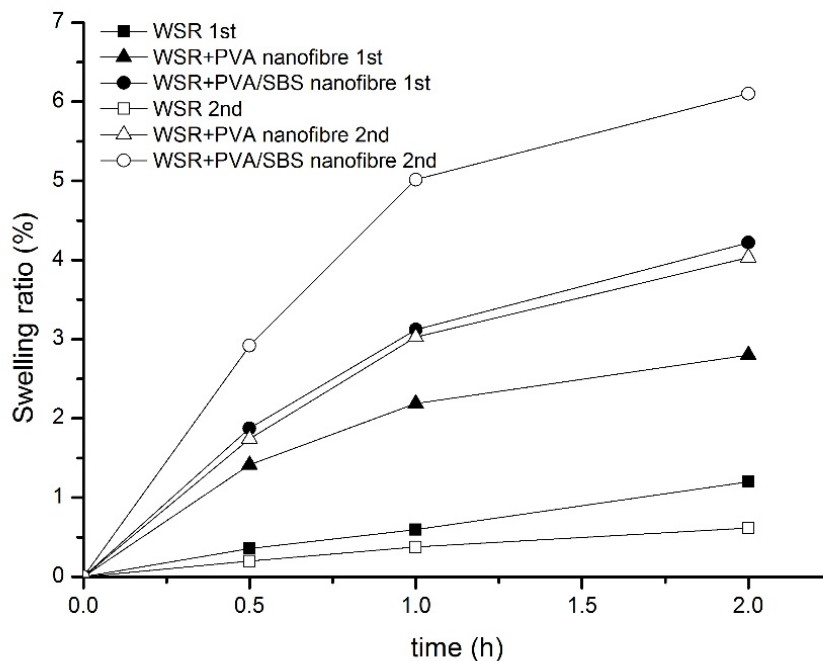


Figure 7.2 Comparison of 1<sup>st</sup> and 2<sup>nd</sup> occasion swelling properties of WSR containing PVA and PVA/SBS nanofibers

Table 7.1 presents the swelling rate changes among the samples in the first and second immersion occasions. The rate of water penetration into the conventional WSR was almost constant in the different swelling occasions, whereas changing the microstructures by the introduction of

hydrophilic/hydrophobic nanofibers significantly affected the water swelling rate in the WSR composites. For the first 2 h of the swelling process, the rate of swelling was almost linear in the conventional WSR, however, the best fit to the swelling characteristic curve of the WSR/PVA nanofiber and WSR+PVA/SBS nanofiber composites was a second degree polynomial. The rate of swelling of the WSR/PVA nanofiber samples almost doubled in the second swelling occasion. However, the initial rate of swelling was greater in the first swelling process in the WSR+PVA/SBS composite. Comparison of the WSR+PVA/SBS nanofiber with the WSR samples showed that the swelling rate was significantly greater in the WSR+PVA/ SBS nanofiber composite in both first and second swelling occasions.

Table 7.1 Mean swelling rate for the WSR composites

<b>Swelling occasion</b>	<b>Composites</b>		
	<b>WSR</b>	<b>WSR/PVA nanofiber</b>	<b>WSR+PVA/SBS nanofiber</b>
<b>1<sup>st</sup></b>	0.49	2.02	1.42
<b>2<sup>nd</sup></b>	0.24	4.10	1.01

Changes in the swelling behaviour of hybrid composites in the short (2 h) and long (350 h) term occurred as a result of alterations to the composites' microstructure created by the PVA or SBS nanofibers. Comparison of the WSR/PVA nanofiber and WSR+PVA/SBS nanofiber samples indicated that, as the PVA nanofibers were water soluble, a small portion of them dissolved and in situ formed water channels within the WSR, while the SBS nanofibers remained unchanged and were mainly incorporated in the mechanical property enhancement. These findings are consistent with the results obtained from mechanical testing and SEM analysis.

### 7.3.2 Contact angle

The contact angle measurements of WSR composites with and without nanofibers are shown in Table 7.2. With the addition of PVA nanofiber into the WSR, the wettability and surface energy of the samples increased as expected, due to the increase in hydrophilicity of the samples. However, the surface properties of the WSR+PVA/SBS nanofiber composites did not change greatly compared with the WSR+PVA nanofiber composites, implying that, although SBS nanofibers caused a reduction in the swelling ratio of the composites, they had only a minor effect on the surface wettability of the composites.

Table 7.2 Comparison of contact angle and surface energy for different samples

Sample	Contact angle (°)	Surface energy (mN/m)
WSR	74	28.9
WSR/PVA nanofiber	54.73	41.9
WSR+PVA/SBS nanofiber	57.21	35.9

### 7.3.3 Morphological study

The effectiveness of nanofibers within the WSR depends on the concentration of nanofibers used, the processing type, and the interface between phases. Figure 7.3 presents SEM images of PVA nanofiber, WSR with PVA and PVA/SBS nanofiber, compared with the conventional WSR. In Figure 7.3(a), PVA nanofiber created tiny empty water channels that could connect isolated SAP particles within the rubber matrix. Some PVA nanofibers with the average diameter of 2 nm were dissolved into water in situ to form these interconnections among isolated hydrophilic SAP particles. The diameter of the observed micro-channels was comparable with that of the PVA nanofiber, as shown in Figure 7.3(b). Change in structural organization of these water channels was seen around the SAPs, as shown in Figure 7.3(a). As indicated in Figure 7.3(c), with combinations

of SBS and PVA nanofibers through the rubber matrix after swelling, a spider web-like structure of SBS nanofiber ranging from submicron (1 mm) to nano size (700-800 nm) developed. In the conventional WSR (Figure 7.3(d)], no channels were observed after swelling. It is suggested that PVA nanofiber were responsible for the transfer of water among isolated SAPs while the SBS nanofibers held the SAPs within the matrix, preventing their migration from the bulk to the surface.

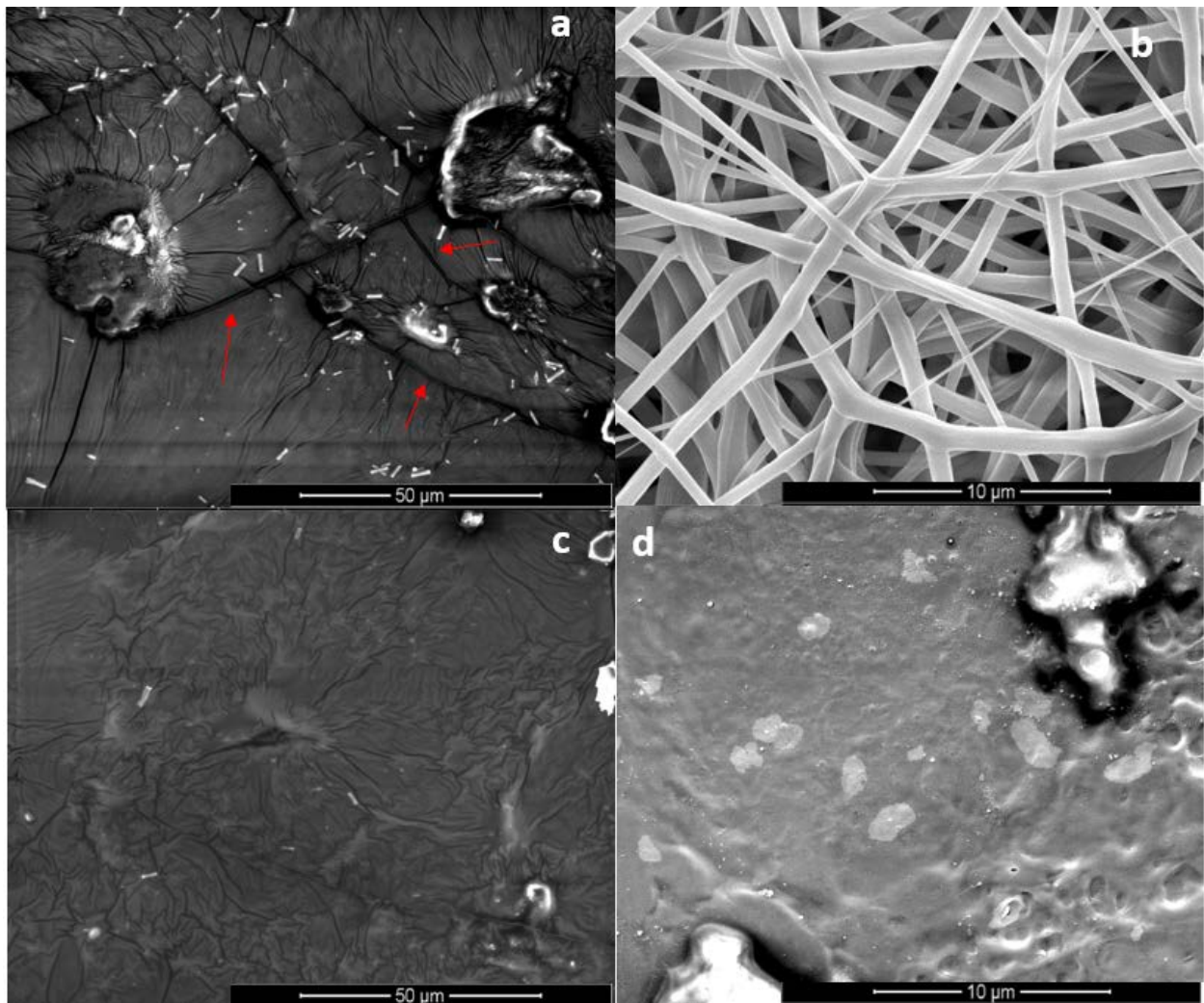


Figure 7.3 SEM micrographs of (a) WSR/PVA nanofiber, (b) PVA nanofibers, (c) WSR+PVA/SBS nanofiber and (d) WSR after 350 h immersing in water

A schematic diagram of water channel formation across WSR+PVA/SBS nanofiber samples is presented in Figure 7.4. By virtue of the distribution of interconnections created by the PVA nanofiber, a consistent network between hydrophilic elements of the composite was formed. This

appearance suggests the existence of specific intermolecular interaction between PVA nanofiber and SAPs. These in situ formed water channels were responsible for water penetration into the composites and improvement of the water absorption properties.

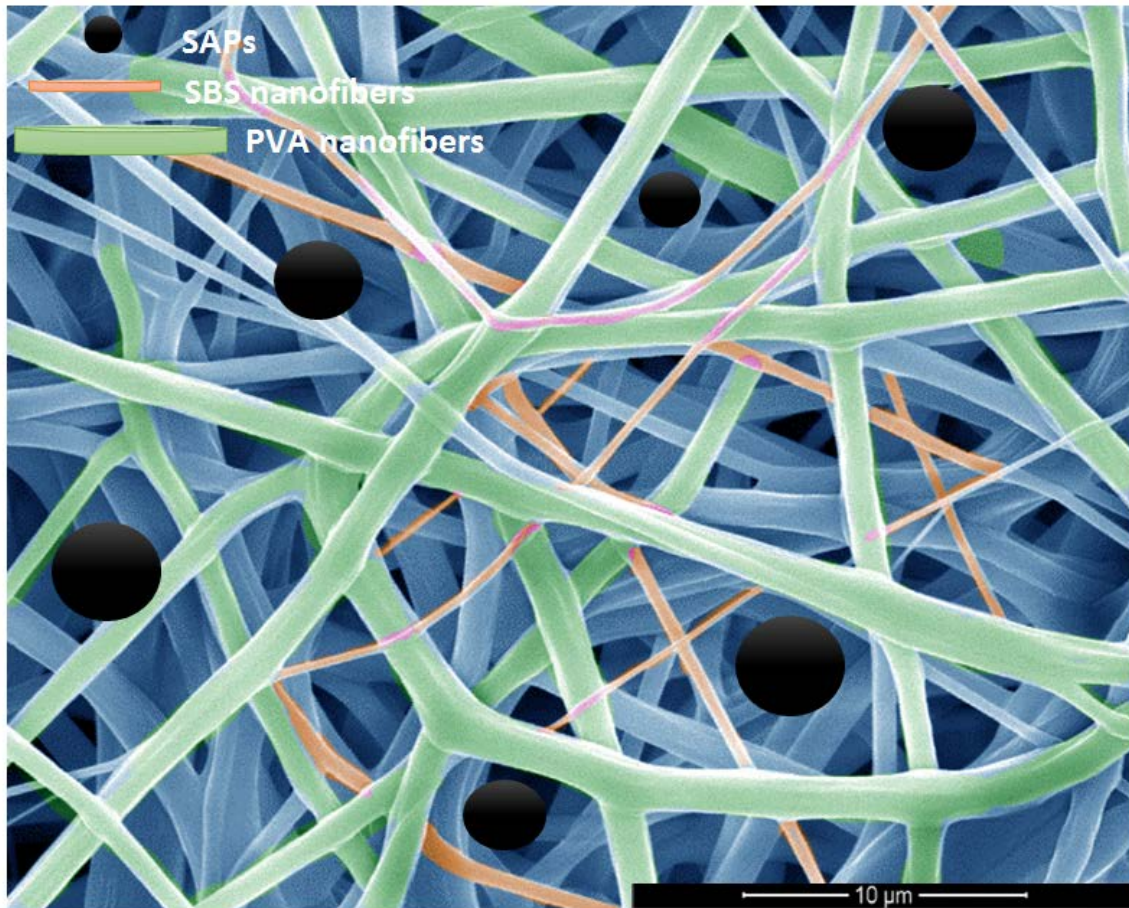


Figure 7.4 Schematic diagram of water channel formation in the WSR+PVA/SBS nanofiber composite

Moreover, PVA/SBS nanofiber (in a mat form) could prevent the migration of SAP particles from the rubber matrix by bonding them together with PVA nanofibers that were dissolved in the water and SBS nanofibers linked the mat and WSR closely. As a result, in this case of studying all investigated composites, introducing PVA/SBS nanofibers was found to enhance both swellability and mechanical properties simultaneously.

### 7.3.4 Mechanical behaviour

One of the prerequisites for good mechanical performance is achieving desirable interactions of fiber-matrix in the composite. In the WSR combined with nanofibers, the ultimate tensile strength (reported as load here) and stiffness increased. The results of measurements of the mechanical properties of WSR without and with nanofibers of PVA and SBS with all investigated composites are presented for the dry state and after the first and second swelling, and shown in Table 7.3 and Figure 7.5. The improvements in ultimate load, stretchability, and stiffness of the WSR+PVA/SBS nanofiber were significantly obvious from other samples.

Table 7.3 Selected mechanical properties for nanofibers and hybrid composites

<b>samples</b>		<b>Extension (%)</b>	<b>Ultimate Load (N)</b>	<b>Stiffness (N.m<sup>-1</sup>)</b>
<b>Dry composites</b>	WSR	1200±60	10.0±0.5	0.40±0.02
	WSR/PVA	600±30	22.0±1.1	1.20±0.06
	WSR+PVA/SBS	600±45	16.0±1.2	0.50±0.02
<b>Composites after 1<sup>st</sup> swelling</b>	WSR	800±40	5.0±0.3	0.20±0.01
	WSR/PVA	300±15	32.0±1.6	2.30±0.01
	WSR+PVA/SBS	600±30	50.0±2.5	3.90±0.20
<b>Composites after 2<sup>nd</sup> swelling</b>	WSR	600±30	2.0±0.1	0.18±0.01
	WSR/PVA	300±30	22.0±2.2	1.80±0.20
	WSR+PVA/SBS	800±80	58.0±6.0	4.00±0.50

Compared with WSR, WSR/PVA nanofiber reached an ultimate load more than twice as high (from 10 N to 22 N) in the dry state. After swelling, WSR/PVA nanofiber samples experienced a decrease in extension from 600% to 300%, which could relate to ultrafine PVA nanofiber dissolving in water and causing weak points to elongate more. In the WSR+PVA/SBS nanofiber samples, an improvement in extension at breaking point (600–800%) was observed alongside a

higher ultimate load (50–58 N) after the first and second swellings, respectively. The improvement in the mechanical properties of the WSR+PVA/SBS nanofiber samples might be a consequence of the impact of SBS nanofiber on stress distribution through the WSR composite [3].

In the second swelling, more water channels were formed by PVA nanofiber such that water channels could act as plasticizer while increasing the composite’s extension ability.

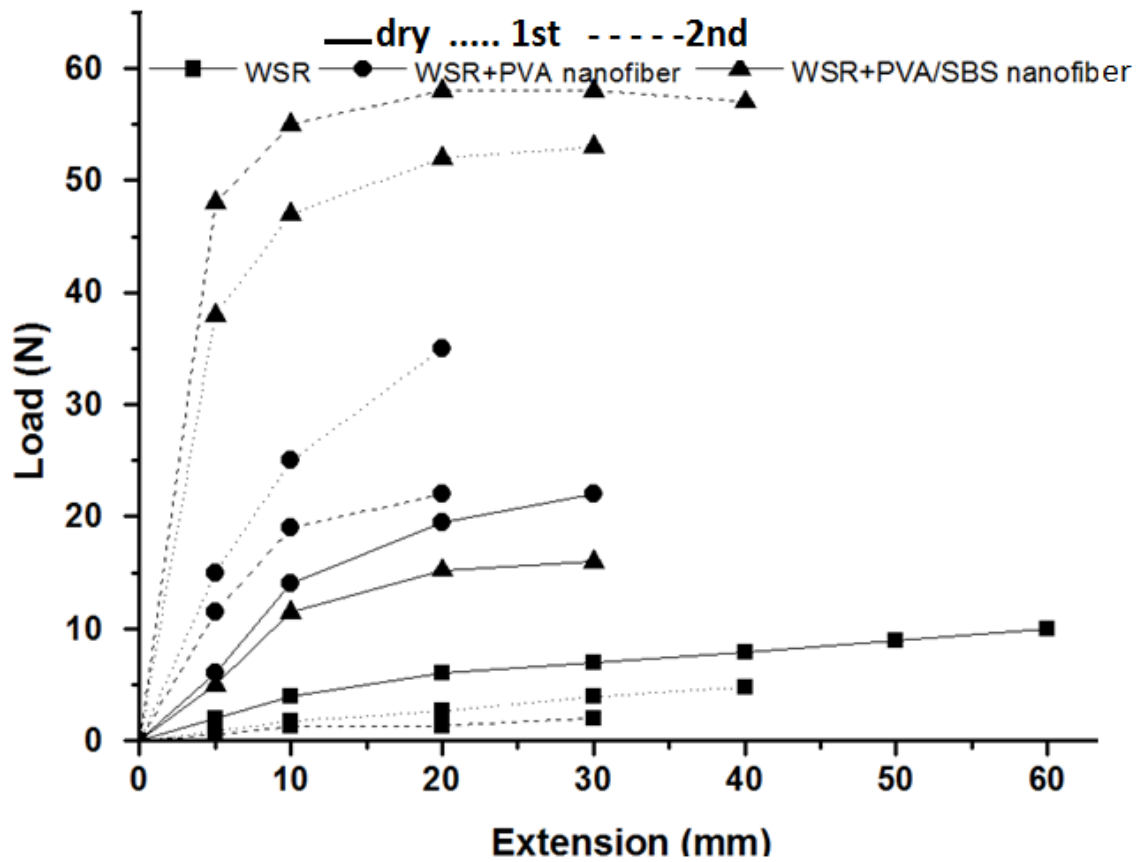


Figure 7.5 Load-extension diagram for WSR, WSR/PVA nanofiber and WSR+PVA/SBS nanofiber in dry state and after first and second swelling

As is well known, the mechanical properties of WSR have an inverse relationship with the swelling behaviour. Penetrating water within the WSR could have caused phase separation between hydrophilic rubber and hydrophobic SAPs. Moreover, migration of SAPs from the bulk could have created some voids/holes within the WSR during the swelling process, reducing the mechanical

properties, as the related defects within the rubber structures created stress concentrations. Also, poor mixing of the SAPs as well as differences in particle size had their own diverse impacts on the strength of the WSR samples. This interpretation is compatible with the results of the measurements of WSRs' swelling.

#### **7.4 Conclusions**

The current chapter mainly focused on the influence of electrospun PVA and SBS nanofibers on the water swellability and mechanical properties of the conventional WSR composites. Swelling behaviours of the composites were enhanced by the addition of PVA nanofiber. Due to their hydrophilic nature, they could in situ dissolve in water and form water channels to transfer water among isolated SAPs in the WSR matrix. Morphological study of the cross-sectional surfaces of samples confirmed the presence of these tiny micro water channels distributed within the matrix. As an important finding, the significant contribution of both PVA and SBS nanofiber led to enhancement in mechanical properties compared with those of the conventional WSR.

#### **7.5 References**

1. Dehbari, N., Zhao, J., Peng, R. and Tang, Y., 2015. Neutralisation and compatibilisation effects on novel water-swellaible rubber composites. *Journal of Materials Science*, 50(15), pp.5157-5164.
2. Hansen, L.M., Smith, D.J., Reneker, D.H. and Kataphinan, W., 2005. Water absorption and mechanical properties of electrospun structured hydrogels. *Journal of Applied Polymer Science*, 95(2), pp.427-434.
3. Gestos, A., 2012. The development of electrospun polymer nanofibres and measurement of their individual mechanical properties with the atomic force microscope.
4. Ren, C., 2013. PAN nanofibers and nanofiber reinforced composites.

5. Blond, D., Walshe, W., Young, K., Blighe, F.M., Khan, U., Almecija, D., Carpenter, L., McCauley, J., Blau, W.J. and Coleman, J.N., 2008. Strong, tough, electrospun polymer–nanotube composite membranes with extremely low density. *Advanced Functional Materials*, 18(17), pp.2618-2624.
6. Wu, M.S., Ou, Y.H. and Lin, Y.P., 2010. Electrodeposition of iron oxide nanorods on carbon nanofiber scaffolds as an anode material for lithium-ion batteries. *Electrochimica Acta*, 55(9), pp.3240-3244.
7. Merzlyak, A., Indrakanti, S. and Lee, S.W., 2009. Genetically engineered nanofiber-like viruses for tissue regenerating materials. *Nano letters*, 9(2), pp.846-852.
8. Zhao, J., Dehbari, N., Han, W., Huang, L. and Tang, Y., 2015. Electrospun multi-scale hybrid nanofiber/net with enhanced water swelling ability in rubber composites. *Materials & Design*, 86, pp.14-21.
9. Dehbari, N., Tavakoli, J., Zhao, J. and Tang, Y., 2017. In situ formed internal water channels improving water swelling and mechanical properties of water swellable rubber composites. *Journal of Applied Polymer Science*, 134(9).
10. Subbiah, T., Bhat, G.S., Tock, R.W., Parameswaran, S. and Ramkumar, S.S., 2005. Electrospinning of nanofibers. *Journal of Applied Polymer Science*, 96(2), pp.557-569.
11. Kim, J.S. and Reneker, D.H., 1999. Mechanical properties of composites using ultrafine electrospun fibers. *Polymer composites*, 20(1), pp.124-131.
12. Park, M., Im, J., Shin, M., Min, Y., Park, J., Cho, H., Park, S., Shim, M.B., Jeon, S., Chung, D.Y. and Bae, J., 2012. Highly stretchable electric circuits from a composite material of silver nanoparticles and elastomeric fibres. *Nature nanotechnology*, 7(12), pp.803-809.
13. Borba, P.M., Tedesco, A. and Lenz, D.M., 2014. Effect of reinforcement nanoparticles addition on mechanical properties of SBS/Curauá fiber composites. *Materials Research*, 17(2), pp.412-419.

14. Li, Y., Neoh, K.G. and Kang, E.T., 2004. Poly (vinyl alcohol) hydrogel fixation on poly (ethylene terephthalate) surface for biomedical application. *Polymer*, 45(26), pp.8779-8789.
15. Tadd, E., Zeno, A., Zubris, M., Dan, N. and Tannenbaum, R., 2003. Adsorption and polymer film formation on metal nanoclusters. *Macromolecules*, 36(17), pp.6497-6502.
16. Park, J.C., Ito, T., Kim, K.O., Kim, K.W., Kim, B.S., Khil, M.S., Kim, H.Y. and Kim, I.S., 2010. Electrospun poly (vinyl alcohol) nanofibers: effects of degree of hydrolysis and enhanced water stability. *Polymer journal*, 42(3), p.273.
17. Lin, W.C., Yu, D.G. and Yang, M.C., 2006. Blood compatibility of novel poly ( $\gamma$ -glutamic acid)/polyvinyl alcohol hydrogels. *Colloids and Surfaces B: Biointerfaces*, 47(1), pp.43-49.
18. Mansur, H.S., Sadahira, C.M., Souza, A.N. and Mansur, A.A., 2008. FTIR spectroscopy characterization of poly (vinyl alcohol) hydrogel with different hydrolysis degree and chemically crosslinked with glutaraldehyde. *Materials Science and Engineering: C*, 28(4), pp.539-548.
19. Park, S.Y., Jun, S.T. and Marsh, K.S., 2001. Physical properties of PVOH/chitosan-blended films cast from different solvents. *Food hydrocolloids*, 15(4), pp.499-502.
20. Zhang, Z., Zhang, G., Wang, C., Liu, D., Liu, Z. and Chen, X., 2001. Chlorohydrin water-swelling rubber compatibilized by an amphiphilic graft copolymer. III. Effects of PEG and PSA on water-swelling behavior. *Journal of applied polymer science*, 79(14), pp.2509-2516.

## **8. [CONCLUSIONS AND FUTURE DIRECTIONS]**

The overriding purpose of this thesis was to determine the importance of WSR when viewed from an industrial perspective. To accomplish that goal, it became necessary to study the possible applications of WSR and compare the achieved WSR with commercial WSR. Determining what parameters are necessary to measure in terms of specific application and how that ideal WSR is connected with the field of technology assumed a high degree of importance during the literature review conducted for this dissertation. This chapter demonstrates a brief discussion of current work, conclusions and some of the directions for future research that stem from the project.

## 8.1 Summary

The research undertaken using superabsorbent polymers (SAPs) within the rubber has established a paradigm shift in materials science and engineering. This has opened new possibilities of fabricating water-swellaible rubber (WSR). The past few years of research, devoted to find some practical ways to control the migration of SAPs from rubber and grow the swelling rate of WSR composites, has resulted in significant advances in this field with the ability to exquisitely tailor the mechanical, physical and chemical properties for targeted applications.

Fabrication of conventional WSR has greatly influenced by filling gaps in field of chemical physics of polymers. The aim of the research herein was to overcome defects of conventional WSR and develop new method(s) for fabricating WSR in a more benign way with this view that it will facilitate transferring the technology to the market place. Although most of the conventional methods for fabricating WSR are significant innovations in engineering and science field, the main issues and limitations that are yet to be addressed are the generation of high levels of waste, energy usage, the need for downstream processing, and also limited scope for scaling up the processes. The use of compatibilizers and high-tech processing in many of those methods are pivotal for stabilising the structures and reducing the migration of SAPs from WSR [1-5]. However, when addressing potential for scalability of a process, these requirements raise concerns due to the high costs and the difficulties of downstream processing. In the present study, we tried to address these issues at the inception of the science.

To summarize the findings in this thesis, the use of electrospun nanofibers into the WSR has resulted in significant advancement in both physical and mechanical properties. The research provides an in-depth study on the use of SAPs and nanofibers within rubber.

A number of significant advancements have been made herein, firstly in preventing the migration of SAPs from WSR by neutralizing and compatibilizing of composites, as detailed in Chapter 3. The addition of NaOH as the neutraliser and aminopropyltriethoxysilane as the compatibilizer, water swelling ability and durability of conventional WSR increased. However, when the compatibilizer and the neutraliser were added together, the water swelling ability and durability of the WSR composites further increased by virtue of the synergistic effects due to the increased interfacial cohesion between the PDMS and PAA [6].

In Chapter 4, another significant advance was investigated by utilizing electrospun multi-scaled hybrid fiber mats into the WSR. The research focused on swelling properties by means of fabricating WSR in presence of nanofiber mats. A remarkable finding of this chapter is formation of internal multi-scale water channels and enhancement of specific surface areas between SAPs and rubber. The electrospun nanofibers of PAA and PAA hybrid fillers with spider web-like structure provide a bridge between isolated PAA particles which wrapped in hydrophobic rubber and link the internal SAPs with the composite surface to enhance the short- and long-term water swelling ability of WSR. The effects and mechanisms of those nanofibers on are also discussed [7].

Chapter 5 provides a detailed study on the use PAA/SBS nanofiber to improve both mechanical and physical properties of WSR. Enhancement of the swellability of WSR+PAA/SBS nanofiber mats was derived from the PAA constituent absorbing water from the surface into the bulk and introducing random internal water channels between discontinuous superabsorbent polymers. The role of SBS nanofibers in the composite of WSR+PAA/SBS nanofiber mats was more related to the mechanical properties, where the breaking force of the composite increased to twice that of the conventional WSR [8].

Chapter 6 mainly focused on toughening of SAP hydrogels without sacrificing the swelling ability. By adding high molecular weight hyperbranched polymers (HB) in PAA networks during in situ polymerisation, formation of hydrogen bonding and physical entanglement can be increased. The characterization results of PAA hydrogel showed well dispersion of spherical HB particles into the PAA matrix, indicating the good compatibility of PAA with HB. The most significant improvements were observed in mechanical properties where the toughness of PAA (with and without notch) was extremely increased. As an example in high depth of notch (14 mm), PAA-HB hydrogel shows 10.5 times higher toughness than pure PAA (from 33 to 347 kJ/m<sup>3</sup>) [9].

The last outcome of this research is using nanofibers of PVA and SBS in WSR, as detailed in Chapter 7. The main advantage of the nanofibers of PVA and SBS in conventional WSR relates to considerable improvement in elasticity and strength without dropping in water swelling ability. After immersion, PVA nanofibers dissolved within the composite to in situ form water channels to connect isolated SAPs. Those water channels led to an increase in water uptake by the WSR composite. Furthermore, the secondary water-swelling behaviours of the WSR composite showed a remarkable increase in swelling rate as well as in mechanical properties. The addition of SBS nanofibers had a marked impact on the mechanical properties of the WSR composite. Their roles became more pronounced after water immersion. However, the results of this study can be used for further optimization. Unique mechanical behaviour of PVA and SBS nanofibers, their networks, and nanofiber-reinforced WSR composites analysed in this work for will be beneficial to a broad variety of applications and can contribute to the development of the next generation structural WSR nanocomposites [10].

## **8.2 Comparison of Commercial WSR with studied WSR**

Classic WSRs can swell when they come into contact with water. It is a given fact, and unless some error has been made in the design of the application, swelling is guaranteed to occur.

Unlike conventional caulking materials, which remain inert and passive following application such as pipe penetration, utility vaults, storage reservoirs and construction joints, the hydrophilic properties of water stop adhesive such as Leakmaster is the most comparable products in market that allow the cured material to swell upon subsequent contact with water. The specifications of Leakmaster are presented in Figures 8.1 and 8.2 and Table 8.1.



Figure 8.1 An example of usage Leakmaster in pre-cast applications such as utility vaults and storage reservoirs [11]

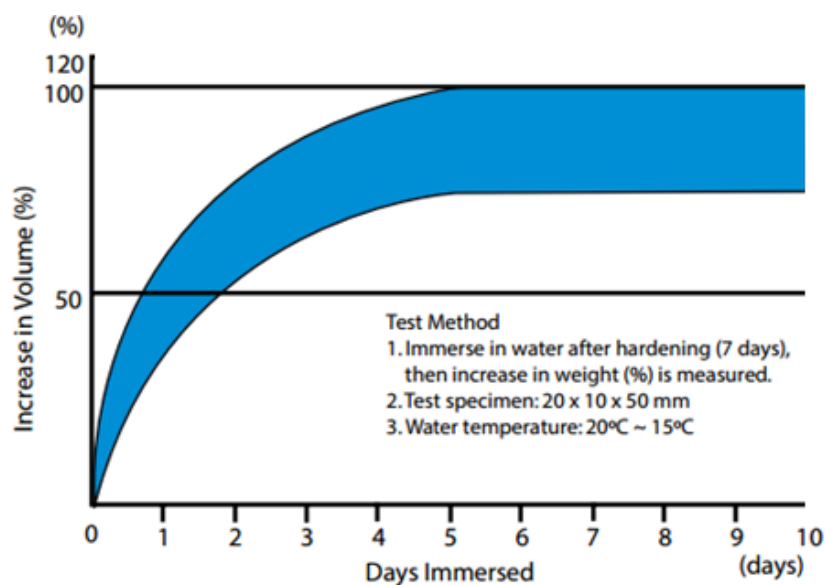


Figure 8.2 Swelling properties of Leakmaster after immersing in water [11]

Table 8.1 Mechanical properties of Leakmaster [11]

<b>Composition:</b> polyurethane prepolymer (TDI-based) <b>Packaging:</b> 320 ml per tube, 24 tubes per carton.	
<b>Before curing</b>	
Appearance: Specific Gravity: Extrudability: Slump: Tack-Free Time:	Grey mastic 1.30 (20°C) under 30 sec less than 3 mm 8 hours at 23°C
<b>After curing</b>	
Hardness: Tensile Strength: Elongation: Tear Strength:	35 SHORE A 30 kg/cm <sup>2</sup> 1250% 10 kg/cm
<b>Adhesion</b>	
50% Tensile Strength: Max. Tensile Strength: Elongation at break:	6.5 kg/cm <sup>2</sup> 11.1 kg/cm <sup>2</sup> 570%
<b>Coverage (bead diameter)</b>	
3 mm: 6 mm: 8 mm: 10 mm:	20–25 m 8–10 m 4–5 m approx. 3 m

### 8.2.1 Experiments

Using similar condition tests to what was achieved for the studied WSR in Chapter 7, provided us information about physical and mechanical properties of the commercial WSR as follows:

The mechanical behaviour of the samples was investigated using a tensile testing machine (Instron, Australia) at strain rate of 5%/min at room temperature until failure. Samples after first and second swelling were taken out from the water after 350 h and gently blotted with tissue paper to remove excess water from the surface. Due to the same dimensions of samples, the ultimate

forces are reported here. All reported mechanical results represent average values from at least three samples.

The swelling properties of commercial WSR was determined by measuring the weight of samples before ( $m_0$ ) and after immersion ( $m_1$ ) in water at ambient temperature for 1 h over several days at regular intervals. The excess surface water of the swollen samples was removed by filter papers prior to measuring. The swelling ratio was calculated using the equation:

$$\frac{m_1 - m_0}{m_0} \times 100$$

where  $m_0$  was the initial dry weight and  $m_1$  was the weight of swollen samples.

For the repeated immersion test, samples were dried at below 70 °C to reach a constant weight. Then they were again immersed in water at room temperature. After a specified time they were taken out and the moisture on the surface was removed. The swelling ratio was calculated for at least three samples.

### **8.2.2 Results and discussion**

The results of tensile measurements for dry state and after the first and second swelling are shown and compared with WSR+PVA/SBS nanofiber composites in Chapter 7 in Figure 8.3. By immersing the commercial WSR into water after 350 hrs, the ultimate load decreased from 44 N to 35 N and 27 N in first and second immersing time, respectively (Figure 8.3 a). However, the improvement in ultimate load for the WSR+PVA/SBS nanofiber is significant from 16 N to 50 N and 58 N in dry state and after immersion for the first and second time, respectively.

The extension at breaking point for commercial WSR is also subjected to change from 24 mm to 18 mm and 15 mm. These results show the mechanical properties of commercial WSR can be affected by immersing time due to the loss of swelling agent within the composite. In the

WSR+PVA/SBS nanofiber samples, an improvement in extension at breaking point (30 mm to 40 mm) after second swelling was observe which may relates to the water channel formed by PVA nanofibers that can act as plasticizer to enhance the extensibility of composite and considerable strength of SBS nanofiber [10, 12-14].

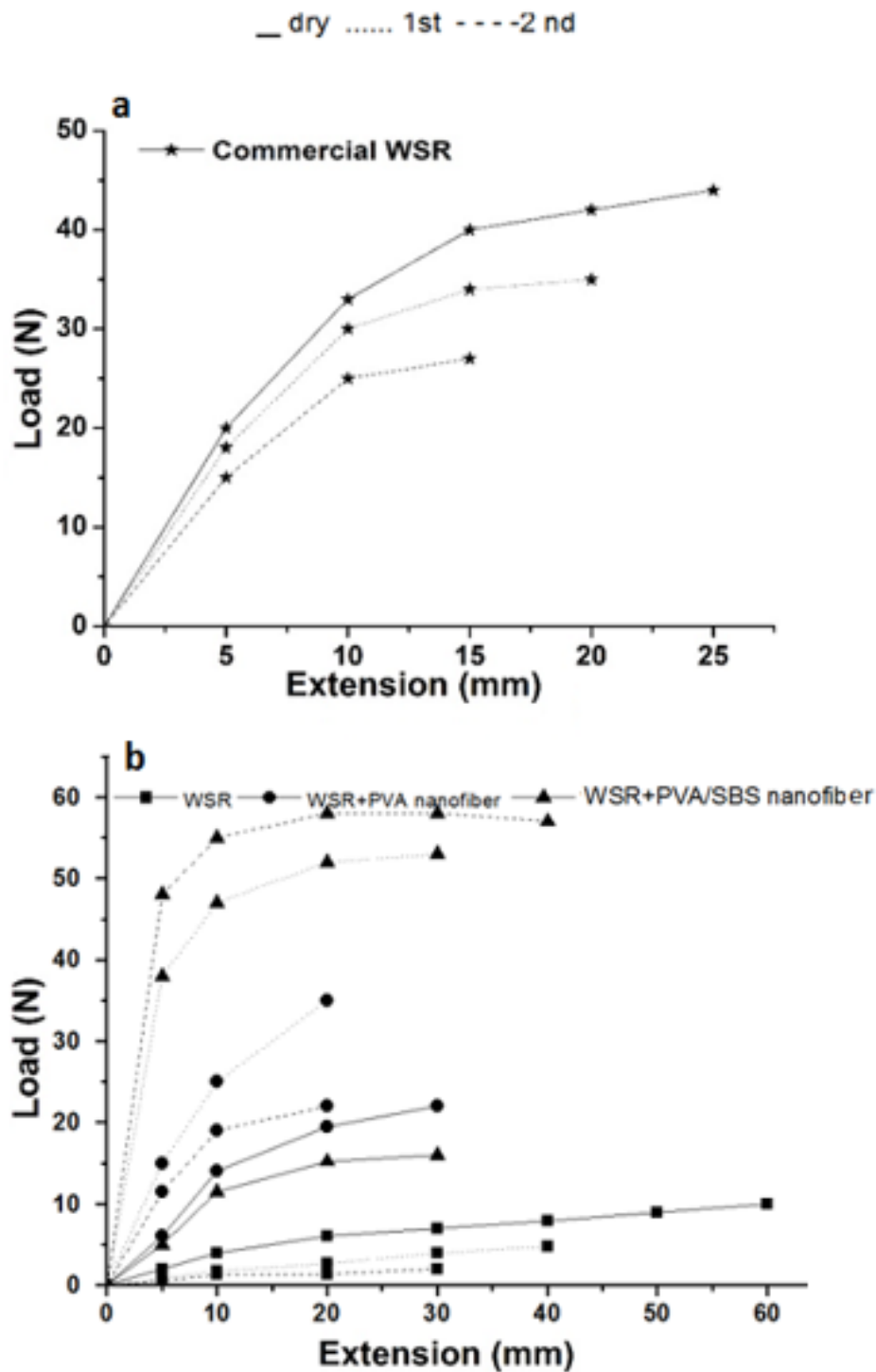


Figure 8.3 Load-extension curves in dry state and after the first and second swelling for a) Commercial WSR and b) WSR+PVA/SBS nanofiber composite

The swelling behaviour of commercial WSR and WSR+PVA/SBS nanofiber after first and second immersion in water are shown in Figure 8.4. As we can see, the swelling ratio in first hour of immersion was quick and after a while, it reached to equilibrium of 58%. In second swelling, same trend was observed with a small loss in swelling about 2% (Figure 8.4 a).

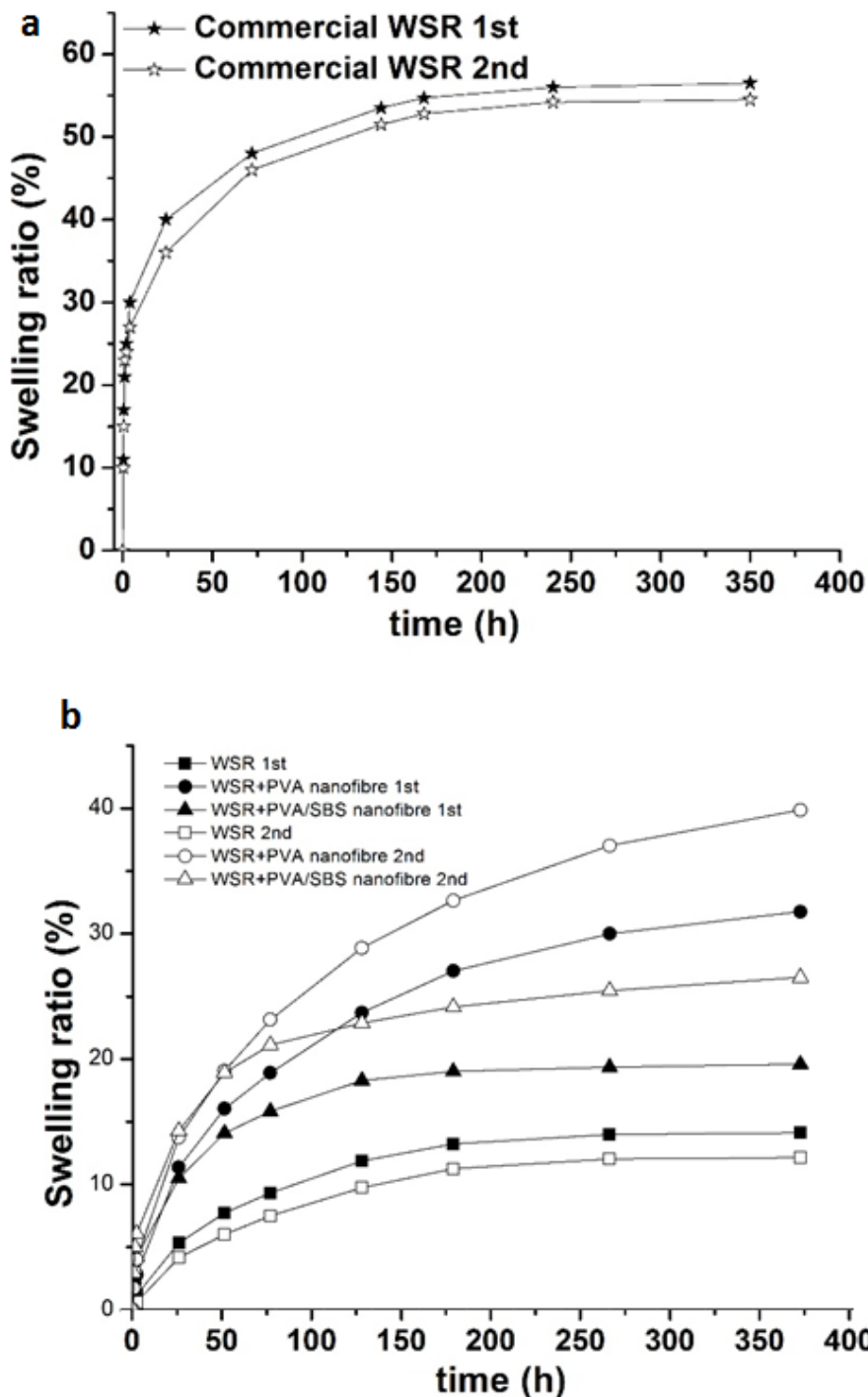


Figure 8.4 Water swellability of a) Commercial WSR b) WSR+PVA/SBS nanofiber composite for first and second swelling

Unlike the commercial WSR, WSR with nanofibers of PVA and SBS did not reach an equilibrium state after 350 h (Figure 8.4 b). By introducing PVA/SBS nanofiber in WSR, the swelling ratio shows an increment of 20%, mainly related to ultrafine PVA nanofibers that could absorb water and form in situ water channels. These channels could connect isolated SAP particles to transfer water within the WSR composite. Interestingly, at the second swelling, swelling ability was enhanced occasion from 20% to 26% in comparison with the first immersion in water, showing greater transport of water among SAPs through water channels created by PVA nanofibers.

Figure 8.5 compares the images of WSRs in dry stage, after 3 months immersion and after 6 months of immersion. Commercial WSR (here Leakmaster) hasn't change in dimensions. However, WSR with nanofibers of PVA and SBS shows a huge change in size due to absorbing water over the time.

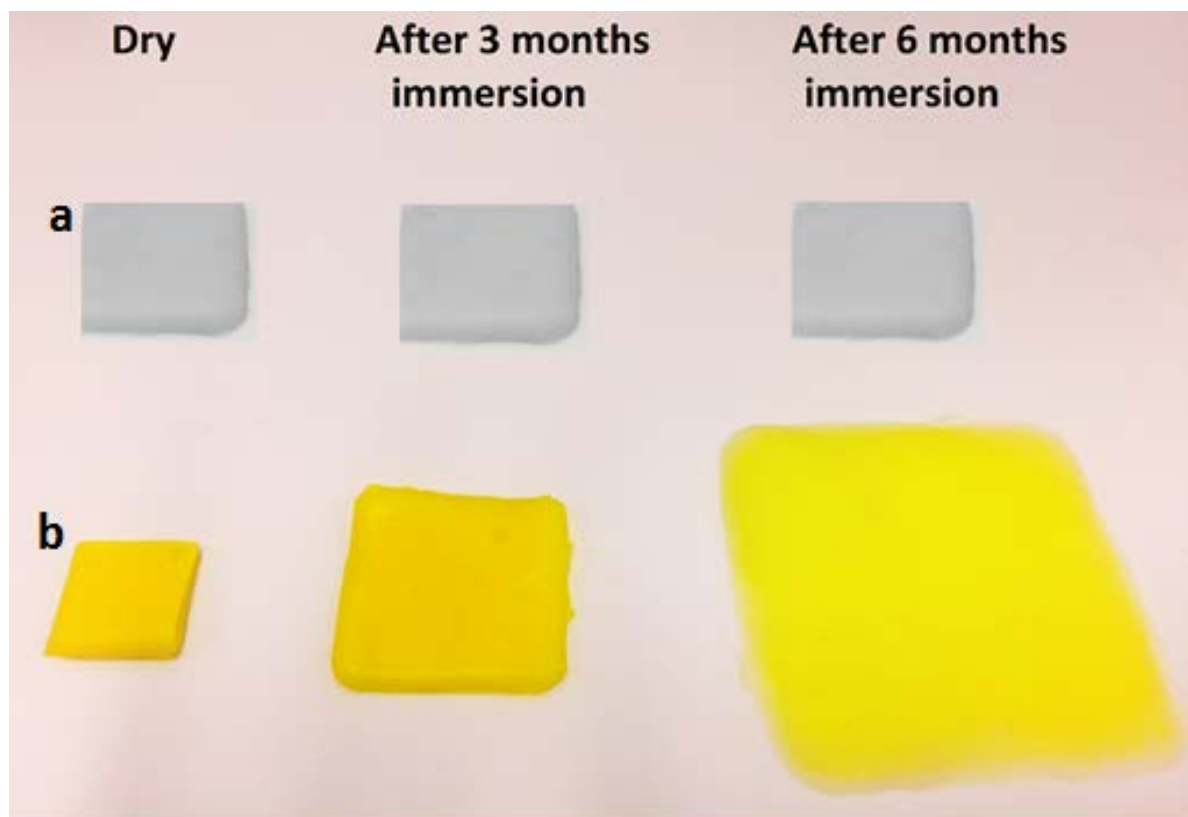


Figure 8.5 Images of a) commercial WSR and b) studied WSR in dry and after 3 months and 6 months of immersion

Thus, it is evident that novel WSR in this study shows great potential for the fabrication in bigger scales rather than classic WSR. This method now allows for translating this novel material towards affording novel hybrid composites.

### **8.3 Recommendations and Future Directions**

Future work about WSR could be focused on (1) how to prepare WSR by utilizing PAA-HB instead of pure PAA resin, (2) the effect of diameter and aspect ratio of nanofibers on the properties of reinforced WSR composites, (3) the range of elasticity of WSR as it classified as elastomers, (4) how to enhance the interaction between SAPs, nanofiber mats and rubber matrix, (5) how to prepare strong hydrogel by using electrospun nanofibers as reinforcements for WSR composite and also (6) the standardization of WSR which need to be addressed.

The advancement of using WSR thus far is still the 'tip of the iceberg'. While this project has demonstrated the potential applications, many opportunities for extending the scope of this thesis still remain. Our main concern herein was related to the utilizing WSR in sealing application such as preventing water leakage from pipes and blocking connections in constructions such as subways or subsea tunnels, preservation of airtightness in machinery, sealing of gaps in construction works, cold joints and working joints in concrete, etc.

Potential applications of WSR in biomedical applications includes tissue engineering, biosensors, materials controlling reversible cell attachment, smart microfluidics and so on. An outstanding example of the potential of WSR, as previous researches show, is in drug delivery system where a hydrophobic material combined with a swelling agent could retard drug release in-vivo and maintain the drug in the body for a longer time.

Obviously, there will be set-backs on the way forward, but the scientific and translational potential of novel WSRs makes us confident in predicting a bright future.

#### 8.4 References

1. Zhang, Y., Gong, F., Zhang, X. and He, P., 2013. Effects of the Reactive Compatibilizer CPE-g-GMA on Water-Absorbing Ability and Mechanical Property of Blending-Type Water-Swellable Rubber. *Advances in Polymer Technology*, 32(S1).
2. Zhang, Z., Zhang, G., Zhang, Y., Wang, Z., Yu, D., Hu, X., Hu, C. and Tang, X., 2004. Mechanical properties, water swelling behavior, and morphology of swellable rubber compatibilized by PVA-g-PBA. *Polymer Engineering & Science*, 44(1), pp.72-78.
3. Gong, F., Han, Y. and He, P., 2010. Synthesis, Characterization and Application of Amphiphilic Copolymer Poly (vinyl alcohol)-g-Poly (butyl acrylate). *Journal of Macromolecular Science, Part A: Pure and Applied Chemistry*, 47(4), pp.318-323.
4. Zhi, X.U., WANG-Yan, L.I. and Fu-cai, Z.E.N.G., 2011. Application of compatibilizer in water swelling rubber. *Journal of Wuhan Institute of Technology*, 10, p.016.
5. Jiang, X.L., Hu, K., Yang, P. and Ren, J., 2013. Study on preparation and properties of water swellable rubber modified by interpenetrating polymer networks. *Plastics, Rubber and Composites*, 42(8), pp.327-333.
6. Dehbari, N., Zhao, J., Peng, R. and Tang, Y., 2015. Neutralisation and compatibilisation effects on novel water-swellable rubber composites. *Journal of Materials Science*, 50(15), pp.5157-5164.
7. Zhao, J., Dehbari, N., Han, W., Huang, L. and Tang, Y., 2015. Electrospun multi-scale hybrid nanofiber/net with enhanced water swelling ability in rubber composites. *Materials & Design*, 86, pp.14-21.

8. Dehbari, N., Tavakoli, J., Zhao, J. and Tang, Y., 2016. Enhancing water swelling ability and mechanical properties of water-swellaable rubber by PAA/SBS nanofiber mats. *Journal of Applied Polymer Science*, 133(47).
9. Dehbari, N., Tavakoli, J., Khatrao, S. and Tang, Y., 2017. In situ polymerized hyperbranched polymer reinforced poly (acrylic acid) hydrogels. *Materials Chemistry Frontiers*.
10. Dehbari, N., Tavakoli, J., Zhao, J. and Tang, Y., 2017. In situ formed internal water channels improving water swelling and mechanical properties of water swellaable rubber composites. *Journal of Applied Polymer Science*, 134(9).
11. <http://hydrotite.ca/products/leakmaster/>
12. Osswald, T.A., Turng, L.S. and Gramann, P.J., 2008. *Injection molding handbook*. Hanser Verlag.
13. Lee, W.F. and Chen, Y.J., 2001. Graft copolymerization of N-isopropylacrylamide on styrene-butadiene-styrene block copolymer. *Journal of applied polymer science*, 82(11), pp.2641-2650.
14. Borba, P.M., Tedesco, A. and Lenz, D.M., 2014. Effect of reinforcement nanoparticles addition on mechanical properties of SBS/Curauá fiber composites. *Journal of Materials Research*, 17(2), pp.412-419.